Stony Brook University

Influence of membrane heterogeneity on G-protein coupled receptor signaling

A Dissertation Presented

by

Rhodora Cristina Calizo

to

The Graduate School

in Partial Fulfillment of the

Requirements

for the Degree of

Doctor of Philosophy

in

Biochemistry and Structural Biology

Stony Brook University

December 2013

Stony Brook University

The Graduate School

Rhodora Cristina Calizo

We, the dissertation committee for the above candidate for the

Doctor of Philosophy degree, hereby recommend

acceptance of this dissertation.

Dr. Suzanne Scarlata – Dissertation Advisor
Professor, Physiology and Biophysics

Dr. Deborah Brown - Chairperson of Defense
Professor, Biochemistry and Cell Biology

Dr. Erwin London
Professor, Biochemistry and Cell Biology

Dr. Mark Bowen
Associate Professor, Physiology and Biophysics

Dr. Susana Neves
Assistant Professor, Pharmacology and System Therapeutics
Mount Sinai Hospital

This dissertation is accepted by the Graduate School

Charles Taber
Interim Dean of the Graduate School

Abstract of the Dissertation

Influence of membrane heterogeneity of G-protein coupled receptor signaling

by

Rhodora Cristina Calizo

Doctor of Philosophy

in

Biochemistry and Structural Biology

Stony Brook University

2013

A highly crowded and heterogenous environment is the emerging picture of the plasma membrane that would explain the efficiency and fidelity of many signal transduction processes. We determined the effect of plasma membrane heterogeneity on the function and diffusion of components from two class A G protein coupled receptor (GPCR) pathways, the bradykinin type 2 (B_2R)/$G\alpha_q$ and the mu-opioid receptor (μOR)/$G\alpha_i$ pathways, as well as the epidermal growth factor receptor. In the first part of this dissertation, we describe the effect of nanoscale plasma membrane heterogeneity, as exemplified by caveolae domains, on the B_2R and μOR pathways. We find that caveolae domains increase the signaling potential of the B_2R/$G\alpha_q$ pathway but not the μOR/$G\alpha_i$ pathway. FRET studies suggest that components of the B_2R/$G\alpha_q$ pathway reside closer to caveolae domains compared to those of the μOR/$G\alpha_i$ pathway and this proximity mediated by molecular interactions of $G\alpha_q$ with Cav1. Diffusion measurements of these membrane proteins by Fluorescence Correlation Spectroscopy (FCS) and Fluorescence Recovery After Photobleaching (FRAP) show a discrepancy in the apparent diffusion coefficients obtained

from the two methods which may be due to the geometry of caveolae domains. By FCS, an increased apparent diffusion was found for both B_2R and $G\alpha_q$ in the presence of caveolae which may be due to the confined, anomalous diffusion of the membrane proteins due to Cav1 interactions. These studies make the prediction that $G\alpha_q$-coupled receptors localize close to caveolae domains and their signaling properties impacted by the presence of caveolae domains, as compared to $G\alpha_i$ coupled receptors. In the second part of this dissertation, we describe studies on the effect of cell shape on the distribution of the EGFR and B_2R. By numerical simulation with experimental validation with fluorescence imaging, we find that cell shape can influence the balance of reaction-diffusion processes of activated membrane receptors, causing a spatial gradient of receptors on the plasma membrane. Studies of membrane heterogeneity on the $B_2R/G\alpha_q$ and EGFR pathways may have implications on the mechanotransduction and mechanosensing of many cells including cardiac, vascular and smooth muscle cells.

Table of Contents

List of Figures

List of Tables

List of Abbreviations

Φ_{local}	Local Thiele modulus
AC	adenylyl cyclase
ATP	Adenosine triphosphate
β2-AR	β-2 adrenergic receptor
B_2R	Bradykinin receptor type-2
B_1R	Bradykinin receptor type-1
Cav1	Caveolin-1
Cav2	Caveolin-2
Cav3	Caveolin-3
CBM	caveolin binding motif
CSD	caveolin scaffolding domain
cAMP	cyclic adenosine monophosphate
cGMP	cyclic guanosine monophosphate
DAG	Diacylglycerol
DAPI	4',6-diamidino-2-phenylindole
DMEM	Dulbecco's modified eagle medium

DRM	detergent resistant membrane
eCFP	enhanced cyan fluorescent protein
ECM	Extracellular matrix
eGFP	enhanced green fluorescent protein
eYFP	enhanced yellow fluorescent protein
EGFR	epidermal growth factor receptor
EGF	epidermal growth factor
eNOS	endothelial nitric acid synthase
FCS	Fluorescence correlation spectroscopy
FRAP	Fluorescence recovery after photobleaching
FLIP	Fluorescence loss in photobleaching
FRET	Förster resonance energy transfer
FRT	Fisher rat thyroid
FRTcav+	Fisher rat thyroid cells stably transfected with Cav1
FRTwt	Fisher rat thyroid cells wild type
GDP	Guanosine diphosphate
GIRK	G-protein inwardly rectifying potassium channel

GM1	monosialotetrahexosylganglioside 1
GM2	monosialotetrahexosylganglioside 2
GM3	monosialotetrahexosylganglioside 3
GPCR	G-protein coupled receptor
GTP	Guanosine triphosphate
H1R	Histamine type-1 receptor
HEK-293	Human embryonic kidney 293 cells
IBMX	3-isobutyl-1-methylxanthine
IP_3	Inositol triphosphate
kDa	kilodalton
μOR	μ-opioid receptor
MAPK	Mitogen activated protein kinase
M_3R	Muscarinic type-3 receptor
N&B	Number and Brightness
NO	nitric oxide
PIP_2	Phosphatidylinositol 4,5-bisphosphate
PKA	Protein kinase A

PKC	protein kinase C
PLC	phospholipase C
PLCβ	phospholipase C β
PMT	photomultiplier
PTRF	polymerase I-transcript release factor
ROI	region of interest
SBT	spectral bleedthrough
SDPR	serum-deprivation response protein
siRNA	small interfering RNA
SRP	Signal recognition particle
TRP6	Transient receptor potential channel type 6
STORM	Stochastic optical reconstruction microscopy
STIM1	Stromal interaction molecule 1
TRP4	Transient receptor potential channel type 4

Acknowledgments

I acknowledge my PhD advisor, Dr. Suzanne Scarlata for her excellent mentorship during my PhD studies. I thank Suzanne for her trust, encouragement and guidance all of which allowed me to mature and find my own voice as a scientist. I learned many techniques and theories on fluorescence and membrane biology under her guidance and I was also given the opportunity to attend workshops and conferences that enabled me to collaborate and think critically of my projects. I will always be indebted to Suzanne's understanding and patience as I went through crucial and sometimes challenging times in my personal and graduate school life.

I thank my dissertation committee members: Dr. Deborah Brown, who generously gave me crucial reagents for my dissertation and for imparting her expertise in membrane biology, Dr. Erwin London, for mentoring me during my first year rotation and for training me to think critically as a membrane biologist, Dr. Mark Bowen for his mentorship and excellent advice in biophysical techniques and Dr. Susana Neves, for her advice and guidance in performing the experiments related to the cell shape project.

I thank our collaborators, Dr. Ravi Iyengar for his support and insightful discussion in the cell shape project and Dr. Padmini Rangamani for carrying out the key simulation experiments that formed the basis of the chapter on cell shape.

I thank my former committee members, who will always remain my advisors, Dr. Steve Smith for mentoring me on my first lab rotation as a graduate student in BSB, and Dr. Roger Johnson who imparted me not only excellent scientific advice, but thoughtful and insightful advice in my career and life as well.

I thank the administrative staff of BSB graduate program: Joann Delucia-Conlon, Carol Juliano and Beverly Piazza and the Physiology and Biophysics graduate program: Michele Leva, Mel Bonnette and Joan Kavanaugh.

I thank the members of the Scarlata lab, who became my surrogate family in Stony Brook. I thank Dr. Yuanjian Guo (Jean), for teaching me all the important techniques that are needed in graduate school in a clever, straightforward and non-stressful way, Dr. Finly Philip for her insights and the discussions we've had especially since the GPCR-caveolae project originated from her dissertation project, Dr. Urszula Golebiewska, for expertise especially in biophysical techniques and for helping me to think critically about my project and Dr. Guiseppe Caso for his helpful comments throughout my dissertation.

I thank my fellow grad students in the Scarlata lab, Siddarth Yerramilli, Shriya Sahu and Imanol Gonzales. My life as a graduate student became livelier with them around, as we discussed science and life in general. I will truly miss their friendships and the times we have shared, in and out of the lab.

I would like to thank my family back in the Philippines, my aunt Nona Segui, mother Victoria, siblings Crispin and Lorena, who have supported me with all their prayers, love and support. I would like to thank the sacrifices of my grandparents Sotero and Josefina, who have given an education, and my father Manuel who has taught me to be persistent and positive in life. I will always miss them. I would like to thank the Chavez family for providing me with all the love and support only a family can truly give. Last but not the least; I would like to thank Tony, my husband and best friend, for giving me unconditional love, support and balance which have inspired me to overcome challenges that I never thought I could overcome.

CHAPTER I – GENERAL INTRODUCTION

The plasma membrane is a highly complex environment. As opposed to the classical model of Singer and Nicholson depicting the plasma membrane as a two dimensional fluid wherein proteins and lipids freely diffuse laterally and are randomly distributed (Singer and Nicolson 1972), the plasma membrane has been revealed to be a crowded place with a high degree of organization and heterogeneity. The heterogeneity may be caused by the natural tendency of membrane proteins to form oligomers because of their α-helical or β-barrel structures, which can further oligomerize to form protein domains (Popot and Engelman 1990), as well as the presence of lipids that segregate into regions that have distinct properties called lipid rafts (Brown and London 1998, Simons and Gerl 2010). Furthermore, the function and mobility of plasma membrane components may also be influenced by the cytoskeleton where a majority of plasma membrane components are anchored (Sheetz 2001, Jaqaman and Grinstein 2012). An increasing number of studies have suggested the compartmentalization of proteins and lipids on the plasma membrane, as evidenced by their anomalous diffusion on the plasma membrane (Kusumi, Nakada et al. 2005) or their visualization in higher resolution imaging techniques (Fotiadis, Liang et al. 2003, Fotiadis, Jastrzebska et al. 2006). The compartmentalization of plasma membrane components could diminish the diffusion time of a membrane protein in order to encounter its binding partners as well as decrease the chances of non-specific binding of a membrane protein with other unrelated membrane proteins. Simple diffusion cannot account for the kinetics observed in G-protein coupled receptor (GPCR) signal transduction events. The signaling cascade of light perception mediated by rhodopsin is triggered within 1 millisecond of light activation and downstream events such as the closing of cGMP

gated ion channels are completed within 200 ms (Makino, Wen et al. 2003). For the β2-adrenergic receptor pathway in native systems, the stoichiometry of GPCR to its corresponding G protein is 1:100. This low stoichiometry between GPCR to its downstream effectors suggests that compartmentalization of GPCR signaling components occurs at the plasma membrane (Ostrom, Post et al. 2000). Compartmentalization of membrane proteins may exist to facilitate and increase the fidelity and efficiency of these signaling cascades. Although plasma membrane organization appears to be a straightforward consequence of the properties of proteins and lipids, studies on how membrane proteins are organized on the cell membrane were hampered over the years because of several reasons. Firstly, membrane proteins often require a lipid environment to fold and function properly. The plasma membrane is challenging to mimic because of the diversity of lipids that constitute it, and there is a gap in knowledge how proteins themselves modify the properties of the membrane. Secondly, the size of complexes and membrane domains such as lipid rafts and protein domains are in the order of tens to hundreds of nanometers. Light microscopy techniques, especially fluorescence imaging, have greatly facilitated the study of membrane proteins in intact cells. However, because of the diffraction of light, conventional light microscopy techniques have an intrinsic resolution limit of approximately 250 nm, causing these domains to be "invisible" by light microscopy.

In recent years, fluorescence microscopy advanced rapidly, providing the specificity and sensitivity needed to visualize and study membrane domains. In this thesis, fluorescence techniques that have sufficient nanometer sensitivity or temporal resolution were used to study the effect of caveolae domains and cell shape on several receptors (i.e. Bradykinin 2 Receptor, μ-opioid receptor, Epidermal Growth Factor Receptor) and their downstream effectors. Förster Resonance Energy Transfer (FRET) microscopy has a sensitivity of 10 nm and can probe

protein-protein interactions in live cells. Fluorescence Recovery after Photobleaching (FRAP) and Fluorescence Correlation Spectroscopy (FCS) determine the mobilities of membrane proteins in intact cells and has a sensitivity / temporal resolution in the order of micro to milliseconds. The use of these techniques prevents any artifacts that may arise because of cell disruption or detergent solubilization. Since these techniques are performed on live, intact cells, these techniques give a picture of how these proteins behave in the highly complex, mammalian cell membrane system.

CAVEOLAE DOMAINS

One of the most well-characterized membrane domains are caveolae. Caveolae are 50-100 nm membrane invaginations discovered more than 50 years ago in electron micrographs ((Anderson 1998, Stan 2005, Parton and Simons 2007)). Caveolae are present in a wide variety of differentiated mammalian cell types including endothelial, epithelial, adipocytes, fibroblasts and muscle cells. Caveolae are structurally composed of caveolin and cavin proteins, as well as enriched in certain lipids such as cholesterol and sphingomyelin, as will be discussed in subsequent sections.

Caveolin proteins

An important milestone in caveolae biology is the discovery of caveolin proteins. Caveolin-1 was first discovered as one of the phosphorylated proteins in chicken embryo fibroblasts transformed with the *v-Src* oncogene (Glenney and Zokas 1989) and was also found

to be the major protein component of caveolae (Rothberg, Heuser et al. 1992). Caveolins are 21-24 kDa integral membrane proteins that form a hairpin loop in the plasma membrane, with both the C and N termini exposed to the cytoplasm. There are three members of the Caveolin family of protein in vertebrates: caveolin-1 (Cav1), caveolin-2 (Cav2) and the skeletal muscle specific caveolin-3 (Cav3) (Tang, Scherer et al. 1996). Cav1, or Cav3 in striated muscle cells, is necessary for the formation of the protein coat on caveolae domains. Cav1 is present as two isoforms α and β, which differ by their N-termini. Both are products of alternate initiation sites during transcription of Cav1 (Kogo and Fujimoto 2000). In some cell lines, expression of Cav1 is sufficient to make caveolae domains *de novo* (Fra, Williamson et al. 1995). In striated muscle cells, Cav3, which has 61% sequence similarity with Cav1, forms the caveolae coat (Scherer, Lewis et al. 1997). Although Cav1 and Cav3 have high sequence similarities, they differ by their N-terminal regions, with Cav1 having a longer N-terminus than Cav3. Cav2 hetero-oligomerizes with Cav1 but by itself is not necessary and sufficient to form caveolae domains (Sargiacomo, Scherer et al. 1995) and has 30% sequence similarity with Cav1. Although So far there has been no caveolin structure obtained in membranes, some information can be gleaned from the amino acid sequence of caveolin proteins. For instance, all caveolin proteins have a central 33-amino-acid long hydrophobic domain that adopts a hairpin conformation and leaves the N and C termini of the protein facing the cytoplasm (Dietzen, Hastings et al. 1995, Monier, Parton et al. 1995). All caveolin proteins also have a hydrophilic amino-terminal sequence FEDVIAEP, called the "caveolin signature motif" (Scherer, Okamoto et al. 1996, Tang, Scherer et al. 1996, Williams and Lisanti 2004). However, the function of this sequence to caveolin function is still not known

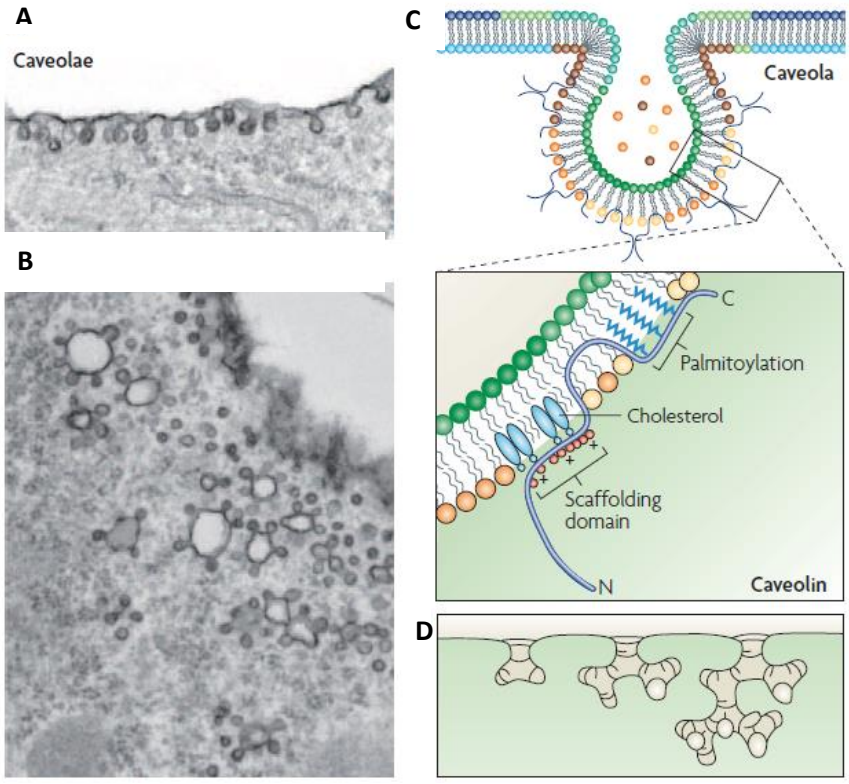

Figure I-1. Caveolae domains. **A** and **B** show caveolae in adipocytes. **C** shows a caveola with the typical flask shaped invagination with caveolin proteins inserted on the inner leaflet of caveolae domains. The caveolin protein has a "hairpin" membrane topology with the N and C termini exposed to the cytoplasm and the intramembrane domain embedded in the membrane. The C terminus of caveolin is triply palmitoylated while the N terminus has a putative scaffolding domain and cholesterol binding region. **D** shows how individual caveola can form numerous invaginations. *Reprinted by permission from Macmillan Publishers Ltd: Parton and Simons, Nat. Rev. Mol. Cell Biol. 8, 186 (2007).*

.

Caveolin scaffolding domain.

Caveolin proteins have been shown to compartmentalize and concentrate signaling molecules via a particular amino acid sequence called the caveolin scaffolding domain (CSD) (Couet, Li et al. 1997). CSD is a ~20 amino acid, aromatic rich region at the N-terminus of Cav1 or Cav3 which may interact with an aromatic-rich caveolin binding motif (CBM) on a binding partner with a common consensus sequences [(ΦXΦXXXXΦ, ΦXXXXΦXXΦ or ΦXΦXXXXΦXXΦ) where Φ is an aromatic acid and X is an unspecified amino acid)]. Various signaling molecules including G-protein subunits, eNOS and small GTPases are thought to bind Cav-1 through the CSD. The Cav-3 is similar to Cav-1 CSD and was shown to also interact with β-dystroglycan as well as a variety of signaling proteins including eNOS, PKC, G-proteins and Src family kinases (Song, Scherer et al. 1996, Sotgia, Lee et al. 2000).

Lipid composition of caveolae.

Purified caveolae domains are enriched in glycosphingolipids, cholesterol and lipid-anchored membrane proteins (Anderson 1998). These biochemical characteristics are similar to detergent resistant membrane (DRM) fraction of cells which is related to lipid rafts (Brown 2006). Because of the biochemical similarities of purified caveolae fractions and detergent resistant membranes, caveolae are believed to be a subset of lipid rafts. Maintenance of caveolae structure is also dependent on cholesterol (Rothberg, Heuser et al. 1992, Hailstones, Sleer et al. 1998). Cholesterol depletion such as treatment of cells with methyl-β-cyclodextrin flattens or collapses the caveolar structure (Rothberg, Heuser et al. 1992) with proteosomal degradation of cavin-2 (Breen, Camps et al. 2012) and increased mobility of caveolin (Pelkmans and Zerial

2005). Caveolins also have specific interactions with cholesterol. Cav1 binds at least 1 mole of cholesterol per mole of protein and cholesterol binding promotes the oligomerization of Cav1 (Murata, Peranen et al. 1995, Hailstones, Sleer et al. 1998). Cav1 and Cav3 (but not Cav2) are also palmitoylated at the C-terminal region. Palmitoylation is believed to cause the partitioning of proteins to lipid rafts (Levental, Lingwood et al. 2010) or cholesterol-rich membrane domains. Several glycosphingolipids (such as GM1 and GM3) as well as sphingolipids (such as sphingomyelin, ceramide and gangliosides) are enriched on the outer leaflet of caveolae domains (Parton 1994, Kabayama, Sato et al. 2007). The enrichment of these molecules is also a characteristic of lipid rafts, which make caveolae domains a specialized subset of non-planar lipid rafts.

Cavin proteins.

Recently, another family of resident proteins in caveolae domains called cavins were found (Hill, Bastiani et al. 2008, Liu and Pilch 2008). The cavin family of proteins, comprised of polymerase I-transcript release factor (PTRF or cavin-1), serum-deprivation response protein (SDPR or cavin-2), and sdr-related gene product (cavin-3), are soluble proteins with putative nuclear localization sequences, leucine zipper and PEST domains (sequences that are enriched in proline, glutamic acid, serine and threonine). Cavin-1 was originally discovered as a transcription factor regulatory protein. Without cavin-1, formation of caveolae is dramatically reduced and Cav1 exhibits lateral mobility and does not form caveolae structures associated with a flat plasma membrane (Hill, Bastiani et al. 2008).

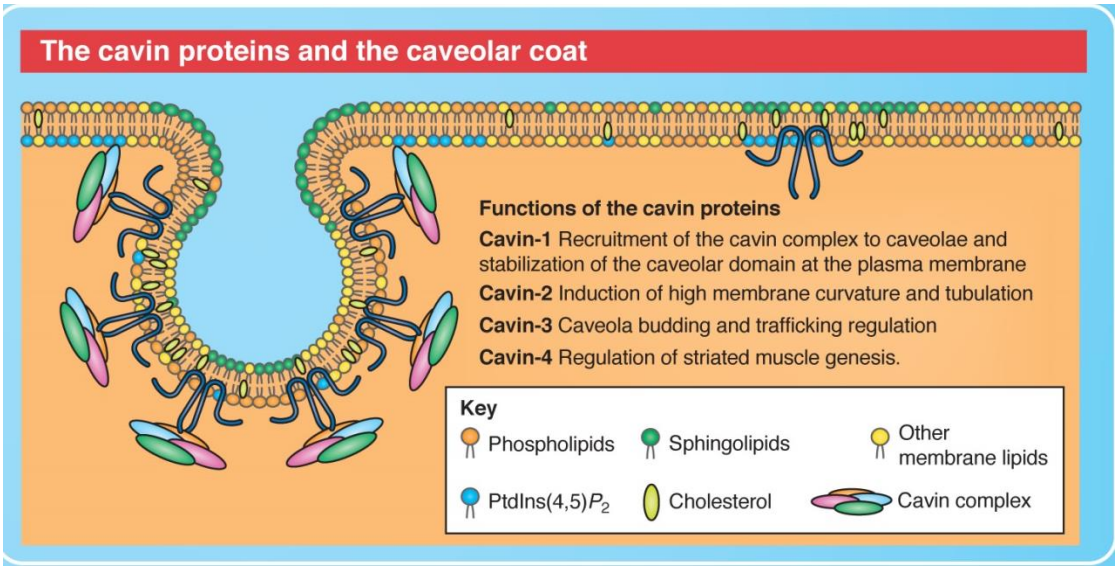

Figure I-2. Caveolae and their resident proteins. Figure shows how cavin proteins are recruited on caveolae domains. The cavin proteins are soluble proteins that interact with caveolin proteins to stabilize caveolae. *Reprinted by permission from The Company of Biologists Ltd: Bastiani M and Parton R, J Cell Sci 123(22) 3831 (2010)).*

Cavin-2 and Cavin-3 were originally discovered as Protein Kinase C substrates. The expression profiles of Cavin-1, Cavin-2 and Cavin-3 parallels the expression level of Cav1. Cavin-4, however is enriched in skeletal and cardiac muscles (Bastiani, Liu et al. 2009). Both Cavin-1 and Cavin-2 are necessary for the formation of caveolae. Cavin1 is necessary for targeting the cavin complex to the plasma membrane while Cavin-2 is necessary for membrane curvature and invaginations. Cavin-3 and Cavin-4 have other important functions in the cavin complex. Cavin-3 regulates endocytosis of caveolae and limits the intracellular trafficking of Cav1 positive vesicles (McMahon, Zajicek et al. 2009). Cavin-4 increases the differentiation of myoblasts into myotubes (Bastiani, Liu et al. 2009).

The cavin complex comprises of 60-80 cavin molecules (Hayer, Stoeber et al. 2010). The interactions of cavin proteins with Cav1 is necessary for cavin recruitment on the plasma

membrane. Cav1 and cavin associate on the plasma membrane but not on the golgi complex suggesting that the incorporation of the cavin coat takes place at a later stage in caveolae biogenesis. It is postulated that cavin proteins may be necessary for the ability of caveolin proteins to form stable caveolae (Hill, Bastiani et al. 2008)

Caveolae biogenesis.

Studies using Fluorescence Recovery After Photobleaching (FRAP) and Fluorescence Loss in Photobleaching (FLIP) in cells that express Cav1-eGFP suggest that caveolae form static and stable structures at the plasma membrane (Thomsen, Roepstorff et al. 2002, Pelkmans and Zerial 2005). Although most of caveolin formed are incorporated in stable caveolae domains, an intracellular pool of caveolins is always present in the golgi complex as well as in the endocytic compartments (Glenney and Soppet 1992, Kurzchalia, Dupree et al. 1992, Liu, Rudick et al. 2002).

Caveolins are synthesized in the endoplasmic reticulum as an integral membrane protein (type II transmembrane protein) and adopts a hairpin configuration in which both N and C termini are exposed to the cytoplasm. The caveolin protein inserts into the membrane of the endoplasmic reticulum in a signal recognition particle (SRP) dependent manner. Cav1 then undergoes the first stage of homo-oligomerization in the ER forming an 8S complex which is composed of approximately 7-14 Cav1 molecules, which then exits the ER due to a DXE sequence on the N-terminus of Cav1 (Monier, Parton et al. 1995). This complex then goes to the golgi complex via the COPII machinery. At the golgi complex, the 8S caveolin complexes undergo another round of oligomerization. Several caveolin mutations disrupt the transport of

caveolin from the Golgi to the plasma membrane (Kirkham, Nixon et al. 2008). After exiting the golgi complex, the caveolin oligomers further assemble into 70S complexes with a molecular weight of 3.3 MDa. The formation of a 70S complex which is composed of ~160 Cav1 and Cav2 molecules is believed to be a mature caveola. Using Total internal reflection (TIRF) microscopy of fluorescently tagged Cav1, it has been suggested that approximately 144 Cav1 molecules are incorporated into one caveola structure (Pelkmans and Zerial 2005). The caveolin complex docks on the plasma membrane and recruits several lipids such as sphingomyelin, glycosphingolipids (GD3, GM1 and GM3), ganglioside and cholesterol to form a specialized lipid domain. Once on the plasma membrane, caveolae are highly stable and long-lived and do not participate in constitutive endocytic pathways (Thomsen, Roepstorff et al. 2002, Pelkmans, Bürli et al. 2004, Tagawa, Mezzacasa et al. 2005).

Phenotypes of caveolin knockdown mice.

Studies of caveolin knockout mice provide the most compelling evidence that Cav1 and Cav3 are necessary for the formation of caveolae domains. Because of the involvement of caveolae domains and caveolin in several signaling pathways, knockout of caveolin gene and disruption of caveolae domains are expected to have pleiotropic effects. Surprisingly, caveolin deficient mice are viable and fertile but have numerous tissue-specific abnormalities. These studies suggest that there are numerous compensatory mechanisms for caveolae function. Cav1 null (Cav-1 -/-) (Drab, Verkade et al. 2001, Razani, Engelman et al. 2001), Cav3 null (Cav-3 -/-) (Hagiwara, Sasaoka et al. 2000, Galbiati, Engelman et al. 2001), Cav1/Cav3 double knockout (Park, Woodman et al. 2002) and Cav2 null (Cav-2 -/-) (Park, Woodman et al. 2002) mice have

been produced. Cav1 null mice display pulmonary fibrosis, hypertension and cardiac hypertrophy and lose Cav2 expression (Razani, Engelman et al. 2001). The acetylcholine and NO pathways are also hyperactivated resulting in increased relaxation of isolated aortic rings of Cav1 null mice (Drab, Verkade et al. 2001). Furthermore, a weaker calcium dependent contractile response to angiotensin II, endothelin-1 and phorbol mice were found in the vascular smooth muscle cells of Cav1 null mice. Cav-1 null mice are also leaner especially when challenged by a high-fat diet, display elevated levels of free fatty acids and triglycerides, decreased leptin and ACRP30, although there are no changes in insulin, glucose and cholesterol levels (Park, Woodman et al. 2002). These results all point to numerous vascular and lipid metabolism defects when the Cav1 gene is knocked out.

Mice with no Cav3 gene (Cav3 -/-) are also viable but showed muscle degeneration in the diaphragm and soleus muscles. The T-tubule system in cardiomyocytes are also disorganized and the dystrophin-glycoprotein are excluded from lipid raft domains (Hagiwara, Sasaoka et al. 2000). Two T-tubule marker proteins, namely the dihydropyridine receptor -1α and ryanodine receptor), are mislocalized in cardiomyocytes of Cav3 null mice. Interestingly, mice overexpressing Cav3 have the same phenotype as Cav3 deficient mice. Transgenic mice overexpressing Cav3 exhibit hypertrophic, necrotic and regenerating skeletal muscle fibers with downregulation of dystrophin, suggesting that Cav3 may play a role in scaffolding of the dystrophin complex in the sarcolemma. (Galbiati, Engelman et al. 2001). These observations suggest the proper amount of Cav3 is required for normal muscle function.

Cav-1/Cav-3 double knockout mice are truly caveolae deficient. These mice develop severe cardiomyopathy and reveal a dramatic increase in ventricular wall thickness and exhibit hypertrophy, disorganization and degeneration of cardiac myocytes and exhibited skeletal

defects (Park, Woodman et al. 2002). These findings underline the importance of caveolae in the cardiovascular system.

Cav2 knockout mice have unaltered number of caveolae demonstrating that Cav2 is not necessary for formation of caveolae (Park, Woodman et al. 2002). Cav2 null mice do not exhibit vascular and lipid metabolism defects as Cav1 null mice but display pulmonary dysfunction with alveolar septal thickening and exercise intolerance. Since these mice displayed normal number of caveolae, these results suggest that Cav2 may perform functions other than those related to caveolae.

Implications of caveolae structure on biophysical studies of caveolae domains

Caveolae were originally found to have 50-100 nm invaginations (Yamada 1955) but later studies show that the dimensions are closer to 60-80 nm (Bastiani and Parton 2010). Using ultrastructural 3D studies of caveolae domains in endothelial cells showed a neck size of ~50 nm and a depth of ~ 50 nm (Figure I-4). These studies also suggest that Cav1 are distributed uniformly on an entire caveola (Richter, Floetenmeyer et al. 2008). If approximately 144 Cav1 molecules are equally distributed in a cup-shaped volume similar to caveolae, two adjacent Cav-1 molecules are within 10 nm of each other. FRET, which is sensitive to molecular interactions or proximity related changes within 10 nm, can therefore be used to see interaction of Cav1 with a caveolae associating molecule, or other proteins residing or in close proximity to caveolae domains.

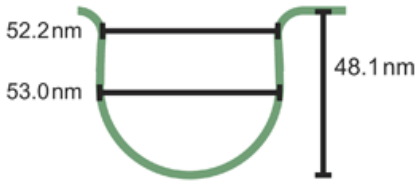

Figure I-3. Dimensions of a caveola averaged over different cell types as determined by high-resolution electron microscope tomography. *Reprinted by permission by John Wiley & Sons, Inc.: Richter T et al. Traffic 9:895 (2008)*

In certain types of endothelial cells, caveolae have specialized structures called stomatal diaphragms. The stomatal diaphragm is a special caveolae sub-domain, which is composed of a thin (~5 -6 nm) protein barrier in the caveolar neck. This protein barrier is characterized by the presence of plasmalemmal vesicle associated protein (PLVAP, gp68, PV1). PV1 is a 60 kDa single span, type II membrane glycoprotein that forms homodimers. The distribution of both stomatal diaphragm and PV1 are similar, suggesting that PV1 is necessary for the formation of stomatal diaphragm (Stan 2002, Stan, Tkachenko et al. 2004). Thus, the neck may be a sub-domain of caveolae domain that has a specialized environment and composition.

Role of caveolae domains in signaling.

Despite its discovery more than 50 years ago and studies unveiling the structure, composition and biochemistry of caveolae, the function of caveolae is still not clearly understood. Caveolae have been associated with many functions in the cell including endocytosis, transcytosis, cholesterol and lipid metabolism, mechanotransduction, cell proliferation and cell signaling.

One of the most important and common roles ascribed to caveolae is its role in modulating membrane signal transduction processes by sequestering membrane signaling proteins (Sargiacomo, Sudol et al. 1993, Chun, Liyanage et al. 1994, Lisanti, Scherer et al. 1994, Schnitzer, Oh et al. 1995). Several signaling proteins such GPI-anchored proteins (Sargiacomo, Sudol et al. 1993), IP3 Receptors (Schnitzer, Oh et al. 1995), heterotrimeric G proteins e.g. (Chang, Ying et al. 1994, Li, Okamoto et al. 1995), small G-proteins such as Ras (Song, Li et al. 1996) and endothelial nitric oxide synthase (eNOS) (Shaul, Smart et al. 1996) among others have been shown to localize in caveolae domains. The enrichment of signaling proteins in caveolae domains led to the "caveolae signaling hypothesis" which postulates that caveolae are signaling platforms that sequester membrane signaling molecules for a faster and more directed signaling effect. (Anderson 1993, Lisanti, Scherer et al. 1994)

G-protein coupled receptor (GPCR).

An important class of signaling proteins that are proposed to localize in caveolae domains are G-protein coupled receptors and their downstream signaling components (for review, see (Chini and Parenti 2004, Insel, Head et al. 2005, Patel, Murray et al. 2008)). GPCRs comprise the largest family of membrane proteins with more than 700 genes encoded in the human genome. They are also the target of more than 30 % of known drugs making them an important pharmaceutical target. GPCRs can sense a wide variety of extracellular signaling including light, hormones, lipids, peptides and odorants. GPCRs can be classified according to their pharmacological properties into four main families: class A rhodopsin-like, class B secretin-like, class C metabotropic glutamate/pheromone and frizzled receptors (class F) (Pin,

Neubig et al. 2007). The structure of a GPCR can be divided into three parts (Figure I-5): 1) an extracellular region which consists of the N-terminus and three extracellular loops (ECL1-ELC3), 2) the transmembrane regions which consists of seven α-helices (TM1-TM7), and 3) the intracellular region consisting of three intracellular loops (ICL1-ICL3), an intracellular amphipathic helix (H8) and the C-terminus (for review of the structure of class A GPCRs, see (Venkatakrishnan, Deupi et al. 2013)). Since we are interested in how caveolae domains may modify the interactions of GPCRs with its downstream binding partners, we will concentrate on the structure of the intracellular loops and C-terminal region which is composed of ICL1-3, H8 and the C-terminus. From current crystal structures of GPCRs, ICL1 is usually 6 amino acids long and contains a helical turn. The length of ICL2 is usually one or two-turns of alpha helix and forms a salt bridge with Asp of the DRY motif in the TM3, which is a highly conserved region in class A GPCRs. Most Class A GPCR structures have a short ampiphatic helix (H8) on their C-termini, which also have palmitoylation sites. According to crystal structures of β-2 adrenergic receptor in complex with $G\alpha_s$, H8 does not contact the G –protein (Rasmussen, DeVree et al. 2011). The ICL3 and C-terminal tail are long and variable regions and are intrinsically disordered in many GPCRs. Furthermore, several residues in the C-terminal tail of beta-2 AR are post-translationally modified and can be phosphorylated and interact with many downstream effectors such as β-arrestin. This makes the C-terminal tail and H8 available to interact with other membrane proteins such as caveolin.

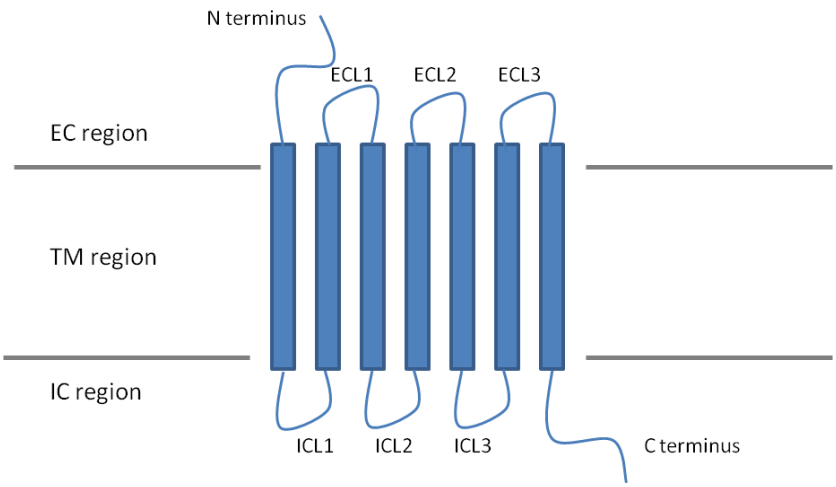

Figure I-4. Main structural features of a G-protein coupled receptor protein showing an extracellular N-terminus, 3 extracellular loops (ECL), 3 intracellular loops (ICL) and an intracellular C terminus.

Of interest to us are two class A (rhodopsin-like) GPCRs: bradykinin 2 receptor pathway and the μ-opioid receptor. We use both GPCRs as our model systems for the $G\alpha_q$ / PLCβ and $G\alpha_i$/ adenylyl cyclase pathways respectively.

Bradykinin 2 Receptor.

Bradykinin Receptors belong to class A GPCRs, and are activated by the agonist bradykinin. Bradykinin signaling is implicated in pain, inflammation, vasodilation and hypertension (for Review see (Marceau and Regoli 2004, Leeb-Lundberg, Marceau et al. 2005)). These receptors signal through the $G\alpha_q$ / PLCβ pathway leading to the increase of intracellular Ca^{2+} and IP_3. Bradykinin receptors also signal through the Phospholipase A_2 pathway causing an increase of arachidonic acid (Burch and Axelrod 1987). Bradykinin 2 receptor and endothelial

nitric oxide synthase (eNOS) pathway are also associated through the agonist bradykinin. Bradykinin activates the release of nitric oxide (NO) from endothelial cells, activating the eNOS pathway (Palmer, Ferrige et al. 1987). There are two types of bradykinin receptors, Bradykinin 1 Receptor (B_1R) and Bradykinin 2 Receptor (B_2R). B_2R is expressed in vascular cells, fibroblasts, epithelial cells, nervous cells and various tumor cells. B_2R is constitutively expressed and desensitizes rapidly, as opposed to B_1R, which requires induction to be expressed and has limited desensitization (Leeb-Lundberg, Marceau et al. 2005). B_2R is post-translationally modified on the extracellular domain by glycosylation and disulfide bond formation similar to most class A GPCRs. B_2R also has a acylation motif (CxxxGC) on the C terminal tail which has shown to be palmitoylated by mass-spectrometry (Soskic, Nyakatura et al. 1999).

Several studies have suggested that B_2R resides in caveolae. By density gradient fractionation and radioligand labeling of B_2R, De Weerd and Leeb-Lundberg showed that bradykinin addition promotes sequestration of B_2R, $G\alpha_q$ and $G\alpha_i$ in caveolae in DDT_1 MF-2 smooth muscle cells (de Weerd and Leeb-Lundberg 1997). In the basal, unstimulated state, B_2R, $G\alpha_q$ and $G\alpha_i$ and are also enriched in caveolin fractions. By immuno-electron microscopy, Haasemann et al. found that Cav1 and B_2R are distributed similarly on caveolae structures on the plasma membrane of A431 cells upon agonist addition (Haasemann, Cartaud et al. 1998). In human airway smooth muscle cell (HSM), plasma membrane caveolin-1 colocalized with B_2R, Muscarinic 3 receptor (M_3R) and Histamine 1 Receptor (H_1R) Receptors as well as STIM1, TRP4 and TRP6. Disruption of caveolae by treatment with methyl-β-cyclodextrin or transfection with Cav1 siRNA attenuated the agonist mediated calcium release in B_2R, M_3R and H_1R, with B_2R showing the most dramatic effect (Prakash, Thompson et al. 2007). The presence of caveolae could impact the function of B_2R. In endothelial cells, ATP, bradykinin or thrombin

stimulation induced calcium waves that specifically originate from caveolin-rich edges, which was dependent on intracellular calcium. Treatment with the microtubule disruption colcemid, altered Cav1 and calcium initiation sites concomitantly (Isshiki, Ando et al. 1998).

μ-Opioid Receptor.

μ-opioid receptor is one of four class A GPCRs that is stimulated by opiates. The other ones are kappa (κOR), delta (δOR) and nociceptive (NOR) opioid receptors. μ-Opioid receptor induces analgesia, bradycardia, hyphothermia and indifference to environmental stimuli. It is coupled to $G\alpha_i$ / $G\alpha_o$ which upon activation inhibits adenylyl cyclase and voltage gated Ca^{2+} channels. It is also known to stimulate G-protein activated inwardly rectifying K^+ channels (GIRKs) and PLCβ. Like other Class A GPCRs, the C terminal tail of the μ-opioid receptor has a putative palmitoylation site (Waldhoer, Bartlett et al. 2004).

Co-immunoprecipitation studies show that μ-opioid receptors localize in Cav1 enriched lipid rafts (Zhao, Loh et al. 2006, Berg, Zardeneta et al. 2007) and colocalize with Cav3 microdomains in adult cardiomyocytes (Head, Patel et al. 2005). Although caveolin expression has not been fully elucidated in the nervous system where μOR is most abundant (Gaudreault, Blain et al. 2005), it is up-regulated in aging brains (Kang, Chung et al. 2006) and its down-regulation induces demyelination of neurons (Yu, Rouen et al. 2008). These observations imply that Cav1 may be indirectly involved with promoting changes in plasticity, neuro-protection, neuro-degeneration and aging.

Heterotrimeric G-proteins.

Heterotrimeric G-proteins are the intracellular binding partners of G-protein coupled receptors. They are composed of α, β and γ subunits. The intracellular loops of the activated GPCR act as a guanine exchange factor (GEF) to the GDP bound α subunit, catalyzing its exchange from GDP to GTP. Gα (GTP) and Gβγ then stimulate downstream effectors. There are 21 Gα subunits encoded by 16 genes, 6 Gβ subunits encoded by 5 genes and 12 Gγ subunits (Downes and Gautam 1999). There are four main classes of the heterotrimeric G proteins based on their Gα subunit: $G\alpha_s$, $G\alpha_i$, $G\alpha_q$ and $G\alpha_{12}$. The Gα subunit has a conserved protein fold composed of a GTPase domain and a helical domain. The GTPase domain hydrolyses GTP and contains switches I, II and III which undergo a major conformational change upon binding with GDP or GTPγS. The helical domain is a six α-helix bundle that forms a lid over the nucleotide-binding pocket. All Gα subunits except $G\alpha_t$ are palmitoylated at the N-terminus, while $G\alpha_i$ is myristoylated at the N-terminus in addition to being palmitoylated. $G\alpha_q$ and $G\alpha_q$ are both dually palmitoylated. $G\alpha_q$ is palmitoylated at cysteines 9 and 10 (Chen and Manning 2001, Smotrys and Linder 2004) while $G\alpha_s$ is palmitoylated at its N-terminal cysteine and N-terminal glycine (Kleuss and Krause 2003).

The Gβ subunit has a seven-bladed β propeller structure each of which is composed of a WD40 sequence repeat. The α helical N-terminus of Gβ forms a coiled-coil interaction with the N-terminus of Gγ while the C terminus of Gγ binds to blades five and six. Gγ subunits are post-translationally modified at their C-termini with either a farnesyl (Gγ1, Gγ8, Gγ11) or geranylgeranyl moiety (Zhang and Casey 1996).

Upon activation of the GPCR, both Gα and Gβγ activate effector molecules. The effector recognition site in all Gα sites is in the C-terminal half of α2 (switch II) together with α3-helix (Sprang, Chen et al. 2007). Each class of Gα target different effectors while Gβγ target similar effectors.

For the G_q pathway, $G\alpha_q$(GTP) activates phospholipase C β (PLC β). Binding of $G\alpha_q$ to PLC β enhances the GTPase activity of the α subunit, turning off $G\alpha_q$. PLC β in turn cleaves phosphatidylinositol 4,5 bisphosphate (PIP_2) into diacylglycerol (DAG) and inositol triphosphate (IP_3). DAG and IP_3 activate Protein Kinase C (PKC) and stimulate the release of intracellular Ca^{2+} (Rhee 2001).

For the G_s pathway, $G\alpha_s$(GTP) stimulates adenylyl cyclase (AC) causing an increase in intracellular cAMP concentrations. Different ACs have varying affinities for $G\alpha_s$, which may cause a variation in cAMP levels. Furthermore, different isozymes of ACs are present in different cell types. The varying degrees of affinities of ACs to $G\alpha_s$ in different cell types are abolished in the presence of 100 μM forskolin, which can regulate coupling of Gα subunits to ACs (Cabrera-Vera, Vanhauwe et al. 2003). In the second chapter, cAMP assays are performed to observe the difference in cAMP levels upon morphine stimulation in the presence and absence of caveolae. Cells were treated with 100 μM forskolin to have a maximal cAMP signal and to abolish the affinities of different ACs present in the cells.

For the G_i pathway, $G\alpha_i$(GTP) inhibits AC causing a decrease in intracellular cAMP. The inhibitory action of GPCRs on AC activity can be blocked by pertussis toxin which catalyzes the ADP-ribosylation of $G\alpha_i$. The AC inhibition of $G\alpha_i$ – coupled receptors are isozyme specific and also cell-type specific (Defer, Best-Belpomme et al. 2000). $G\alpha_i$, acts as a

noncompetitive inhibitor of $G\alpha_s$-stimulated AC5 and AC6 but has no effect on AC2 and AC8. Like $G\alpha_s$, the cAMP profile of $G\alpha_i$ may therefore vary on different cell type depending on which ACs are present in the cell.

The $G\beta\gamma$ subunit can also play roles in cAMP levels. $G\beta\gamma$ can activate AC2 and AC4 but only in the presence of $G\alpha_s$. The $G\beta\gamma$ subunit can also directly inhibit AC1 activity resulting in a further decrease in cAMP compared to the actions of $G\alpha_i$ alone (for review please see (Defer, Best-Belpomme et al. 2000).)

The $G\alpha$ subunit of the heterotrimeric G-proteins have also been found to colocalize in caveolae domains. $G\alpha_{i2}$, $G\alpha_{q/11}$, $G\alpha_s$, $G\alpha_{i3}$ are enriched in caveolae fractions (Sargiacomo, Sudol et al. 1993, Chang, Ying et al. 1994, Li, Okamoto et al. 1995). However, there is confusion in the literature regarding which $G\alpha$ subunits localize in caveolae domains. Freeze-fracture immunoelectron microscopy by Nomura et al. found that $G\alpha_{i2a}$ is enriched only by approximately two-fold, as opposed to the 3-40 fold enrichment reported from biochemical fractionation studies (Nomura, Inuo et al. 1997). Using subcellular fractionation and confocal microscopy in lung tissue, endothelial and epithelial cells, $G\alpha_q$ without $G\beta\gamma$, was found to interact with caveolin, while $G\alpha_i$, $G\alpha_s$ as well as $G\beta\gamma$ colocalize with GPI anchored proteins associated with non-caveolae lipid rafts (Oh and Schnitzer 2001).

In our lab, we have found that $G\alpha_q$ has a specific interaction with Cav1. The presence of Cav1 decreases FRET between $G\alpha_q$ (GTP) and $G\beta\gamma$ upon B_2R stimulation, with concominant prolongation of calcium signaling (Sengupta, Philip et al. 2008). This result suggests that the presence of Cav1 prolongs the lifetime of $G\alpha_q$(GTP), causing a sustained Ca^{2+} signal. In adult cardiomyocytes that amply express Cav3, a peptide that disrupts interaction between $G\alpha_q$ and

Cav3 extinguishes calcium waves that are not seen in neonatal cardiac myocytes, which do not have caveolae. This results suggest that caveolae might play a role in regulating basal calcium activity in cardiomyocytes (Guo, Golebiewska et al. 2011).

CELL SHAPE AND RECEPTOR GRADIENT ON THE PLASMA MEMBRANE

Cell shape may also regulate GPCR distribution on the plasma membrane. Studies of cell shape are an empirical and straightforward way of determining how cells behave under different conditions and it is for this reason that pathology uses cell morphology as a diagnostic tool to assess tissue disease states. Drastic changes in cell morphology are indicators of oncogenic transformation by Ras as it transforms from a normal, spread out, circular morphology to a fusiform and elongated shape with compact nuclei and disrupted cytoskeleton (Kim, Burns et al. 1999). An earlier study demonstrates that cell shape is tightly coupled to DNA synthesis and growth in non-transformed cells (Folkman and Moscona 1978). It can therefore be hypothesized that cell shape can modulate signal transduction processes and may even be used as a repository of signaling information.

Numerous studies have suggested that signaling proteins and formation of microdomains are influenced by cell shape and size. Most of these studies were carried out by controlling the microenvironment by performing experiments on cells cultured in micropattern substrates. Micropattern technology involves the fabrication of substrates to which cells can

attach and take on different shapes (Théry 2010). Control of the cell shape, in particular alignment and constriction, can induce myogene differentiation of bone-marrow-derived human mesenchymal stem cells, with an upregulation of myogenic gene markers upon incubation in well-aligned, constricted micropatterns. The authors hypothesize that lineage commitment of mesenchymal stem cells can be induced by controlling the micropattern (Yu, Chua et al. 2013). Cell confinement can control the development of three-dimensional epithelial cell polarity by modulating the initial steps in the formation of the central lumen into the apical membrane (Rodriguez-Fraticelli, Auzan et al. 2012, Rodriguez-Fraticelli and Martin-Belmonte 2013). Cell shape also affects cell locomotion. The authors found that the direction and speed of cell migration can be controlled by manipulating the divergence angles and the widths of the micropatterns respectively (Yoon, Kim et al. 2012). In neuronal cells, glutamate treatment and electrical stimulation results in the enrichment of PKCγ in membrane regions with smaller surface to volume ratios such as synaptic spines and dendritic branches compared to regions with higher surface to volume ratios such as cell soma or thicker branches (Craske, Fivaz et al. 2005).

Cell shape is controlled by many factors including interactions of small GTPases with the cytoskeleton (Sheetz 2001, Hall 2012), membrane dynamics (endocytosis and exocytosis) and membrane tension to name a few (Diz-Muñoz, Fletcher et al. 2013). The cell senses these factors collectively to respond to the environment by changing its shape or motility. Rho family of GTPases control cytoskeletal remodeling. There are 20 Rho GTPases in mammals. RhoA, Rac1 and Cdc42 are the three best characterized Rho GTPases (Hall 2012). Cell shape is also influenced by membrane tension (reviewed in (Diz-Muñoz, Fletcher et al. 2013)). One of the ways for the cell to regulate membrane surface area is by exocytosis, stimulated by high membrane tension and clathrin-coated endocytosis, stimulated by low membrane tension. These

two opposing forces maintain membrane homeostasis (Sheetz 2001). Recently, caveolae have been shown to play a role in the control of membrane tension by acting as membrane reservoirs enabling cells to accommodate sudden changes in membrane tension (Gervásio, Phillips et al. 2011, Sinha, Köster et al. 2011). Increase in cell tension by cell stretching or hypo-osmotic shock causes disassembly of caveolae suggesting that caveolae are capable of buffering plasma membrane tension.

Theoretical models integrate the above mentioned factors to collectively simulate forces that control cell shape and motility (for review (Holmes and Edelstein-Keshet 2012)). One of them is the perimeter model, which represents the cell as a closed curve. The boundary is identified as the cell membrane and the 2D interior of the shape is identified as the cytosol. One such application that uses the perimeter model is the Virtual Cell suite (Loew and Schaff 2001). In chapter 4 of this dissertation, Virtual Cell was used to model different cell shapes and to perform numerical simulations of the concentration of growth factor receptor and GPCR in the basal and stimulated states.

One of the ways that membrane heterogeneity could arise is through the changes in membrane curvature. It can be hypothesized that the curvature of the plasma membrane results in spatial gradients of activated signaling components on the plasma membrane due to the balance of reaction-diffusion processes along the plane of the membrane (Rangamani, Lipshtat et al. in press). In chapter four of this dissertation, this hypothesis was tested numerically and experimentally. Numerically, reaction-diffusion formulations were used to analyze the effect of cell shape of the boundary on the spatial distribution of activated signaling components in the plane of the plasma membrane and in the cytoplasm as a function of time. To test this experimentally, the concentration of membrane signaling components in different cell shapes are

quantified using imaging and correlation methods. The ellipsoid cell shape is closest to the fusiform shape, which is a characteristic of neoplastic transformed cells, while the circular, spheroidal cells are associated with normal cell shape. From these studies we can answer the question whether cell shape could modulate receptor distribution on the plasma membrane.

FLUORESCENCE METHODS USED IN THIS DISSERTATION

Förster/Fluorescence Resonance Energy Transfer Microscopy (FRET)

Förster Resonance Energy Transfer (FRET) is a non-radiative energy transfer that occurs between an excited donor (D) molecule and an acceptor (A) molecule in a ground state. The rate of energy transfer depends on the overlap between the donor emission and the acceptor excitation spectra, quantum yield of the donor, the orientations of the donor and acceptor dipoles and the distance between the donor and acceptor molecules (Lakowicz 2006). The relationship between the rate of energy transfer, k_T, from donor to acceptor is given by the equation

$$k_T(r) = \frac{1}{\tau_D}\left(\frac{R_0}{r}\right)^6 \qquad (1)$$

where τ_D is the lifetime of the donor emission in the absence of acceptor, R_0 is the Förster distance, and the r is the distance between the donor and the acceptor. The distance at which the efficiency of energy transfer is 50% efficient is called the Förster radius. For a eCFP / eYFP FRET pair, the Forster radius is ~ 50 Å. There are many modes of FRET microscopy in use (for Review see (Sun, Wallrabe et al. 2011)). In this dissertation, sensitized emission is used, which

measures the amount of acceptor emission which results from energy transfer from the donor emission. The eCFP/eYFP FRET pair was used to tag two proteins and study their interactions. Most crucial in performing sensitized emission FRET is correcting for the spectral overlaps, which contaminates the signal of the sensitized emission channel. There are two spectral overlaps that need to be corrected: 1) the overlap of the donor emission with the acceptor detection channel that causes spectral bleedthrough, and 2) the overlap of the acceptor excitation with the donor excitation spectra, causing cross-excitation. The raw FRET image can be corrected for the above-mentioned spectral overlaps using Precision FRET (PFRET) algorithm (Chen, Elangovan et al. 2005). PFRET calculation is based on post-acquisition image analysis that corrects for the contaminating signal using singly labeled reference samples. PFRET is defined as:

$$PFRET = UFRET - DSBT - ASBT \quad (2)$$

where UFRET is the uncorrected FRET, DSBT is the donor spectral bleedthrough, and ASBT is the acceptor spectral bleedthrough. DSBT is the donor emission bleedthrough to the acceptor emission channel and can be corrected by a donor-only sample, by measuring the amount of donor emission signal that leaks through the acceptor channel. ASBT is the signal bleedthrough coming from the cross-excitation of the acceptor from the donor excitation. It is corrected by using a sample with only the acceptor (acceptor-only sample), and the amount of acceptor emission upon excitation with the donor wavelength is measured. The amount of acceptor species is determined by exciting the acceptor with the acceptor excitation wavelength. It is notable that since the images of the sample containing both donor and acceptor are corrected using images of different samples (donor only and acceptor only controls), individual pixel locations cannot be compared. In this algorithm, pixels with matching fluorescence and in the

same intensity range are compared. Therefore, this method also takes into account the expression levels of the acceptor and the donor. This approach works on the assumption that doubly labeled samples and acceptor and donor only controls are imaged under the same conditions and exhibit the same bleedthrough dynamics. Therefore, all settings used for taking control images should be used for the sample images, including laser power, PMT voltages, magnification, zoom, in the case of performing FRET in confocal laser scanning microscope.

The DSBT can be obtained by the following equations:

$$rd_{(j)} = \frac{\sum_{i=l}^{i=m} b_i}{\sum_{i=l}^{i=m} a_i}$$

$$DSBT_{(j)} = \sum_{p=l}^{p=n} \left(e_p * rd_{(j)}\right)$$

$$DSBT = \sum_{j=l}^{j=k} DSBT_{(j)}$$

Where j is the jth range of intensity, $rd_{(j)}$ is the donor bleed-through ratio for the jth intensity range, m is the number of pixel in ‘a’ for the jth range, where ‘a’ is the image containing donor only, excited at the donor wavelength and the signal collected at the donor emission wavelength and ‘b’ is the same sample containing donor only, excited at the donor wavelength and the signal collected at the acceptor emission wavelength, $a_{(i)}$ is the intensity of pixel (i), $DSBT_{(j)}$ is the donor bleed-through for the range j, n is the number of pixel in ‘e’ for the jth range, where ‘e’ is the image containing both donor and acceptor, excited at the donor wavelength and the signal collected at the donor emission wavelength, $e_{(p)}$ is the intensity at pixel (p), k is the number of range and DSBT is the total donor bleedthrough.

The ASBT can be obtained similarly:

$$ra_{(j)} = \frac{\sum_{i=l}^{i=m} c_i}{\sum_{i=l}^{i=m} d_i}$$

$$ASBT_{(j)} = \sum_{p=l}^{p=n} (g_p * ra_{(j)})$$

$$ASBT = \sum_{j=l}^{j=k} ASBT_{(j)}$$

Where j is the jth range of intensity, $ra_{(j)}$ is the acceptor bleed-through ratio for the jth intensity range, m is the number of pixel in 'd' for the jth range, where 'd' is the image containing acceptor only, excited at the acceptor wavelength and the signal collected at the acceptor emission wavelength and 'c' is the same sample containing acceptor only, excited at the donor wavelength and the signal collected at the acceptor wavelength, $d_{(i)}$ is the intensity of pixel (i), $ASBT_{(j)}$ is the donor bleed-through for the range j, n is the number of pixel in 'g' for the jth range, where 'g' is the image containing both donor and acceptor, excited at the acceptor wavelength and the signal collected at the acceptor emission wavelength, $g_{(p)}$ is the intensity at pixel (p), k is the number of range and ASBT is the total acceptor bleedthrough.

The energy transfer and distance from sensitized emission is

$$E = 1 - \left(\frac{I_{DA}}{I_D}\right) \qquad (3)$$

Where I_{DA} is the pixel intensity a donor image in the presence of acceptor, while I_D is the intensity in the absence of acceptor. Since PFRET is the energy transfer from the donor emission to the acceptor,

$$I_D = I_{DA} + PFRET \qquad (4)$$

Equation (3) can therefore be expressed as

$$E = 1 - \frac{I_{DA}}{[I_{DA} + g^{-1}(PFRET)]} \qquad (5)$$

Where g^{-1} is the spectral sensitivity for donor and acceptor channel images. The distance between donor and acceptor, r

$$r = R_0 \left\{\left(\frac{1}{E}\right) - 1\right\}^{1/6} \qquad (6)$$

For a comprehensive discussion of the determination of spectral sensitivity, please see (Chen, Elangovan et al. 2005).

Fluorescence Recovery After Photobleaching (FRAP).

Fluorescence Recovery After Photobleaching (FRAP) is a technique to determine the mobilities of fluorophore-tagged proteins. A region of the cell expressing the fluorophore-tagged protein is bleached using high-powered laser, and the time dependent recovery in fluorescence is observed, as the non-bleached population diffuses into the bleached region using low-powered laser (for review (Reits and Neefjes 2001, Sezgin and Schwille 2011)). Two parameters can be obtained from a FRAP curve: the diffusion coefficient and the mobile fraction of the fluorescently labeled protein.

The mobile fraction is defined as

$$R = \frac{(F_\infty - F_0)}{(F_i - F_0)} \qquad (7)$$

where F_∞ is the fluorescence in the bleached region after full recovery, F_i is the pre-bleaching fluorescence, and F_0 is the fluorescence right after bleaching.

For membrane proteins diffusing on the plasma membrane, unrestricted two-dimensional diffusion is assumed. Diffusion coefficient D, is related to the diffusion time τ_D by the modified Einstein equation for two-dimensional diffusion.

$$\tau_D = \frac{\omega^2 \gamma}{4D} \qquad (8)$$

where ω is the radius of the of the laser beam at e^{-2} intensity and γ is a correction factor to account for the amount of bleaching.

FRAP is suited for processes on a second scale while FCS is suited for microsecond time scale processes. A FRAP curve might contain information regarding binding as well as diffusion. Since FRAP averages over many molecules, extensive modeling may be necessary to interpret the FRAP curve.

Fluorescence Correlation Spectroscopy (FCS).

Another technique to determine the mobility of membrane proteins is by Fluorescence Correlation Spectroscopy (FCS). FCS is based on the analysis of time-dependent intensity fluctuations as a fluorophore diffuses into and out of diffraction limited spot produced by a focused laser beam. The excitation or detection volume has a shape of an ellipsoid with a radius of 200-300 nm radius and a height of 2 μm, and has a volume of approximately 1 fL. The signal fluctuations contain information such as the average deviation from the mean, amplitude and frequencies. The amplitude is linearly reciprocal to the concentration of the fluorophore, while

the frequency contains information about the diffusion rates of the fluorophore. Fast diffusing particles give rise to faster signal fluctuations while slower or bigger particles have slower fluctuations. This information can be more easily extracted by obtaining the autocorrelation function $G(\tau)$ of the fluorescence fluctuations. To obtain the autocorrelation function, the product of two channels separated by a certain lag time, τ, is normalized by the square of the average intensity and is plotted against the logarithm of the increasing lag time.

$$G(\tau) = \frac{\langle F(t) \cdot F\,(t+\tau)\rangle}{\langle F\rangle^2} - 1 = \frac{\langle \delta F(t) \cdot \delta F(t+\tau)\rangle}{\langle F\rangle^2} \qquad (9)$$

For three-dimensional diffusion, using complex mathematics that are described elsewhere (Lakowicz 2006, Weidemann and Schwille 2009), the autocorrelation function can be written as

$$G\,(\tau) = {N_{eff}}^{-1}\left(1 + \frac{\tau}{\tau_D}\right)^{-1}\left(1 + \frac{\tau}{S^2\tau_D}\right)^{-1/2} \qquad (10)$$

where N_{eff} is the effective number of molecules in the confocal volume, τ_D is the diffusion time, which is the fluorophore's time of transit in the focus and S is the structural parameter which describes the shape of the detection volume (i.e the ratio of the axial and lateral radii, $S = \frac{z_o}{\omega_o}$). The fluorescence autocorrelation curve from equation (9) is fitted to (10) to obtain τ_D which is related to diffusion coefficient, D.

$$\tau_D = \frac{{\omega_o}^2}{4D}$$

Although FCS can be used to study any process that results in intensity fluctuations, we used FCS mainly to study diffusion on the membrane. In this case, the autocorrelation function is fitted to a modified version of (10), which assigns a fixed high value for the structural parameter

S, which is a pseudo- two dimensional diffusion, correcting the three-dimensional diffusion into a two-dimensional diffusion.

Aside from obtaining diffusion coefficients, FCS can also measure binding kinetics, rotational diffusion and macromolecule dynamics. While FRAP can measure processes on the seconds time scale while FCS is sensitive to events occurring from tens of nanoseconds to millisecond making both methods complementary.

RESEARCH AIMS INCLUDED IN THIS DISSERTATION

Do B_2R and μOR and their Gα binding partners localize to caveolae domains? This question is addressed by measuring the colocalization and distance between Cav1 and a fluorescently labeled protein by using immunofluorescence and FRET respectively. More importantly, are the functions of these GPCR pathways modified in the presence of caveolae domains? To answer this question, assays utilizing the Cav-1 deficient FRTwt cell and a sister cell line stably transfected with Cav1, FRTcav+, were used to assess the effect of Cav1 on the function of these receptors. These topics are discussed in Chapter 2. Does the presence of caveolae change the mobilities of B_2R, μOR and their downstream Gα binding partners? This question is addressed in Chapter 3. Does cell shape have an effect on the cell surface distribution of different membrane proteins? This question is addressed in Chapter 4. The future directions and general discussion of this dissertation is in Chapter 5.

CHAPTER II – INFLUENCE OF G-PROTEINS IN G-PROTEIN COUPLED RECEPTOR-CAVEOLAE LOCALIZATION

ABSTRACT

Caveolae are membrane domains that may influence cell signaling by sequestering specific proteins such as G-protein-coupled receptors (GPCRs). While previous reports largely show that $G\alpha_q$ subunits, but not other G-proteins, interact strongly with the caveolae protein, Caveolin-1 (Cav1), the inclusion of GPCRs in caveolae is controversial. Here, we have used fluorescence methods to determine the effect of caveolae on the physical and functional properties of two GPCRs that have been reported to reside in caveolae, bradykinin receptor type 2 (B_2R), which is coupled to $G\alpha_q$, and the μ-opioid receptor (μOR), which is coupled to $G\alpha_i$. While caveolae do not affect cAMP signals mediated by μOR, they prolong Ca^{2+} signals mediated by B_2R. In A10 cells that endogenously express B_2R and Cav1, downregulation of Cav1 ablates the prolonged recovery seen upon bradykinin stimulation in accord with the idea that the presence of caveolae prolongs $G\alpha_q$ activation. Immunofluorescence and Förster resonance energy transfer (FRET) studies show that a significant fraction of B_2R resides at or close to caveolae domains while none or very little μOR resides in caveolae domains. The level of FRET between B_2R and caveolae is reduced by downregulation of $G\alpha_q$ or by addition of a peptide that interferes with $G\alpha_q$-Caveolin-1 interactions, suggesting that $G\alpha_q$ promotes localization of B_2R to caveolae domains. Our results lead to the suggestion that $G\alpha_q$ can localize its associated receptors to caveolae domains to enhance their signals.

---

*Reprinted with permission from Biochemistry Vol 51 (47), R.C. Calizo and S. F. Scarlata, "A role for G-proteins in directing G-protein-coupled receptor-caveolae localization", pp. 9513-9523. Copyright 2012 American Chemical Society.

INTRODUCTION

Caveolae are 50-100 nm membrane domains that were discovered in electron micrographs more than 50 years ago (Anderson 1998). Many proteins that reside in caveolae domains are signaling proteins which has led to the speculation that caveolae may be involved in the formation of signaling domains in the membrane (Anderson 1993, Lisanti, Scherer et al. 1994). Membrane domains may sequester signaling proteins from a distinct pathway and facilitate rapid and efficient signaling. However, despite numerous studies suggesting the enrichment of various signaling proteins in caveolae domains, there is still no consensus which signaling proteins are sequestered in caveolae domains. Limitations of the various methods used may be the reason for contradictory results. Immunofluorescence methods may not have sufficient spatial resolution that is compatible with the size of caveolae domains and fractionation studies require cell membrane disruption which would also disrupt the weak interactions of signaling proteins within the membrane domains.

An important class of signaling proteins that target caveolae are G-protein coupled Receptors (GPCRs) (Chini and Parenti 2004, Insel, Head et al. 2005). GPCR signaling occurs through a series of molecular interactions that begin with the binding of an extracellular agonist which cause a conformational change on the GPCR so the signal is transmitted to downstream effectors in the cytoplasm through the activation of heterotrimeric G-proteins (Alberts, Bray et al. 1994). A variety of GPCRs and G-protein subunits have been reported to be in caveolae domains (Schnitzer, Oh et al. 1995, Oh and Schnitzer 2001, Insel, Head et al. 2005). There is recent evidence that components of G-protein coupled receptor signaling reside in pre-formed

complexes and that Cav1 may alter their interactions by binding to some of the signaling components (Dowal, Provitera et al. 2006, Philip, Sengupta et al. 2007). Caveolae may play a significant role in GPCR signaling by altering the receptor association with agonists, G-proteins and with other GPCRs by homo and hetero-oligomerization. Previous studies have suggested that $G\alpha_q$ subunits reside in caveolae domains whereas $G\alpha_o$, $G\alpha_i$, and $G\beta\gamma$ subunits prefer non-caveolae domains (Oh and Schnitzer 2001). Our laboratory has shown that $G\alpha_q$ and $G\beta\gamma$ localize in caveolae domains in the basal state (Sengupta, Philip et al. 2008). Activation of $G\alpha_q$ causes a conformational change that causes it to strengthen its interaction with Cav1, promoting the release of $G\beta\gamma$ from caveolae domains and extending the time of $G\alpha_q$ activation (Sengupta, Philip et al. 2008, Guo, Golebiewska et al. 2011). This stabilization of activated $G\alpha_q$ results in a prolonged calcium response which is believed to be a combination of the stabilization of the activated state of $G\alpha_q$ and the extended time for $G\beta\gamma$ recombination. This effect of prolongation of recombination time is not seen in other $G\alpha$ families.

In this dissertation chapter, we determined whether the presence of caveolae can alter the function and membrane properties of two class A GPCRs, the μ-opioid receptor (μOR), which is coupled to $G\alpha_i$ and the bradykinin type 2 receptor (B_2R), which is coupled to $G\alpha_q$. Both receptors have been reported to localize in caveolae. We study these receptors in Fisher rat thyroid (FRTwt) cells, which do not express any Cav1 and do not exhibit any caveolae domains, and a sister cell line which is stably transfected with canine Cav1 (FRTcav+) and displays caveolae domains (Lipardi, Mora et al. 1998, Mora, Bonilha et al. 1999). Additionally, FRT cells do not have endogenous μOR or B_2R, the contribution of which could complicate analyses of FRET measurements and functional assays.

μOR is a target of opiates and other analgesics. μOR activates $G\alpha_i$, which inhibits adenylyl cyclase resulting in a decrease of cellular cAMP (Law, Wong et al. 2000). Using co-immunoprecipitation methods, μOR has been shown to localize to caveolin-related lipid rafts (Zhao, Loh et al. 2006, Berg, Zardeneta et al. 2007), and has been shown to localize in Cav3 microdomains in adult cardiomyocytes (Head, Patel et al. 2005). B_2R is a key mediator of the inflammation response. B_2R signals through $G\alpha_q$, which activates PLCβ and resulting in an increase in the intracellular calcium levels and activation of protein kinase C (PKC). B_2R is constitutively expressed in a wide variety of cells, while B_1R expression is limited (Faussner, Bathon et al. 1999). Previously, we have found that in the presence of Cav1, activation of $G\alpha_q$ by muscarinic receptors results in a prolonged calcium response as a result of a sustained activated $G\alpha_q$ signaling (Philip, Sengupta et al. 2007). Thus, caveolae may promote inflammatory responses through a sustained and synergistic B_2R signaling.

Here, we have used fluorescence methods to study the influence of caveolae domains on the function and membrane properties of the μOR and B_2R signaling pathways. The use of fluorescence methods allows us measure receptor localization and dynamics in live cells in real time, eliminating problems associated with cell disruption. We find that the function and localization of μOR are largely unaffected by the presence of caveolae. Alternately, B_2R-$G\alpha_q$ signaling is affected by the presence of caveolae domains. Our FRET studies suggest that receptors do not directly localize to caveolae but require $G\alpha_q$ to scaffold them to caveolae domains.

MATERIALS AND METHODS

FRTwt and FRTcav+ cells and canine caveolin-eGFP DNA were gifts from Dr. Deborah Brown (Stony Brook University). μOR-eYFP, μOR-eCFP and $G\alpha_i$-eYFP wer e from Dr. Lakshmi Devi (Mount Sinai Medical Center, New York, NY). $G\alpha_q$-eGFP and $G\alpha_q$-eYFP were from Catherine Berlot (Geisinger Research). B_2R and B_2R-GFP were from F. Leeb-Lundberg (University of Texas Health Science Center). The plasmid of eCFP and eYFP linked by a 12-amino acid peptide chain as a positive control for FRET experiments was from J. Pessin (Albert Einstein College of Medicine, Bronx, NY). mCherry-Cav1, eYFP-Cav1 and eCFP-Cav1 were constructed from canine Cav1-eGFP by excising it as a XhoI and BamHI fragment and subcloning it into the same sites in pmcherry-C1, pEFYP-C1 and pECFP-C1 (Clonthech). Sequencing these plasmids showed an in-frame fusion of mcherry, eYFP or eCFP at the N-terminus of Cav1 and a six-amino acid linker (SGSRAA) between the Cav1 and fluorophore constructs.

Cell Culture.

Fisher Rat Thyroid cells (FRTwt) and a sister cell line stably transfected with canine Cav1 (FRTcav+) have been described previously (Lipardi, Mora et al. 1998, Mora, Bonilha et al. 1999). Fisher rat thyroid cells were grown in F-12 Coon's Modification Media (Sigma) supplemented with 10% FBS and 1% Penicillin/Streptomycin. FRTcav+ cells were grown in the same media supplemented with 0.2 mg/mL G418. Immunofluorescence of Cav1 was routinely performed to check for the expression of Cav1 in FRTcav+ cells. FRTwt and FRTcav+ cells

were transfected by Lipofectamine according to manufacturer's instructions. Briefly 1 x 10^5 cells were incubated in the DNA – Lipofectamine complex (1 µg DNA : 3 µL lipofectamine) in complete antibiotic-free media and assayed 48 hours after transfection. Expression levels of GFP-tagged proteins were compared by measuring the intensities of cells under the same viewing conditions and by western blot using GFP antibody. A10 (rat aortic smooth muscle cells) and HEK 293 were maintained in DMEM (Gibco) supplemented with 10% FBS and 1 % Penicillin/Streptomycin. HEK293 cells were transfected by Fugene according to manufacturer's instructions using a µg DNA: µL Fugene ratio of 1:3. Expression of Cav1 in A10 cells was downregulated by treating cells with siRNA from Dharmacon, Inc. according to the manufacturer's instructions. Briefly, 1 x 10^5 cells were seeded in 6-well plates and transfected with the lipid-siRNA complexes with 25 nM Cav1 siRNA. Cells were grown in complete antibiotic-free media (DMEM supplemented with 10% FBS) and assayed 48-hours post-transfection. The efficiency of downregulation was determined by immunofluorescence using anti-Cav1 antibody bound to Alexa-647 conjugated secondary antibody in which the fluorescence intensities per cell of wild-type A10 cells ($n = 11$; $43 \pm 13\%$) versus the Cav1 knockdown ($n = 17$; $21 \pm 7\%$) cells imaged under the same conditions were obtained and compared. These measurements showed Cav1 knockdown efficiency of approximately 51%. Western blot analyses were also performed to compare Cav1 levels.

The levels of expression of Cav1 in FRTcav+ cells and in transfected HEK293 cells were found to be similar to the endogenous level of expression of Cav1 in NIH3T3, A10 and MDA MB-231 cells by Western blotting. Additionally, B_2R expression levels in transfected FRT cells were found to be similar to endogenous levels in NIH3T3 cells and A10 cells. Similar expression levels of cells transiently transfected with B2R and cells endogenously expressing B_2R (NIH3T3

and A10 cells) correlate with the comparable extents of calcium release upon stimulation with bradykinin.

FRET Spectroscopy of Membrane Fractions.

HEK293 cells were separately transfected with either B_2R-eYFP, μOR-eYFP or eCFP-Cav1 using Fugene according to manufacturer's instructions. Forty eight hours post-transfection, approximately 3 x 10^7 cells transiently expressing expressing B_2R-eYFP, μOR-eYFP or eCFP-Cav1 were homogenized in ice-cold lysis buffer [250 mM sucrose, 20 mM HEPES (pH 7.4), 1.5 mM $MgCl_2$, 1 mM EDTA, 1 mM EGTA, protease inhibitor cocktail, 1% Triton-X, 0.5 % NP-40 and 1 mM DTT]. The membrane fractions were collected by centrifugation at 50,000g for 1 hour at 4° C. The concentrations of B_2R-eYFP and eCFP-Cav1 were found to be 0.12 μM and 0.30 μM respectively, by Western blot analysis using GFP antibody as a probe and soluble GFP as the protein standard. Expression and purification of recombinant $G\alpha_q$ and $G\alpha_i$ through baculovirus infections of Sf9 cells have been described previously (Runnels and Scarlata 1999). $G\alpha_q$ and $G\alpha_i$ were activated by incubation in 1 mM GTPγS in 50 mM HEPES, 100 mM NaCl, 4 mM $MgCl_2$, 1 mM DTT, and 50 mM $(NH_4)SO_4$ for 1 hour at 30 °C. B_2R-eYFP (5 nM) and eCFP-Cav1 (10 nM) were titrated and purified $G\alpha_q$ or $G\alpha_i$. FRET measurements between B_2R-eYFP or μOR-eYFP and eCFP-Cav1 were performed by monitoring the increase in the emission of eYFP (560 nm) upon excitation of eCFP (450 nm) and normalized using the intensities of eYFP emission upon eYFP excitation.

Ca^{2+} Measurements.

Intracellular Ca^{2+} levels in cells were measured by loading cells with Fura-2 AM or Calcium Green AM. Cells expressing B_2R-GFP or μOR-eGFP were harvested and incubated with 1 μM Fura-2 AM in Hanks Balanced Salt Solution (HBSS, Gibco) with 1% BSA. Cells (1 x 10^7) were incubated with 1 μM Fura-2 AM for 30 min, pelleted, washed twice with HBSS, and incubated for an additional 15 min for de-esterification of Fura-2 AM. Fluorescence of suspended cells were measured using ISS spectrofluorometer. The ratio of fluorescence emitted at 510 nm upon excitation with 340 nm and 380 nm was converted to Ca^{2+} using the Grynkiewicz equation (Grynkiewicz, Poenie et al. 1985) :

$$[\mathrm{Ca}^{2+}] = K_d \left(\frac{F - F_{min}}{F_{max} - F} \right)$$

For adherent cells, calcium changes were measured using 5 μM Calcium Green, or Calcium Orange if the cells were already expressing a GFP-labeled receptor. Zeiss Confocor II was used using 488 nm Argon ion laser to image calcium green and 543 HeNe laser to image calcium orange. Intensities were acquired every 1 second up to 200 seconds.

Intracellular cAMP Measurements.

μOR-expressing cells were serum-starved and pretreated with 1 mM 3-isobutyl-1-methylxanthine (IBMX) and stimulated with different morphine concentrations in the presence of 10 μM forskolin. Cells were treated with 1% perchloric acid for 1 hour to stop the assay and to lyse the cells. Cyclic AMP from cell lysates were measured from the supernatant using a [^{3}H]

cAMP assay kit (GE Healthcare) following the manufacturer's instructions. Inhibition of cAMP by morphine is expressed as the percent forskolin activation in the absence of agonist.

Immunofluorescence Studies.

FRTcav+ cells transfected with μOR-eGFP or B_2R-eYFP were seeded onto glass bottom dishes (MatTek Corp.). Forty-eight hours post-transfection, cells were washed and fixed with 4% paraformaldehyde for 1 h and permeabilized with 0.2% NP-40. Cells were incubated with rabbit polyclonal anti-Cav1 antibody (N20) (Santa Cruz Biotechnology) and then incubated with AlexaFluor secondary antibodies. Fixed cells were imaged with an Olympus Fluoview laser scanning microscope equipped with a 488 nm argon ion laser for excitation of eGFP, a 543 nm HeNe laser for Alexa594, and a 633 nm HeNe laser for Alexa 647. Z-stack of Cav1 or GFP tagged receptors were performed by taking 1 μm confocal slices of the cells. No significant bleedthrough was observed from the eGFP or eYFP channel to the Alexa647 channel. Colocalization and z-stack analyses were performed using the MacBiophotonics version of ImageJ.

FRET Imaging.

Sensitized emission of FRET was performed with an Olympus Fluoview1000 instrument on HEK293 cells co-expressing eCFP- or eYFP-tagged proteins. eCFP and eYFP were excited using 458 and 515 nm argon ion laser lines, respectively, and 480-495 and 535-565 nm bandpass filters to collect emission images, respectively. The FRET efficiency was calculated by the

method used by Chen and co-workers (Chen, Elangovan et al. 2005). Using this algorithm, FRET images are corrected for spectral bleedthrough by analyzing images of control cells expressing donor proteins alone or acceptor proteins alone with the same intensity distributions as the sample. Using controls with the same intensity distributions as the samples, we found that FRET efficiency values did not change significantly over a 10-fold range of acceptor:donor intensity ratios (e.g., Figure II-5). Background FRET values were obtained by imaging cells co-expressing eCFP and eYFP. Positive control values were obtained using a dodecapeptide labeled with eCFP and eYFP on both ends (i.e, eCFP-X_{12}-eYFP).

Microinjection of HEK293 cells.

Microinjections were performed on an Axiovert 200M (Zeiss) using InjectMan NI2 with a Femtojet pump (Eppendorf). Samples were microinjected into the cytoplasm with a typical injection pressure of P_i = 30 hPa, compensation pressure (P_c) of 15 hPa and injection time (t) of 0.5 s. DAPI dye (0.5 µM) was added to the peptide solution to facilitate viewing of microinjected cells. FRET microscopy was immediately performed on microinjected cells that had comparable expression levels of B_2R-eYFP and eCFP-Cav1. Cells that exhibited drastic change in morphology or compartmentalization dyes in vesicles were not included in the analysis.

RESULTS

Distribution of Caveolae Domains in Cells.

Before characterizing the effect of caveolae on the signaling of B_2R and μOR in Fisher rat thyroid cell lines, we determined the cellular distribution of Cav1 in FRTcav+ cells by immunofluorescence (Figure II-1a). FRT cells are derived from FRT-L cells which are polarized epithelial cells exhibiting basolateral and apical membranes. Since Fisher rat thyroid cells are not maintained under conditions that would cause differentiation in the basal and apical membranes, it is possible that FRT cells have lost their polarity, therefore we only call the top and bottom membranes instead of apical and basolateral membranes respectively. We find that Cav1 is mainly localized to the bottom membrane closest to the substrate and is sporadically distributed on the top membrane. This is in agreement with the work of Mora and others, who found that more than ~99% of Cav1 in FRTcav+ cells preferentially go to the bottom membrane (Mora, Bonilha et al. 1999). Several studies have suggested that Cav1 may be one of the many protein players in focal adhesions and also has been shown to interact with integrins (Salanueva, Cerezo et al. 2007). Additionally, Cav1 is localized in regions of cell-cell contact. The observation that Cav1 is concentrated in cell contact regions correlates well with the observation that they may organize proteins involved in intercellular signaling, such as connexins (Schubert, Schubert et al. 2002, Langlois, Cowan et al. 2008).

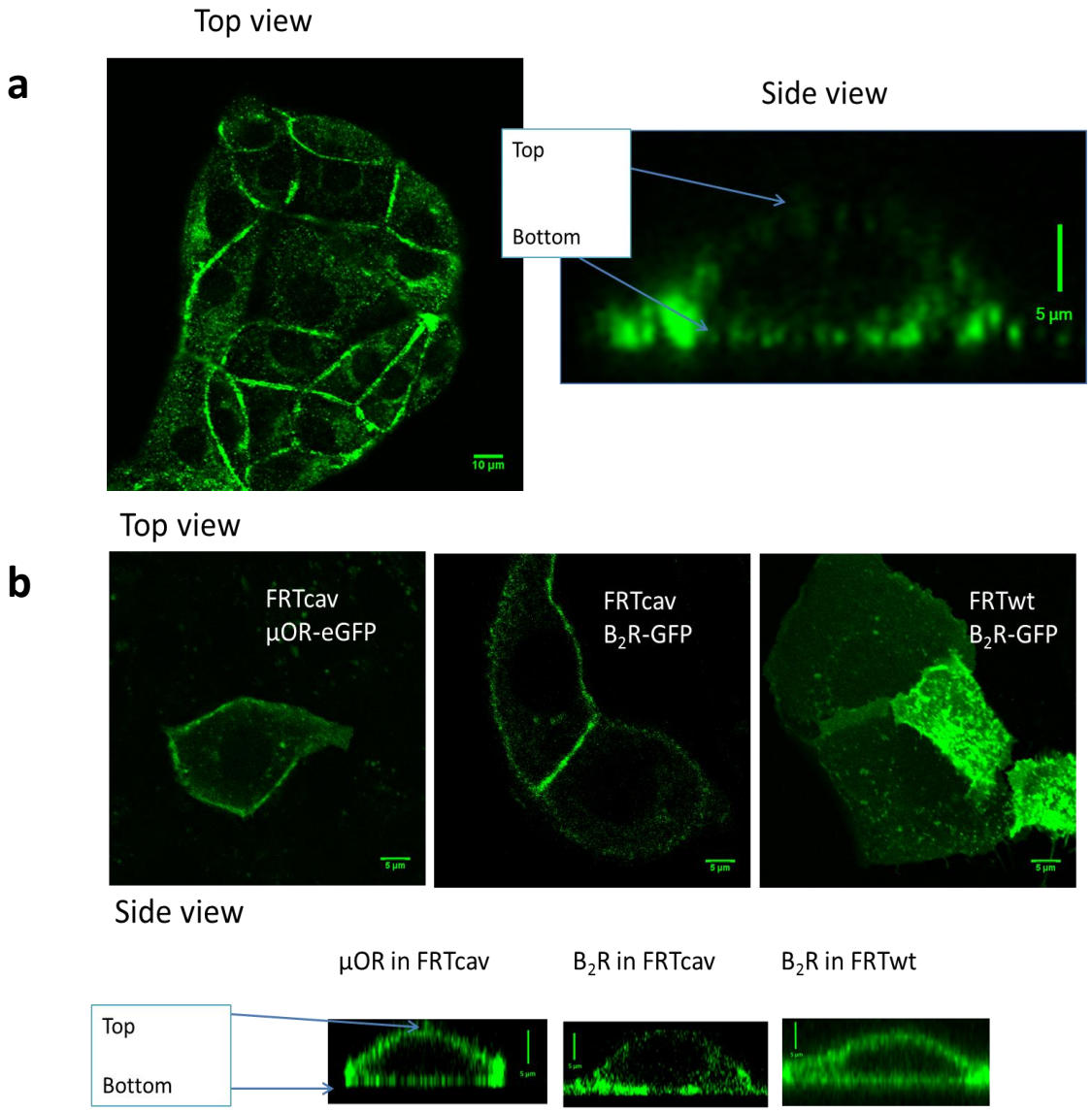

Figure II-1. **a** - Immunofluorescence image of FRTcav+ cells showing the distribution of Cav1 as viewed from the top of the cells. The right figure is a side view of a cells showing that Cav1 is mainly distributed on the bottom plasma membrane. **b** - Distribution of Cav1, µOR and B_2R in FRT cells. µOR-eGFP in FRTcav+ cells shows a uniform distribution on the top and bottom membranes while the majority of B_2R-GFP localizes to bottom membrane of FRTcav+ similar to Cav1 distribution. This preferential localization of B_2R to the bottom membrane is not seen when it is expressed in FRTwt cells.

We wanted to determine whether the presence of caveolae impacts the plasma membrane distribution of B_2R and μOR. We looked at the z distribution of B_2R-GFP and μOR-eGFP in FRTwt and FRTcav+ cells to see whether they would have a distribution similar to that of Cav1. We found that μOR has a uniform plasma membrane distribution on both the bottom and top membrane (Figure 1b). Alternatively, B_2R largely resides on the bottom membrane, paralleling the distribution of Cav1 in contrast to μOR. To verify whether the distribution of B_2R is caused by the presence of Cav1, we checked the z distribution of B_2R in FRTwt cells, which do not have caveolae. In FRTwt cells, B_2R did not exhibit a preferential localization on the bottom membrane. These observations suggest that Cav1 is responsible for B_2R localization at the bottom of the membrane.

Caveolae Affect Signals from B_2R but not from μOR.

We determined whether the presence of caveolae affect the secondary messengers in the signaling of B_2R and μOR. Stimulation of μOR by morphine activates $G\alpha_i$, which inhibits adenylyl cyclase, resulting in a decrease of cellular cAMP. We measured the decrease in cAMP

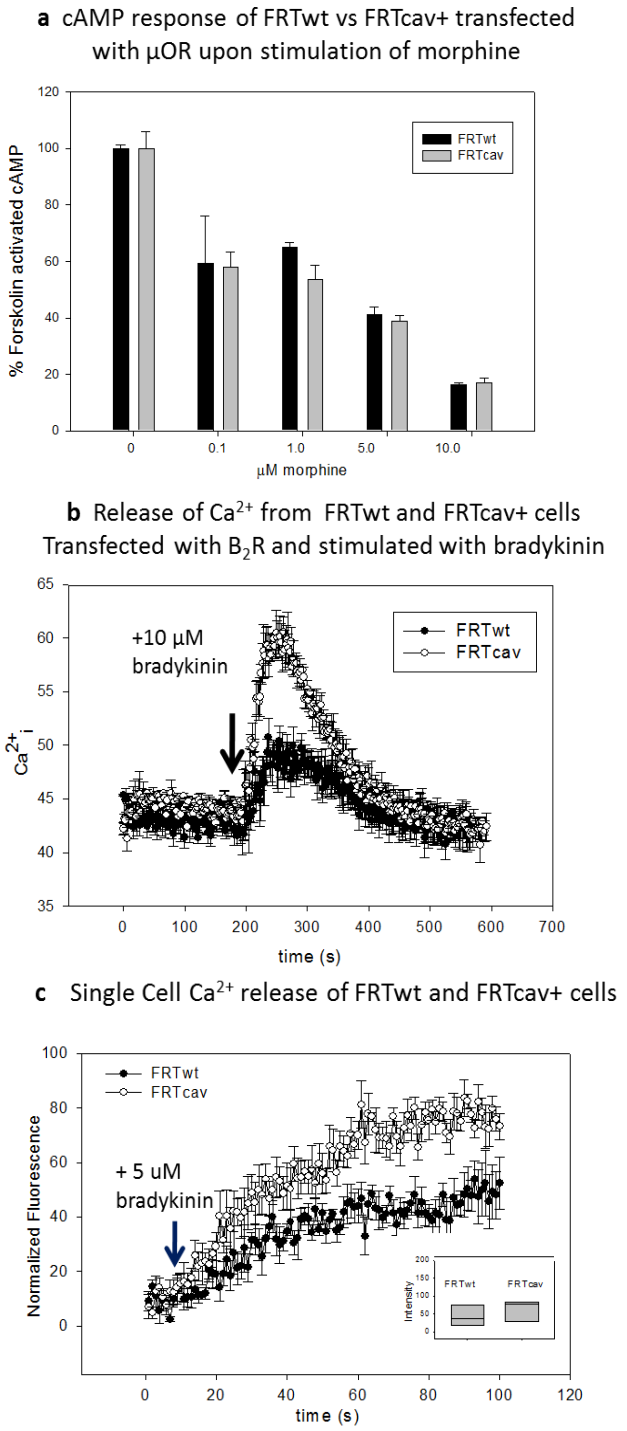

Figure II-2. Functional studies of suspensions of FRTwt and FRTcav+ cells transfected with µOR, at identical µOR expression levels, showing the differences in cAMP levels stimulated at four different morphine concentrations (*see methods*) where n=3 independent experiments. Mean±SEM is shown. **b** – Determination of intracellular Ca^{2+} release (in nM) in cell suspensions upon the addition of 10 µM bradykinin, as measured using Fura-2, of FRTwt and FRTcav+ transfected with B_2R where the expression levels of the receptor were similar in both cell types as determined by western blot analysis, where n=3 independent experiments. Mean±SEM is shown. **c** - Single cell measurements of Ca^{2+} release from FRTwt cells transfected with B_2R-GFP and stimulated with 5 µM bradykinin where the curves are an average of responses of 8 cells and S.D. is shown. Signal was normalized to each cells' response to A23187, which gives maximal intracellular Ca^{2+} *Inset* - The level of B_2R-GFP intensity (y-axis) in arbitrary units of the measured cells.

in FRTwt and FRTcav+ cells transfected with μOR using a standard radiometric method which measures the binding competition between tritiated cAMP and cellular cAMP on a cAMP binding protein. We verified that the receptor is expressed at similar levels in both cell types by visualizing the fluorescently tagged receptors before proceeding with the assay. The results of these studies (Figure II-2a) demonstrate that caveolae do not affect the cAMP response generated through μOR and $G\alpha_i$. For these cell types, stimulation of μOR and $G\alpha_i$ did not increase the level of intracellular Ca^{2+} even at saturating morphine concentrations (0.1 – 50 μM).

We have previously found that the affinity between Cav1 and $G\alpha_q$ is strengthened when $G\alpha_q$ is activated through muscarinic receptors, resulting in a prolonged Ca^{2+} signal (Sengupta, Philip et al. 2008). Here, we tested whether a similar increase in the level of calcium is seen for B_2R-mediated $G\alpha_q$ activation. To this end, we measured the change in Ca^{2+} levels with bradykinin stimulation in FRTwt and FRTcav+ cells expressing B_2R. Again, similar B_2R expression levels in the two cell lines were verified by fluorescence imaging of the tagged receptor (see inset in Figure II-2c). In addition we find that the presence of caveolae significantly increases the amount of Ca^{2+} released upon the addition of bradykinin in both calcium assays for cells in suspension (Figure II-2b) (t-test; $p = 0.007$) and single-cell calcium measurements (Figure II-2c) (Mann-Whitney test; $p = 0.008$). In addition to the increase in the intensity and concentration of intracellular Ca^{2+} in the presence of Cav1, the duration of increased Ca^{2+} levels were prolonged ~2.5 fold.

Caveolae Affect B_2R-Mediated Ca^{2+} signaling in A10 cells.

To support the idea that B_2R signaling can be affected by the presence of caveolae in cells that endogenously express both Cav1 and B_2R, we carried out studies using rat aortic

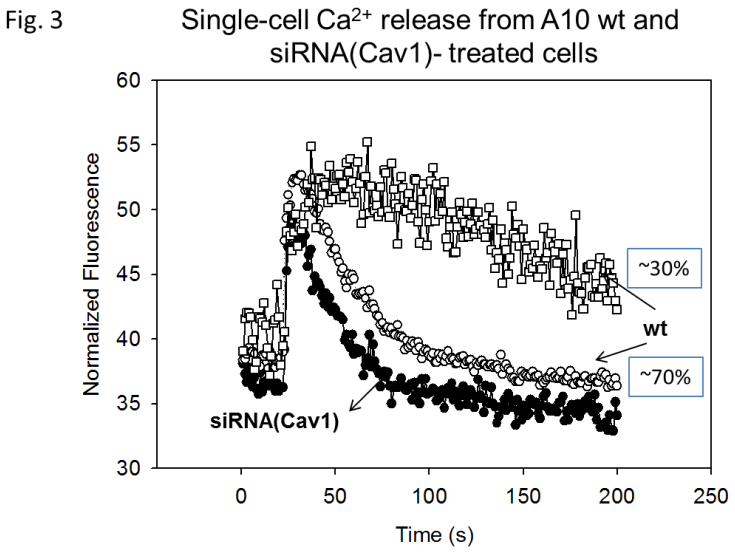

Figure II-3. Single cell measurements of Ca^{2+}, as determined by Calcium green (*see methods*) for wild type A10 cells and cells treated with siRNA(Cav1), and treated with 10 μM bradykinin. Signal was normalized to each cells' response to A23187, which gives maximal intracellular Ca^{2+}. Two wild type traces are shown in open symbols: (○) is for an average of 8 traces for the cell population (~70%) that displayed short recovery while (□) is for a sample trace of cells in the 30% population that showed prolonged recovery (~30%). (●) is for an average of 7 traces for cells that have been treated with siRNA(Cav1). SEM, which is not shown for clarity, ranged between 0.6 – 2.5% from the beginning to the recovery period for both (○) and (●), and 2.4 – 5.7% for the recovery. Error for the prolonged Ca^{2+} signal was high in the recovery period but always at least 40% higher than the short duration cells.

smooth muscle cells (A10). In these studies, we compared intracellular Ca^{2+} release in wild type cells and cells where expression of Cav1 was downregulated by ~50% [as estimated by immunofluorescence and Western blotting] through treatment with Cav1 siRNA. In wild-type cells, we find that at least one-third of the cells showed a prolonged Ca^{2+} signal (i.e. > 200 s) upon bradykinin stimulation. In the case of Cav1 knockdown cells, none of the ~50 siRNA (Cav1) treated cells showed this prolonged Ca^{2+} recovery. In Figure II-3, we show data extracted for several cells, although many more were viewed.

Colocalization of B_2R and μOR with Cav1.

The preferential distribution of B_2R on the bottom membrane, where Cav1 is also localized (Figure II-1b) and strengthened Ca^{2+} signals generated with B_2R-$G\alpha_q$ activation (Figure II-2b, c) in FRTcav+ cells suggest that B_2R, but not μOR interacts with caveolae domains. As a first step in determining whether this is the case, we measured the amount of colocalization between the receptors and Cav1, using anti-Cav1 antibody and fluorescent protein tagged receptors. These results, summarized in Figure II-4, show a significant colocalization between B_2R-eYFP and Cav1 labeled with anti-Cav1 and Alexa 647 labeled secondary antibody as seen on the lateral membrane (0.76 ± 0.01; n = 7) compared to a positive control consisting of Cav1-eGFP labeled with anti-Cav1 labeled with Alexa647 in FRTwt cells (0.93 ± 0.01; n = 9) and a negative control consisting of Cav1-eGFP stained with Alexa 647 secondary antibody alone (0.17 ± 0.02; n = 7). In contrast, a smaller amount of colocalization is seen between μOR-eGFP and Cav1 (0.51 ± 0.01; n = 9).

a

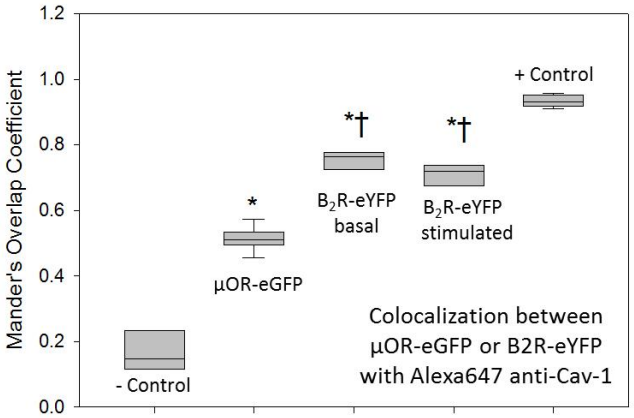

b

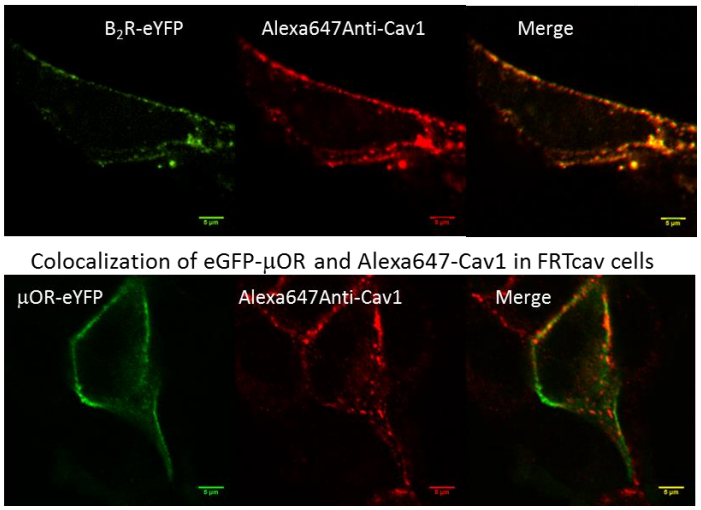

Figure II-4. Summary of colocalization of Cav1 with μOR and B_2R as compared to negative and positive controls, where n=7 for negative control (Cav1-eGFP and secondary Antibody (Alexa 647) alone), n=9 for μOR-eGFP, n=7 for B_2R-eYFP unstimulated, n=6 for B_2R-eYFP stimulated with 1 μM bradykinin for 5 minutes, and n=9 for positive control (Cav1-eGFP and Cav-1 Antibody labeled with Alexa647 conjugated secondary antibody). Asterisk indicates significant difference from negative control while cross indicates significant difference from μOR-eGFP/Cav-1 Colocalization Values (ANOVA $p < 0.001$). **b** – Sample images of some of the cells that were used in the data presented in **3a**.

A

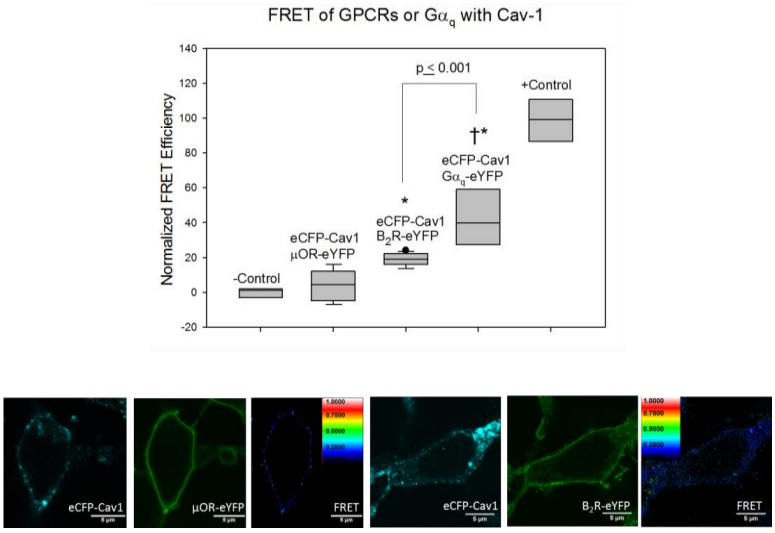

B

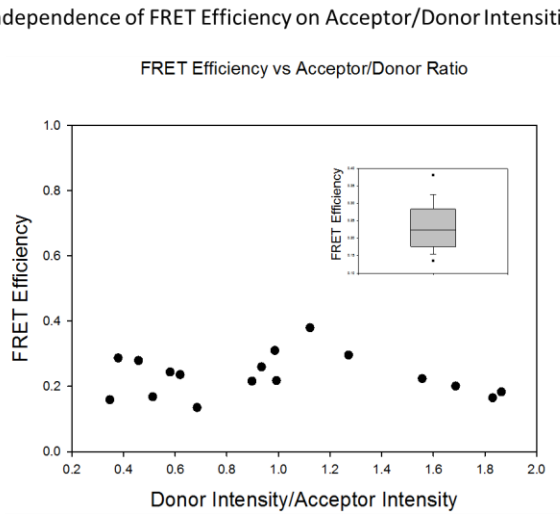

Figure II-5. A. Normalized FRET efficiencies (see methods) of eCFP-Cav-1/μOR-eYFP (n=9), eCFP-Cav-1/B_2R-eYFP (n=15), eCFP-Cav1/$G\alpha_q$-eYFP (n=7). Normalization was performed using free eCFP and eYFP which showed low FRET efficiency (- Control, n=10) and a dodecapeptide with an eYFP and eCFP on either ends which showed high FRET efficiency (+ Control, n=8). Asterisk indicates significant difference from negative control while cross indicates significant difference from eCFP-Cav1/B_2R-eYFP values (ANOVA $p<0.001$). (*bottom*) Sample raw images of a cell expressing eCFP-Cav1, μOR-eYFP acceptors and raw FRET (*left*) and a cell expressing eCFP-Cav1, B_2R-eYFP and raw FRET (*right*). We note that previous studies of eCFP-Cav-1 and -$G\alpha_i$-eYFP expressed in FRTwt cells gave a FRET efficiency of 4 $\pm$ 6% (n=3). **b** – Plot showing that the FRET efficiency between B_2R-eYFP and eCFP-Cav1 (Box plot, Inset) does not change significantly over a 10-fold range of donor /acceptor intensity ratios with the FRET algorithm used.

B_2R and μOR Interact Differently with Cav1 as determined by Forster Resonance Energy Transfer.

Concerns with colocalization measurements are the low spatial resolution and the dependence on the strength and specificity of the antibodies, as well as the exposure of the epitope which may be a problem with integral membrane proteins. To gain more sensitive localization information, we used FRET. Cav1 was tagged with an enhanced cyan fluorescent protein (eCFP) on its N-terminus, and B_2R and μOR were tagged with an enhanced yellow fluorescent protein (eYFP) tag on their C-termini. HEK293 cells were chosen for their high transfection efficiency and the exclusive plasma membrane distribution of the receptors and G-proteins. Cells expressing eCFP-Cav1 and B_2R-eYFP at similar levels were selected. The increase in eYFP emission in the presence of eCFP was then measured using the method of Chen and others (Chen, Elangovan et al. 2005). For the eCFP/eYFP pair, the distance at which 50% donor fluorescence is lost to transfer is 30 Å, and on the basis of the estimated size of the proteins, the presence of FRET should indicate physical association. FRET values for each sample were compared to a positive control consisting of free eCFP and eYFP expressed in the same cells. Additionally, we verified that a high level of FRET occurs between Cav1-eGFP and mCherry-Cav1, showing that the tagged Cav1 proteins can still oligomerize and form caveolae domains (Normalized FRET Efficiency = 24.4 $\pm$ 3.0 , n = *4*). FRET results are shown in Figure II-5.

Despite previous data suggesting that μOR localizes in caveolae domains, we could not detect significant FRET between Cav1 and μOR. In contrast, B_2R and Cav1 display a weak but significant and reproducible FRET, suggesting that a population of receptor localizes to these domains.

A

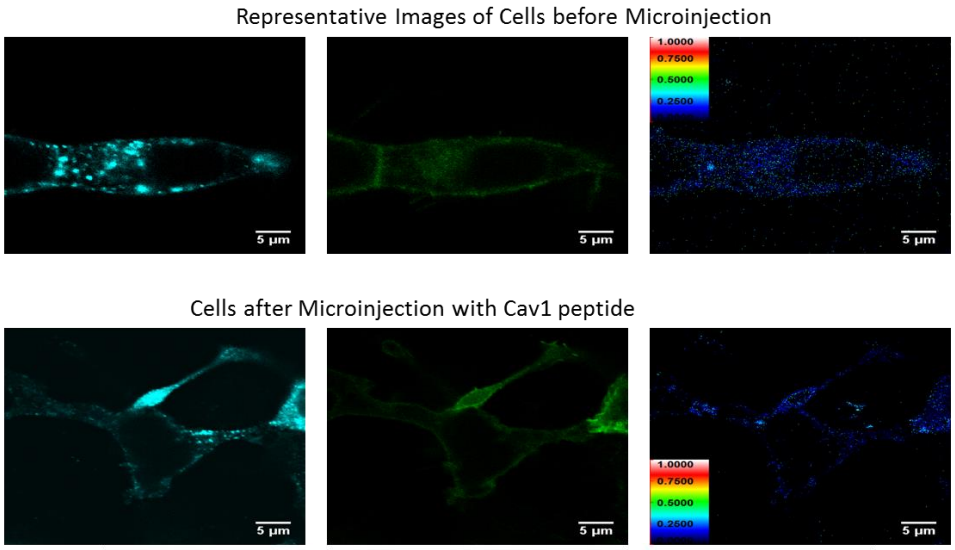

B

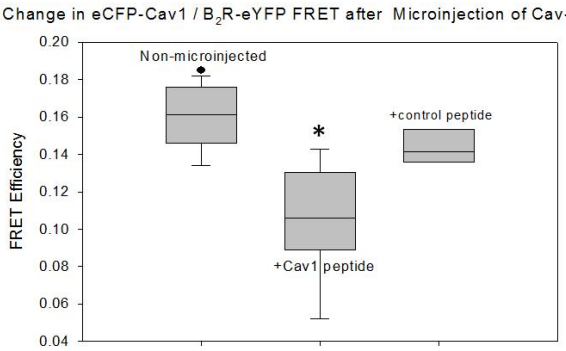

Figure II-6. A - Raw images showing the change in FRET between eCFP-Cav1 and B_2R-eYFP before and after injection with 200 nM solution of a peptide that disrupts $G\alpha_q$ - Cav1 association (Cav1 peptide). We note that the injected cell presented was one that gave a FRET value in the upper range for display purposes. **B -** A summary of the change in eCFP-Cav1 /B_2R-eYFP FRET in cells that were not injected (n=15), cells injected with the Cav1 peptide (n=9) or a control peptide (n=8). ANOVA calculations show significant differences ($p<0.001$) between uninjected and Cav1 peptide samples, and between Cav1 peptide and control peptide data.

The value of $G\alpha_q$-Cav1 FRET is two-fold higher than the value of B_2R-Cav1 FRET (Figure II-5). These results might suggest that $G\alpha_q$ has a higher degree of caveolae association or interaction with Cav1 than B_2R. The higher level of FRET between $G\alpha_q$ and Cav1 than between B_2R and Cav1 is unexpected because a relatively high level of normalized FRET for B_2R-eYFP and $G\alpha_q$-eCFP was observed (i.e. 24.7 $\pm$ 1.8 for FRTwt and 29.1 $\pm$ 3.3 for FRTcav+). Moreover, we found that in the basal, unstimulated state in HEK293 cells, B_2R forms a complex with $G\alpha_q$ and $G\beta\gamma$. Nevertheless, the presence of FRET suggests close association and localization among B_2R, $G\alpha_q$ and Cav1.

Role of $G\alpha_q$ -Cav1 Interactions in B_2R-Cav1 Interactions.

The FRET studies suggest that $G\alpha_q$-Cav1 interactions are stronger than B_2R-Cav1 interactions. $G\alpha_q$-Cav1 interactions may be promoting B_2R-Cav1 interactions. If this is the case, then disrupting the interactions of Gαq-Cav1 would lessen or eliminate B_2R-Cav1 interactions. Thus, we measured the amount of FRET between B_2R-eYFP and eCFP-Cav1 in the presence and absence of a microinjected caveolin peptide (DGIWKASFTTFTVTKYWFYRC)), which interferes with the association between purified Gαq and partially purified membrane fractions containing overexpressed Cav1 (Sengupta, Philip et al. 2008). This peptide, but not a control peptide, with the same length and charge also disrupts $G\alpha_q$-Cav3 colocalization in cultured cells and cardiomyocytes, although there is a possibility that the peptide might disrupt other caveolin interactions (Guo, Golebiewska et al. 2011).

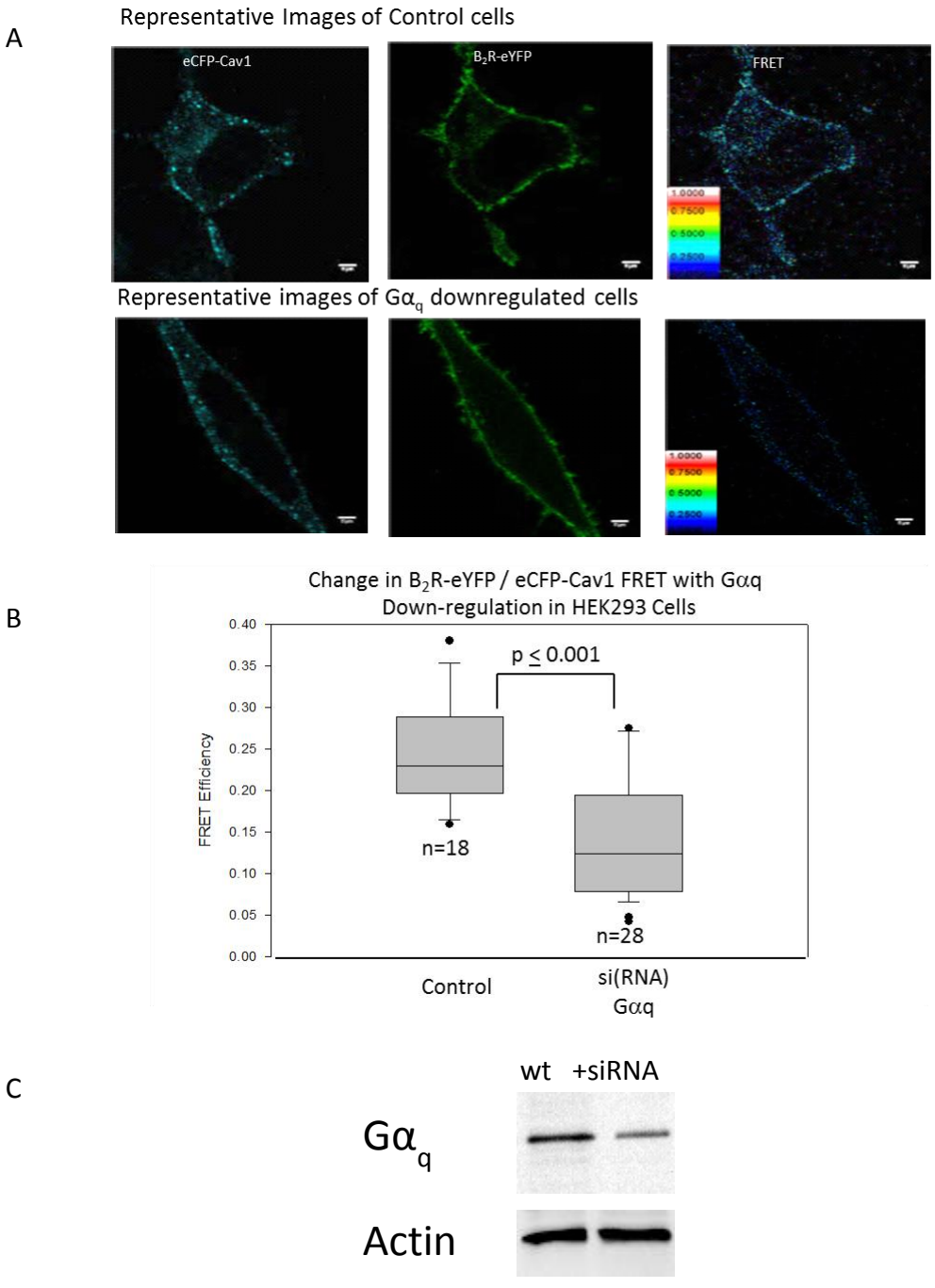

Figure II-7. A - Raw images showing the change in FRET between eCFP-Cav1 and B_2R-eYFP in control cells and in cells where $G\alpha_q$ was down-regulated using siRNA **B** - A summary of the change in eCFP-Cav1 /B_2R-eYFP FRET in control cells (n=18), and cells transfected with Cav1 siRNA (n=28). T-test calculations show significant differences ($p<0.001$) between control and $G\alpha_q$ transfected cells. **C** – $G\alpha_q$ and actin blots showing the siRNA mediated downregulation of $G\alpha_q$ by ~39 $\pm$ 11% compared to wildtype.

HEK293 cells expressing B_2R-eYFP and eCFP-Cav1 at similar levels were microinjected with 200 nM peptide, and changes in B_2R-Cav1 FRET were determined (e.g. Figure II-6a). By comparing the amount of FRET from microinjected versus uninjected cells to that in cells injected with 200 nM control peptide, we found that the cells injected with caveolin peptide had significantly lower FRET values (Figure 6b). We compared the amount of FRET from microinjected cells with un-injected cells as well as cells injected with 200 nM control peptide, which has the same charge and length as Cav1 peptide. We found that cells injected with Cav1 peptide had significantly lower FRET values (Figure 6b). The FRET values between B_2R-eYFP and eCFP-Cav1 in microinjected cells were similar to negative control cells, suggesting that the amount of Cav1 peptide microinjected is enough to disrupt the entire population of B_2R-eYFP associated with Cav1. This study suggests that the population of B_2R-eYFP that participates in the energy transfer from eCFP-Cav1 is mediated by interactions between $G\alpha_q$ and Cav1.

We further tested whether $G\alpha_q$ mediates the interaction between B_2R and Cav1 by transfecting HEK293 cells with eCFP-Cav1 and B_2R-eYFP and measuring the decrease in the level of FRET by siRNA mediated down-regulation of $G\alpha_q$ (Figure II-7). $G\alpha_q$ was down-regulated by ~39 $\pm$ 11% as estimated by Western blotting. Downregulation of $G\alpha_q$ did not affect the expression levels or cellular localization of eCFP-Cav1 or B_2R-eYFP. Our results show that reducing the level of $G\alpha_q$ decreases FRET between B_2R-eYFP and eCFP-Cav1.

To support the hypothesis that $G\alpha_q$ is directing B_2R-Cav1 interactions, we performed spectroscopic FRET of purified membrane fractions from HEK293 overexpressing either B_2R-eYFP or eCFP-Cav1. We then mixed B_2R-eYFP and eCFP-Cav1 membrane fractions and added $G\alpha_q$ inactive (GDP) or activated, GTP bound $G\alpha_q$ (GTP). The increase in FRET between B_2R-eYFP and eCFP-Cav1 indicates that $G\alpha_q$ promotes association between B_2R and Cav1.

Addition of 30 nM activated $G\alpha_q$ in the absence or presence of a control peptide resulted in an increase in the FRET. This increase is indicative of B_2R-Cav1 association (Figure II-8). This increase in FRET was reduced in the presence of caveolin-1 peptide or deactivated $G\alpha_q$(GDP). Addition of activated or deactivated $G\alpha_i$ had no measurable effect on the level of FRET. These results show that $G\alpha_q$ promotes association between B_2R and Cav1 and that the affinity between Cav1 and $G\alpha_q$(GDP) is not sufficiently high to displace endogenous proteins from Cav1.

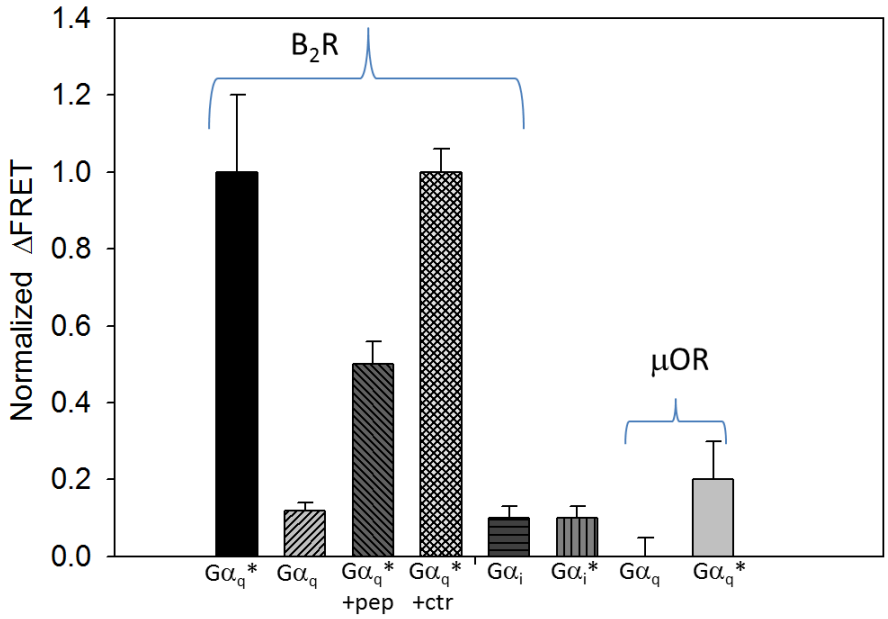

Figure II-8. FRET between B_2R-eYFP and eCFP-cav1in HEK293 membrane fractions mixed with activated (30 nM) ($G\alpha_q$ * or $G\alpha_i$ *) or inactivated $G\alpha_q$ or $G\alpha_i$ (30 nM) in the absence and presence of Cav1 peptide (+pep), 200 nM or a control peptide (+ctr), 200 nM. FRET efficiencies were calculated from the increase in eYFP emission upon eCFP excitation. Data are shown as Mean±SEM, where n=3 independent experiments.

DISCUSSION

In this study, we have determined the influence of caveolae on the properties of two GPCRs that are coupled to different Gα subunits. The rationale for this work is to verify observations that certain signaling proteins, such as $G\alpha_q$, partition into caveolae domains that may alter their signaling properties. Because many GPCRs that are coupled to $G\alpha_i$ and $G\alpha_q$ have been reported to reside in caveolae domains, we wanted to determine the influence of caveolae domain on GPCR signaling. In these studies, intact living cells expressing fluorescently labeled GPCRs were used, which avoids some of the problems in interpreting results using methods that involve cell disruption. It is arguable that fluorescent labels used in live cell studies may influence the results. However, the plasma membrane localization and functional studies of these proteins argue against this possibility.

We first found that Cav1, and presumably caveolae domains, are not evenly distributed in Fisher Rat thyroid cells. It is important to note that the localization of caveolae may differ depending on a variety of factors, including the cell type, confluency (Volontè, Galbiati et al. 1999), migration state (Isshiki, Ando et al. 2002) or its stage in the mitotic cycle (Boucrot, Howes et al. 2011). In FRTcav+, we observe Cav1 mainly on the bottom membrane and in areas of cell to cell contact supporting the idea that they may play a role in sensing contact inhibition or cell communication by organizing proteins such as connexins (Volontè, Galbiati et al. 1999, Schubert, Schubert et al. 2002, Langlois, Cowan et al. 2008). It is notable that in muscle tissue in which cells are arranged in arrays, such as cardiomyocytes, caveolae have a dense and fairly uniform membrane distribution along actin lines (e.g. (Guo, Golebiewska et al. 2011) (Woodman, Park et al. 2002)). In fluid cells, transformed

cells or immortalized cells, caveolae are either absent or their presence is greatly diminished (Koleske, Baltimore et al. 1995, Engelman, Wykoff et al. 1997). We also observe that the distribution of B_2R on the bottom membrane close to the substrate, mirrors Cav1 in these cells while μOR does not.

We studied the effect of caveolae on the functional and physical properties of two types of GPCRs, B_2R and μOR, which have both been implicated to localize in caveolae domains (de Weerd and Leeb-Lundberg 1997, Haasemann, Cartaud et al. 1998, Lamb, Zhang et al. 2002, Head, Patel et al. 2005, Zheng, Chu et al. 2008). μOR and B_2R are coupled to two different families of G proteins, $G\alpha_i$ and $G\alpha_q$, respectively. Cav1 expression does not appear to affect cAMP signals generated through μOR / $G\alpha_i$. It is noteworthy that stimulation of μOR / $G\alpha_i$ pathway may also increase intracellular Ca^{2+}, possibly through co-activation of a $G\alpha_q$–coupled receptor or by the release of $G\beta\gamma$ subunits which can then activate PLCβ2 or PLCβ3 (Philip, Kadamur et al. 2010). However, in our hands, FRTwt and FRTcav+ cells expressing μOR did not exhibit intracellular Ca^{2+} release. In contrast, Ca^{2+} signaling through the B_2R pathways is clearly affected by the presence of caveolae as seen in both single cell and cell suspension measurements similar to the behavior seen for muscarinic receptors (Sengupta, Philip et al. 2008). It is important to note that the effect of caveolae on Ca^{2+} release is seen immediately after stimulation and before detachment of B_2R from $G\alpha_q$ and subsequent sequestration since $G\alpha_q$-B_2R FRET is constant for the first 2 minutes after stimulation. This effect of caveolae on Ca^{2+} signals is interpreted to be due to stabilization of the activated state of $G\alpha_q$ by strong Cav1 binding and release of $G\beta\gamma$ from caveolae domains which lengthens the time for recombination of the heterotrimer (Sengupta, Philip et al. 2008). These studies and the ones presented here suggest that both B_2R and muscarinic receptors may reside in or close caveolae.

We find both receptors colocalize with Cav1. It is notable that Head and coworkers found that μOR and Cav3 colocalize to a higher degree in adult cardiomyocytes (Head, Patel et al. 2005) although direct comparison between their studies and ours is difficult since Cav3 shows a much higher expression and is uniformly distributed throughout cardiomyocytes as opposed to FRT cells. Additionally, the C-terminus of Cav3 is significantly different from Cav1 which may enable direct or indirect μOR binding. It is notable that the resolution of colocalization measurements is quite low compared to FRET and we could not detect a significant amount of FRET between μOR and Cav1 but did find a low (~20%) amount FRET between B_2R and Cav1. Additionally, we observed a larger amount of FRET between $G\alpha_q$-Cav1, implying that $G\alpha_q$ is localized within caveolae domains. We also observe an equally large amount of FRET between the $G\alpha_q$ and B_2R (**Fig. 3** and (Philip, Sengupta et al. 2007)). Together with our functional results, these data show that $G\alpha_q$ can interact with Cav1 and change its signaling properties while being in close proximity to B_2R. The lower FRET observed between B_2R and Cav1 compared to $G\alpha_q$ and Cav1 might be correlated to a weaker interaction although it could also be traced to orientations of eCFP and eYFP that make transfer less favorable.

It has been shown that Cav1 stabilizes $G\alpha_q$–mediated Ca^{2+} signals generated through bradykinin in B_2R–transfected cells (Sengupta, Philip et al. 2008). This receptor population is large enough to undergo FRET with Cav1 in the nanosecond time scale, and to influence $G\alpha_q$ signaling. $G\alpha_q$ / Cav1 FRET is two-fold higher than B_2R / Cav1 FRET, despite the high FRET values between B_2R / $G\alpha_q$. One explanation of this result is that GPCRs do not significantly penetrate into Cav1 domains and their association depends on the strength of their attached Gα family. $G\alpha_q$, which interacts strongly with Cav1, promotes caveolae localization of its coupled receptors, while $G\alpha_i$–coupled receptors, such as μOR have little interaction with these domains. Our fluorescence and

functional studies suggest that the interaction between B_2R and Cav1 could be mediated through $G\alpha_q$. We find a loss of B_2R /Cav1 FRET when $G\alpha_q$ is down-regulated or displaced from caveolae, and we find that $G\alpha_q$ but not $G\alpha_i$ increases FRET between B_2R and Cav1. The idea that G proteins mediate receptor association with caveolae is also supported by observations that μOR and B_2R can be pre-assembled with their G protein subunits , and that $G\alpha_q$, but not other G proteins interact with Cav1 (Oh and Schnitzer 2001), (Murthy and Makhlouf 2000). Additionally, previous FRET studies suggest that $G\alpha_q$ can interact simultaneously with $G\beta\gamma$, B_2R and Cav1 (Philip, Sengupta et al. 2007, Sengupta, Philip et al. 2008).

Even though FRT cells have been used extensively to study caveolae, we tested the effects of caveolae on Ca^{2+} signals mediated through bradykinin in A10 cells which endogenously express B_2R and Cav1. Single cell measurements show two distinct Ca^{2+} responses which we interpret to be due to caveolae and non-caveole localized $G\alpha_q$. The basis for these two populations is uncertain. It is possible that only ~30% of A10 cells have fully formed caveolae domains where $G\alpha_q$ can properly localize and impact the signaling. Based on the localization of caveolae on plasma membranes, we suggest that the caveolae-localized $G\alpha_q$ population is in regions of cell-to-cell contact. This idea leads to the hypothesis that signaling in intercellular regions differ from other regions of the cell.

It is possible that instead of stabilizing the activated state of $G\alpha_q$, Cav1 mediates a step downstream of $G\alpha_q$ that is coupled to B_2R and to muscarinic receptors. We have previously found that PLCβ associates strongly and similarly to $G\alpha_q$ in FRTwt and FRTcav+ cells and since the activity of PLCβ is low in the basal state, then its activity mirrors the activation state of $G\alpha_q$, which has been observed to be prolonged in the presence of caveolae (Guo, Golebiewska et al. 2011). It is also possible that specific partitioning of PIP_2 in caveolae contributes to the observed changes in Ca^{2+} release although preferential localization of PIP_2 in caveolae domains is

controversial (see (Morris, Huynh et al. 2006)). Interestingly, PIP_2 was shown to localize to the periphery of caveolae (Fujita, Cheng et al. 2009) where we suggest that $G\alpha_q$ -receptors localize. Partitioning of PIP_2 in the neck of caveolae would be expected to impact the magnitude of calcium release which we see in our FRTcav+ cells when stimulated with bradykinin, but we find that caveolae impacts the duration of the signal rather than the extent ((Sengupta, Philip et al. 2008) and Figure II-2b and Figure II-3).

Support for the idea that GPCRs coupled to $G\alpha_q$ interact more extensively with caveolae than receptors coupled to other G protein families comes from several reports. Many receptors that are reported to be localized and/or internalized via caveolae are coupled to $G\alpha_q$ (i.e. B_2R (de Weerd and Leeb-Lundberg 1997, Haasemann, Cartaud et al. 1998, Ju, Venema et al. 2000, Lamb, Zhang et al. 2002), endothelin Etb (Teixeira, Chaverot et al. 1999, Yamaguchi, Murata et al. 2003), GnRH(Navratil, Bliss et al. 2003, Pawson, Maudsley et al. 2003), serotonin 5HT2 (Dreja, Voldstedlund et al. 2002) TRH (Drmota, Novotny et al. 1999) and muscarinic receptor M3 (Gosens, Stelmack et al. 2007)). With the exception of somastostatin SST2 (Krisch, Feindt et al. 1998, Mentlein, Held-Feindt et al. 2001)), which was shown by electron microscopy to go to caveolae domains upon agonist stimulation, the two $G\alpha_i$ coupled GPCRs that have been reported to be in caveolae have been studied using methods that require cellular disruption (sphingosine EDG-1 (Igarashi and Michel 2000) , muscarinic M2 (Feron, Smith et al. 1997, Dessy, Kelly et al. 2000)). Additionally, these receptors may be coupled to $G\alpha_q$ as well as $G\alpha_i$ and form heterodimers with $G\alpha_q$-coupled GPCRs. It is also notable that disruption of caveolae domains by methyl-β-cyclodextrin attenuated the Ca^{2+} response of the $G\alpha_q$-coupled 5HTA receptor, but did not affect the Ca^{2+} release from the $G\alpha_q$ coupled α_1-adrenergic receptor (Dreja, Voldstedlund et al. 2002). However, it is possible that methyl-β-cyclodextrin treatment does not completely disrupt the strong

Cav1- $G\alpha_q$ association that results in dissociation of $G\beta\gamma$ subunits resulting in prolonged Ca^{2+} signals.

Localization of signaling proteins in caveolae would be expected to impact their signaling properties if this sequestration prevented or promoted access to proteins in their pathway. The studies here suggest that caveolae may impact $G\alpha_q$ signaling without a direct incorporation of GPCRs in the domain. This idea might explain many of the controversial reports pertaining to GPCR–caveolae associations. Super-resolution studies are underway to better understand the organization of these domains.

ACKNOWLEDGMENT

We thank Drs. Deborah Brown, Yuanjian Guo, Urszula Golebiewska, and Finly Philip for their helpful comments throughout this work.

CHAPTER III – DISCREPANCY BETWEEN FLUORESCENCE CORRELATION SPECTROSCOPY (FCS) AND FLUORESCENCE RECOVERY AFTER PHOTOBLEACHING (FRAP) DUE TO THE PRESENCE OF CAVEOLAE IN MEMBRANES

ABSTRACT

Fluorescence recovery after photobleaching (FRAP) and fluorescence correlation spectroscopy (FCS) are the two most direct methods to measure the diffusion of molecules in intact living cells. Ideally, these methods should produce similar results for an identical system. We have used these methods to monitor the diffusion of two G-protein-coupled receptors and their associated proteins in the plasma membranes of cells that do not or do contain invaginated protein domains called caveolae. FRAP studies show that caveolae domains increase the immobile fraction of receptors without significantly changing their mobility. On the other hand, FCS studies show an unexpected increase the mobility of caveolae-associated proteins. Our data suggest that the geometry of caveolae domains gives rise to a confined diffusion of its attached proteins, resulting in an apparent increase in mobility.

---

*Reprinted from Analytical Biochemistry, Vol. 440, Issue 1, R.C. Calizo and S. F. Scarlata, Discrepancy between Fluorescence Correlation Spectroscopy (FCS) and Fluorescence Recovery After Photobleaching (FRAP) due to the Presence of Caveolae in Membranes, pp. 40-48.

INTRODUCTION

Fluorescence correlation spectroscopy (FCS) and fluorescence recovery after photobleaching (FRAP) are routinely used to measure the diffusion of fluorescent proteins in cells. FRAP monitors the recovery of fluorescence by the diffusion of fluorophores into a region that has been bleached by a high intensity laser. Usually the bleach spot is on the micron scale, and the recovery is over a minute depending on the mobility of the fluorophore (Alexrod, Koppel et al. 1976). FCS, on the other hand, monitors the fluctuations of fluorescence intensity as molecules diffuse in and out of a small (i.e. ~1fL) confocal volume (Schwille, Haupts et al. 1999). The most common type of FCS measurement is single point FCS, which has the drawback of being only sensitive to diffusing fluorophores and the immobile population of fluorophores are not detected. Alternately, FRAP measurements give a good indication of the population of species that are immobile during the sampling period. In principle, FCS and FRAP should offer similar and complementary information. However, because the size of the sampling areas differs greatly in the two methods, discrepancies may arise due to local structural barriers that impede or corral the movement of probes. This is particularly true on the plasma membranes of living cells where diffusion barriers exist (e.g. (Suzuki, Ritchie et al. 2005)).

Here, we have used FCS and FRAP to determine the effect of membrane domains called caveolae on the diffusion of two related integral membrane proteins. Caveolae are flask-shaped membrane invaginations (see Fig. III-1 (Anderson 1998, Schlegel, Volonte et al. 1998, Parton and Simons 2007)) formed from the caveolin and cavin family of proteins (see (Rothberg, Ying et al. 1990, Rothberg, Heuser et al. 1992, Monier, Dietzen et al. 1996, Lipardi, Mora et al. 1998, Parton and Simons 2007, Hansen and Nichols 2010)). Caveolae are found on the plasma

membrane of many mammalian cells. These domains appear to participate in vesicle trafficking and endocytosis. Additionally, caveolin proteins (i.e. Cav1 and Cav3) may specifically bind to other cellular proteins involved in transmission of extracellular signals (e.g. (Rybin, Xu et al. 2000, Zajchowski and Robbins 2002)).

An important class of signaling proteins that may target caveolae are G-protein coupled receptors (GPCRs) (Chini and Parenti 2004). GPCRs are the largest family of mammalian receptors that structurally consist of seven transmembrane helices. When an extracellular agent interacts with its specific GPCR, it initiates a series of sequential molecular interactions that involve activation of surface associated heterotrimeric G proteins, and subsequent activation or inhibition of cytosolic enzymes that result in various cellular responses (Alberts, Bray et al. 1994). Many GPCRs and G-protein subunits have been reported to localize in lipid rafts and caveolae domains (see (Oh and Schnitzer 2001, Chini and Parenti 2004)). By corralling GPCRs and G proteins, caveolae may impact signaling by promoting their oligomerization, their association with agonists, as well their interaction with intracellular G proteins.

Heterotrimeric G proteins are activated by GPCRs, and consist of a Gα and a Gβγ subunit. There are 4 families of Gα subunits and only the $G\alpha_q$ subtype has been reported to reside in caveolae domains (Oh and Schnitzer 2001). Our laboratory used live cell fluorescence imaging to show that in the basal state, $G\alpha_q G\beta\gamma$ localizes to caveolae domains (Sengupta, Philip et al. 2008) due to strong interactions between $G\alpha_q$ and Cav1 (Sengupta, Philip et al. 2008, Guo, Golebiewska et al. 2011). For those studies, we used Fisher rat thyroid (FRTwt) cells with corroborating experiments in other cell lines. FRTwt cells do not express detectable levels of Cav1 but a sister line that is stably transfected with canine Cav1 (FRTcav+) displays caveolae domains as visualized by electron microscopy (Lipardi, Mora et al. 1998, Mora, Bonilha et al.

1999). In this cell line, caveolae appear at high density on the bottom membrane and very little on the top membrane. Furthermore, caveolae are enriched in regions of cell to cell contact in accord with the observations that they may organize proteins involved in intercellular signaling such as connexins (Calizo and Scarlata 2012).

$G\alpha_q$ is coupled to many GPCRs and its activation results in an increase in intracellular calcium resulting in mitogenic and proliferative changes in the cell (see (Alberts, Bray et al. 1994)). One of the more notable GPCRs that is coupled to $G\alpha_q$ is the bradykinin type 2 receptor (B_2R). B_2R binds the extracellular agonist bradykinin, which is a key mediator of the inflammation response (Bachvarov, Houle et al. 2001). The binding of bradykinin to B_2R activates $G\alpha_q$ resulting in activation of phospholipase Cβ (PLCβ) enzymes that ultimately results in an increase in intracellular calcium and activation of many calcium sensitive proteins. FRT cells do not express B_2R receptors allowing us to monitor the effect of caveolae domains on the homo-oligomerization of these receptors.

We have found that the presence of caveolae greatly impacts B_2R/ $G\alpha_q$ signaling correlating with a significant increase in calcium release in FRTcav+ cells as compared to FRTwt (Sengupta, Philip et al. 2008, Calizo and Scarlata 2012). Additionally, we have found a significant amount of Förster resonance energy transfer (FRET) between eCFP-Cav1 and B_2R-eYFP, and between eCFP-Cav1 and $G\alpha_q$-eYFP supporting a caveolae localization of these proteins (Sengupta, Philip et al. 2008, Calizo and Scarlata 2012). These studies, as well as sedimentation studies, suggest that B_2R localizes to caveolae domains (de Weerd and Leeb-Lundberg 1997). In contrast, the presence of caveolae does not affect the function of another GPCR pathway, the μ-opioid receptor (μOR) / $G\alpha_i$ system correlating with a lack of FRET between these proteins and Cav1 (Calizo and Scarlata 2012).

Here, we have measured the impact of caveolae on the diffusion properties of B_2R using FCS and FRAP. While FRAP studies show a small increase in the immobile population of B_2R in the presence of caveolae, FCS show an unexpected increase in receptor mobility with caveolae. We postulate that this surprising FCS result is caused by confined movement of B_2R to the periphery of caveolae domains.

MATERIALS AND METHODS

Materials.

FRTwt and FRTcav+ cells and canine Cav-1-eGFP DNA were gifts from Dr. Deborah Brown (Stony Brook University, NY) and were cultured in F-12 Coon's modified media obtained from Sigma as previously described (Sengupta, Philip et al. 2008). Cells were imaged in Leibovitz's L-15 media from Gibco (see (Lipardi, Mora et al. 1998)) and transfected using Lipofectamine (Invitrogen, Inc.) following the manufacturers' protocol.

μOR-eGFP and $G\alpha_i$-eYFP were from Dr. Lakshmi Devi (Mount Sinai Medical Center, NY). $G\alpha_q$-eYFP was from Dr. Catherine Berlot (Geisinger Research). B_2R and B_2R-GFP were from Dr. Leeb-Lundberg (Lund University, Sweden). We have found that expressed proteins are functional (Philip, Sengupta et al. 2007, Sengupta, Philip et al. 2008, Calizo and Scarlata 2012). The membrane marker is an eYFP fused with the first 20 amino acids of GAP-43 and is palmitoylated on cysteines 3 and 4 post-translationally (Clontech, Inc.).

FRAP measurements.

FRTwt and FRTcav cells expressing fluorescently tagged proteins were seeded on glass bottom dishes (MatTek Corporation). Cells were imaged with a 60x oil objective (N. A. 1.42) using Olympus Fluoview1000. For variable radius FRAP (vrFRAP), the focal plane was set on either the top or the bottom membranes and circular regions of interest with increasing radii (1 μm, 2 μm or 3 μm) were selected for bleaching. For areas of bottom membranes and cell to cell contact, an approximately 2 μm x 2 μm rectangular region was selected for bleaching. The region of interest was illuminated with high intensity (100% transmittivity) 488 nm Argon ion laser for 500 milliseconds and the recovery was observed for 120 seconds under low-intensity illumination (2% transmittivity). Under these bleaching conditions, at least ~50% of the original intensity was bleached after 500 ms of the bleaching pulse. To correct for photobleaching, a similar region of interest in a non-bleached cell located in the same field of view was selected and the time dependent decrease in fluorescence was used to correct the recovery curves. Cells that exhibited cell movement or excessive photobleaching were not considered for the analysis. The corrected fluorescence recovery was fitted as described previously, using one component exponential fit. Comparison of the normalized FRAP curves was performed using Student t-test with a statistical significance of $P < 0.010$ using SigmaPlot (Jandel Scientific, Inc).

FCS measurements.

FCS measurements on cells expressing the membrane protein of interest were performed on a LSM 510-Confocor 2 system equipped with 40x (N. A. 1.2) water immersion objective. GFP and YFP were excited using 488 nm or 514 nm Argon ion laser lines respectively, and the fluorescence emission was recorded using an avalanche photodiode through a long pass emission

filter. The beam waist, ω_0, and focal volume were calibrated with 10 nM Rhodamine 6G solution (D = 2.8 x 10^{-6} cm^2/s). Measurements of each cell were taken over 30 seconds and repeated for more than four times. For each cell, the traces were averaged to obtain the final ACF to be used for fitting. The power of the excitation laser was adjusted such that there is sufficient signal to noise ratio and minimal photobleaching. Photobleaching was assessed by observing the time dependent decrease in intensity of the time trace. This was achieved using 55% output of a 500 mW maximum output Argon ion laser and 1% transmittivity for both the 488 nm and 514 nm laser lines. Traces that showed a decrease or increase of intensity over time were not used for analysis. Autocorrelation functions were analyzed using a two-component, pseudo-two dimensional diffusion model by modifying the three dimensional diffusion fitting routine provided by the Confocor2 software with following equation, and setting the structural parameter to quasi-infinite:

$$G(\tau) = 1 + \frac{1}{N}\left\{\left(1 + \frac{\tau}{\tau_D}\right)^{-1}\left(1 + \frac{\tau}{S^2\tau_D}\right)^{-1/2}\right\}$$

where τ is the correlation time, τ_D is the average time a particle spends in the confocal volume, N is the average number of molecules in the confocal volume and S is the structural parameter. S was set to 100 (quasi-infinite) for two-dimensional diffusion. Diffusion Coefficient, D, is calculated from the τ_D of a molecule using Einstein relation for diffusion: $r^2 = 4D \times \tau_D$ where r is the radius of the observation volume. For GFP tagged proteins, a fast component (~100-300 μs) is attributed to autofluorescence (Brock, Hink et al. 1998) while for YFP tagged proteins, the fast component in the time scales of 10-30 μs due to flickering of the eYFP was observed (Schwille, Kummer et al. 2000). In both cases, a slow component in the 10-50 ms time range due to membrane diffusion could be clearly resolved in the autocorrelation curves.

Number and Brightness Analysis.

Olympus Fluoview FV1000 was used to determine the molecular brightness and number (Dalal, Digman et al. 2008, Digman, Wiseman et al. 2009). Data was taken at 12.5 μs/pixel and an image series of one hundred slices were acquired in the pseudo-photon counting mode with a pixel size of 107 nm using Argon 488 nm laser, 0.1 % transmittivity as previously described (Golebiewska, Johnston et al. 2011).

RESULTS

Visualization of caveolae domains.

The size of a caveolae domain is too small to observe by fluorescence microscopy (i.e. ~50-100 nm in diameter, see (Anderson 1998, Schlegel, Volonte et al. 1998, Parton and Simons 2007)). In FRT cells, caveolae are concentrated on the bottom membrane as opposed to the top membrane (Calizo and Scarlata 2012). To ensure that we will be viewing caveolae domains in FCS measurements, we estimated the number of caveolae that would be illuminated in a confocal volume. Confocal imaging of GFP fluorescence in FRTwt cells transfected with Cav1-eGFP suggests that 82% of the fluorescence intensity is on the bottom membranes (n=20, and Figure III-1). By analyzing the fluorescence intensity of Cav1-eGFP on the bottom membranes of these cells (n=20), we estimate that caveolae domains account for ~40% of the bottom and lateral membrane areas. Even though this model is based on the diffraction-limited measurements of Cav1-eGFP and should be considered only as an estimated assessment of the area, it indicates that there is a high probability

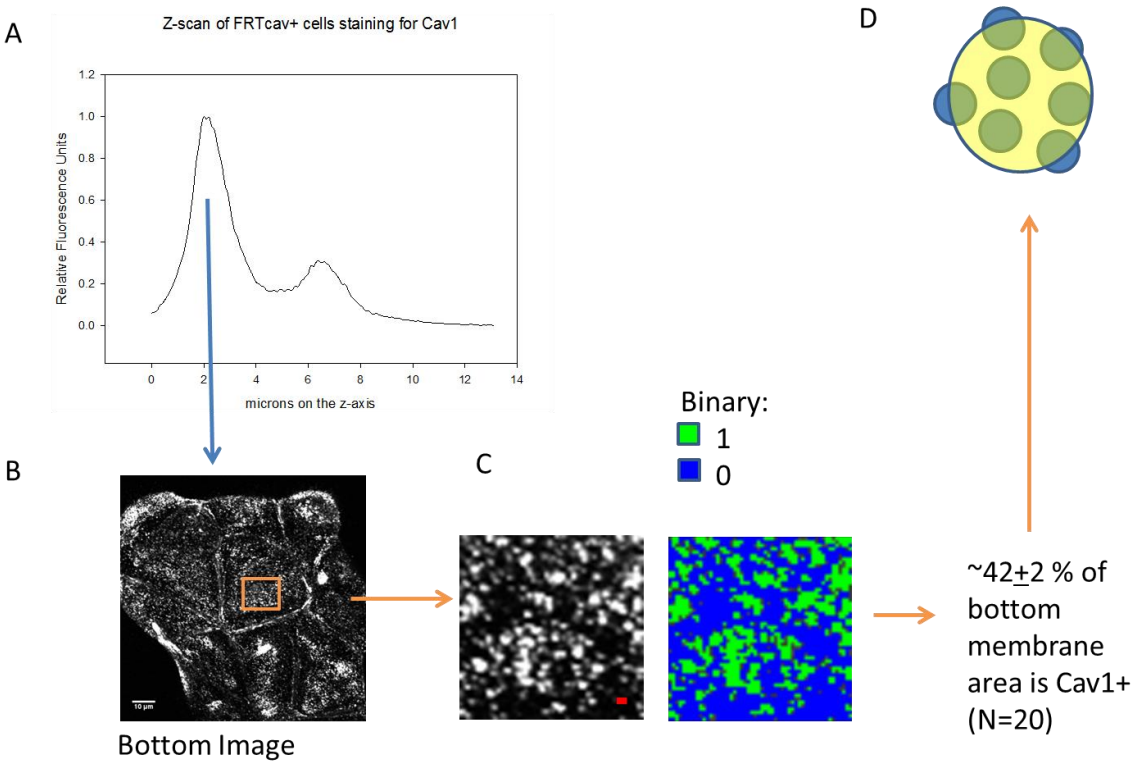

Figure III-1. A. Example of the distribution of Cav1-eGFP in the Z direction expressed in an FRTwt cell. **B.** The corresponding image of the cell. **C.** Expanded view of a region of the image in black and white and binary depiction. **D.** Cartoon depicting caveolae in an FCS-based illuminated measurement.

of viewing caveolae on the basal and lateral membranes in FCS measurements. Since larger areas are bleached in FRAP measurements which may encompass other regions besides the caveolae-rich bottom membrane, it is possible that a smaller percentage of caveolae are viewed.

***FRAP studies*.**

We determined the impact of caveolae on receptor diffusion by FRAP. These studies were initiated by measuring the diffusion of Cav1-eGFP expressed in FRTwt cells that do not contain caveolae. We find that after bleaching the fluorescence of Cav1-eGFP does not recover over a 100s period suggesting an extremely limited diffusion. This immobility is consistent with Cav1 forming protein domains (Figure III-2a). We then measured the diffusion of a commercially available plasma membrane marker consisting of an eYFP linked to a small peptide with two hydrocarbon chains that anchor the fluorophore to the membrane surface. This construct is introduced into cells by transient transfection (see Methods). This marker should be freely diffusing on the membrane surface and we find that its diffusion is unaffected by the presence of caveolae (Figure III-2b) suggesting that caveolae does not affect diffusion of small lipid components. Additionally, $G\alpha_q$, which is only peripherally bound to the membrane surface is not sensitive to the presence of caveolae in FRAP measurements suggesting that surface diffusion of this protein is similar on caveolae and non-caveolae surfaces (Figure III-2c). If B_2R is incorporated into caveolae domains, we would expect its diffusion to be slower on the bottom membrane where caveolae are localized, but not on the top membrane where little caveolae are found. In accord with this idea, we find either no significant or small differences in the diffusion coefficients of B_2R in the top membranes of FRTwt cells and FRTcav+ cells, which may be attributed to small differences in membrane structure

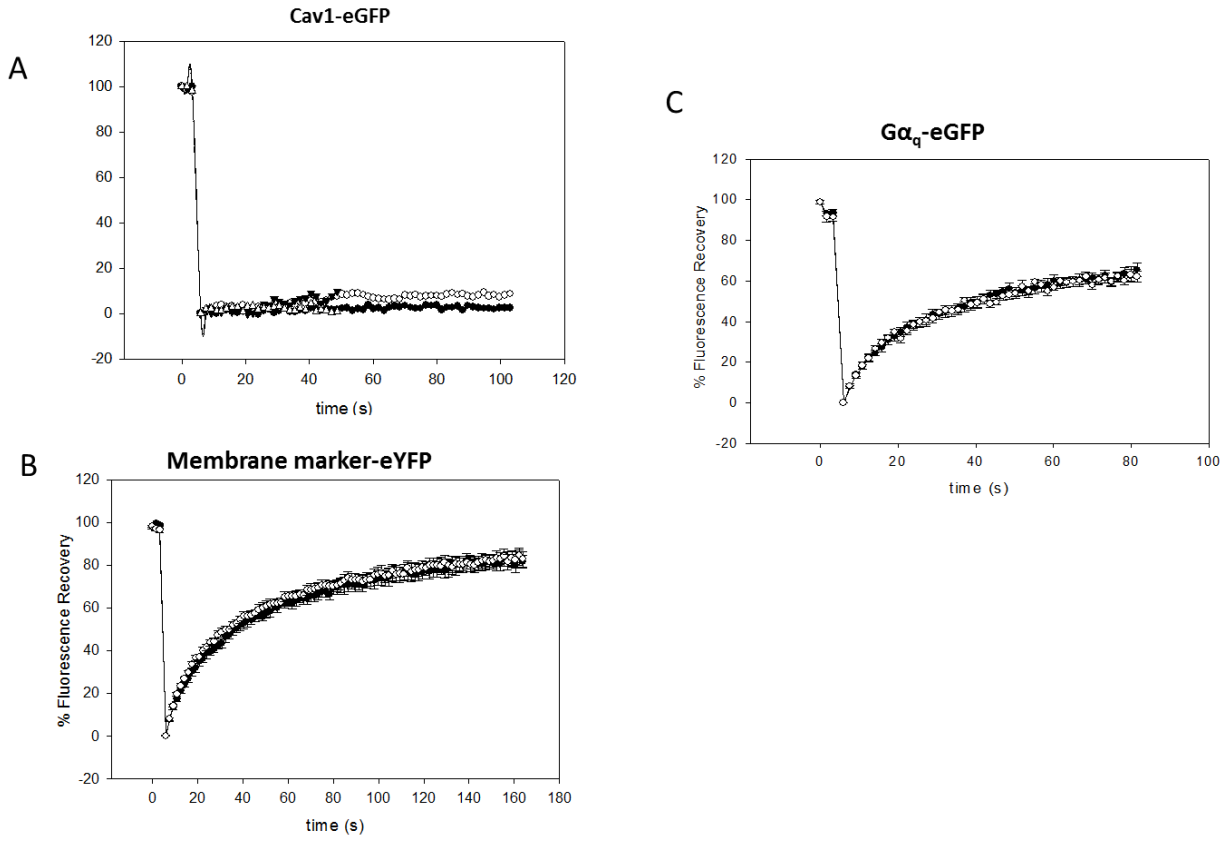

Figure III-2. FRAP measurements of different membrane proteins diffusing on the bottom membranes of FRTwt or FRTcav+ cells. Recovery curves of **A** Cav1-eGFP, **B** membrane-marker-eYFP (Clontech, Inc.) and **C** $G\alpha_q$-eGFP diffusing in the bottom membrane of FRTwt and FRTcav+ cells. The open and closed circles are for data taken in FRTwt and FRTcav+ cells, respectively, where n=10-13 (see Table 1). The data shown are average values and SD is shown.

(i.e. curvature of the top membrane since it is not bound to glass, or small folds in the lateral membrane etc.) (Figure III-3a-b).Additionally, the recoveries of μOR in the top membranes were within error, as were the recoveries of μOR in the absence and presence of caveolae domains (Table III-1, Figure III-3a-b). However, when viewing caveolae-rich FRTcav+ bottom membranes, the mobile fractions of both receptors are significantly reduced (Figure III-3c). Since both receptors show high mobility as compared to Cav-1-eGFP and since the presence of caveolae similarly affects their diffusion, these results suggest only a weak association of the receptors to caveolae domains. FRAP results are summarized in Table III-1**.**

The distribution of caveolae is not uniform and diameter of the bleach spot is relatively large, and so there is a possibility that diffusion from membrane regions besides the bottom membrane contribute to the observed recovery. We repeated the FRAP measurements with increasing radius of bleach spot (vrFRAP) on the bottom membrane. This method has been previously used to investigate the lateral confinement of NK2 receptors in HEK293 cells (Cézanne, Lecat et al. 2004) and in μOR in a neuronal cell line (Saulière, Gaibelet et al. 2006, Saulière-Nzeh, Millot et al. 2010). For receptors exhibiting confined diffusion within a domain size *r*, the authors found an inverse linear relationship between the mobile fraction, *M* and the radius of the bleach spot:

$$M = M_P + 0.63\,\frac{r}{R}$$

where M_P is the permanent mobile fraction. The diffusion coefficients obtained from each size of the bleached spot are apparent diffusion coefficients that depend on the domain size, r, the mobile fraction and the size of the bleach spot R. We see this relationship between the mobile

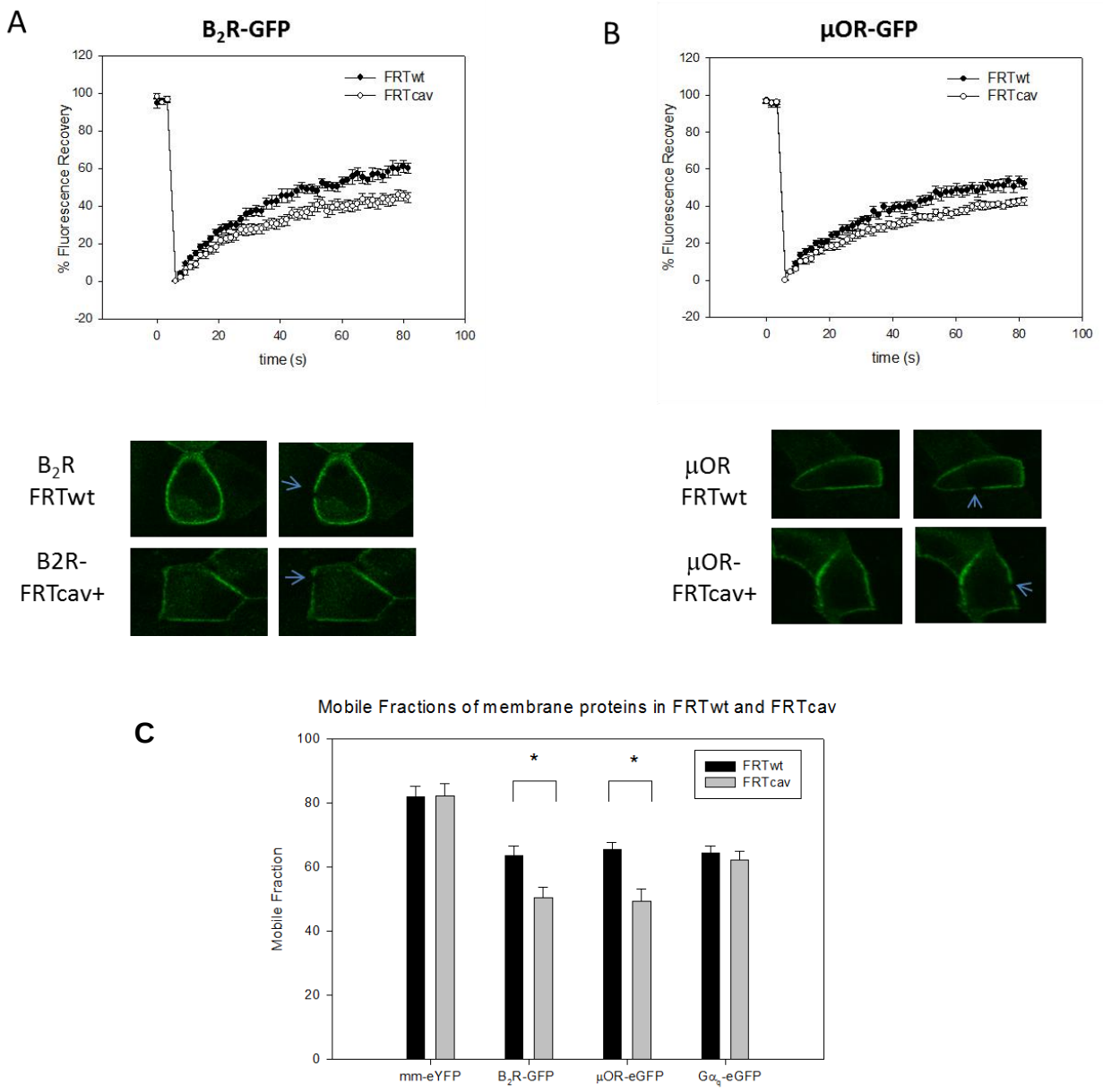

Figure III-3. FRAP Measurements of B_2R and µOR diffusing in the bottom membranes of FRTwt and FRTcav+ cells. Recovery curves of **A-** B_2R-GFP and **B-** µOR-GFP diffusing in the bottom membrane of (●) FRTwt and (○) FRTcav+ cells showing compiled data (*top*) and sample images (*bottom*) where n=12,13 (see **Table III-1**) and the arrow points to the bleached spot. **C** – Comparison of mobile fractions in FRTwt and FRTcav+ cells obtained from FRAP curves in **A** and **B**. Data are shown with error in SD. A student t-test was performed between FRTwt and FRTcav+ for each membrane protein. Asterisks indicate statistical difference in the mobile fractions of membrane proteins between FRTwt and FRTcav ($p < 0.001$).

Table III-1 FRAP and FCS results for Proteins in FRT cells

Cell type	Protein	Diffusion Coefficient	Mobile Fraction	(cells)
a-FRTwt	μOR-eGFP	4.7 ± 0.9 x 10^{-11} cm^2/s	0.80 ± 0.04	12
a-FRTcav+	μOR-eGFP	4.1 ± 0.7 x 10^{-11} cm^2/s	0.77 ± 0.02	12
a-FRTwt	B_2R-GFP	4.6 ± 0.6 x 10^{-11} cm^2/s	0.80 ± 0.03	6
		5.0 ± 0.6 x 10^{-9} cm^2/s		**22**
a-FRTcav+	B_2R-GFP	4.3 ± 0.6 x 10^{-11} cm^2/s	0.79 ± 0.04	6
		6.3 ± 0.7 x 10^{-9} cm^2/s		**21**
b-FRTwt	μOR-eGFP	5.7 ± 0.7 x 10^{-11} cm^2/s	0.66 ± 0.04	12
		3.2 ± 0.2 x 10^{-9} cm^2/s		**18**
b-FRTcav+	μOR-eGFP	5.3 ± 0.7 x 10^{-11} cm^2/s	0.49 ± 0.02	12
		3.4 ± 0.2 x 10^{-9} cm^2/s		**16**
b-FRTwt	B_2R-GFP	6.8 ± 0.7 x 10^{-11} cm^2/s	0.64 ± 0.03	13
		8.1 ± 0.8 x 10^{-9} cm^2/s		**80**
b-FRTcav+	B_2R-GFP	6.0 ± 0.8 x 10^{-11} cm^2/s	0.51 ± 0.03	12
		14.9 ± 0.9 x 10^{-9} cm^2/s		**86**
b-FRTwt	mm-eYFP	5.7 ± 0.6 x 10^{-11} cm^2/s	0.82 ± 0.04	10
		12.3±0.3 x 10^{-9} cm^2/s		**81**
b-FRTcav+	mm-eYFP	5.7 ± 0.3 x 10^{-11} cm^2/s	0.82 ± 0.03	13
		9.3 ± 0.3 x 10^{-9} cm^2/s		**60**
b-FRTwt	$G\alpha_q$-eGFP	2.0 ± 0.2 x 10^{-10} cm^2/s	0.64 ± 0.03	12
		6.2 ± 0.3 x 10^{-9} cm^2/s		**75**
b-FRTcav+	$G\alpha_q$-eGFP	2.1 ± 0.2 x 10^{-10} cm^2/s	0.62 ± 0.02	10
		11.0± 0.1 x 10^{-9} cm^2/s		**74**

Table III-1. Diffusion results for proteins and membrane marker (Mm-eYFP) in FRTwt and FRTcav+ cells where (a-) denotes the top membrane and (b-) denotes the bottom membrane. Values in black and normal font are those derived from FRAP measurements while FCS measurements are bold and in red. Diffusion coefficients assuming a 2 x 2 x 2 μm area reflecting the beam dimensions in the x, y and z planes and are thought to be appropriate for viewing membrane proteins diffusing in the bottom membrane. Diffusion coefficients assuming a 2 x 4 μM area (not shown) were consistently 1.7+ 0.1 fold lower in magnitude and may better diffusion in the top membrane that is expected to be curved, but the comparative results are unchanged. The data have a normal distribution as determined by Shapiro-Wilk test, and SEM values are shown. Differences in the mobile fractions for μOR and B2R in the bottom membranes of FRTwt and FRTcav+ cells are significant ($p<0.001$) whereas differences for Mm-eYFP and $G\alpha_q$-eGP are not. Statistical analysis for the mobile fraction data can be found in Fig. III-3c. These results show similar FRAP diffusion properties of the receptors in the absence and presence of caveolae.

fraction and bleach spot size for both B_2R and μOR, but we could not detect significant differences in immobile fractions or apparent diffusion coefficients between FRTwt and FRTcav+ cells. This suggests that there are other mechanisms of receptor confinement in the absence of caveolae. We also find that the diffusion coefficients obtained using variable radius FRAP are similar to reported values (Table III-1 and Figure III-4). Taken together, the FRAP results are inconsistent with a caveolae localization of B_2R but instead correlate with a transient localization.

FCS measurements.

We measured the mobility of B_2R and μOR using single point fluorescence correlation spectroscopy (FCS). Figure III-5 shows an example of raw data and residuals while the compiled results are listed in Table III-1. We found that the apparent diffusion coefficients of μOR-eGFP on the bottom membranes of FRTwt and FRTcav+ cells were identical. Also, the apparent diffusion coefficients of B_2R-GFP in the top membranes of FRTwt and FRTcav+ cells were similar. Also, the mobility of the membrane marker, mmYFP, slowed in the presence of caveolae (Table III-1). This reduced mobility is interpreted as being due to small amount of incorporation of the palmitoyl groups into the domain, as saturated lipids tend to incorporate into caveolae (Anderson 1998, Schlegel, Volonte et al. 1998). We note that the diffusion coefficients determined by FCS are faster than FRAP measurements (see Table III-1) but are comparable to other reports of GPCR diffusion measured by FCS (see compilation in (Philip, Sengupta et al. 2007)).

In contrast to observations for diffusion on the top membrane, when we focused on the caveolae-rich bottom membrane of FRTcav+ cells, we found a significant shift in the apparent diffusion of B_2R toward faster mobilities: $D=8.1 \pm 0.8 \times 10^{-10}$ cm^2/s (n=80) for FRTwt, and $D= 14.9 \pm 0.9 \times 10^{-9}$ cm^2/s (n=86) for FRTcav+ (p = <0.001). Additionally, we found that the distribution of

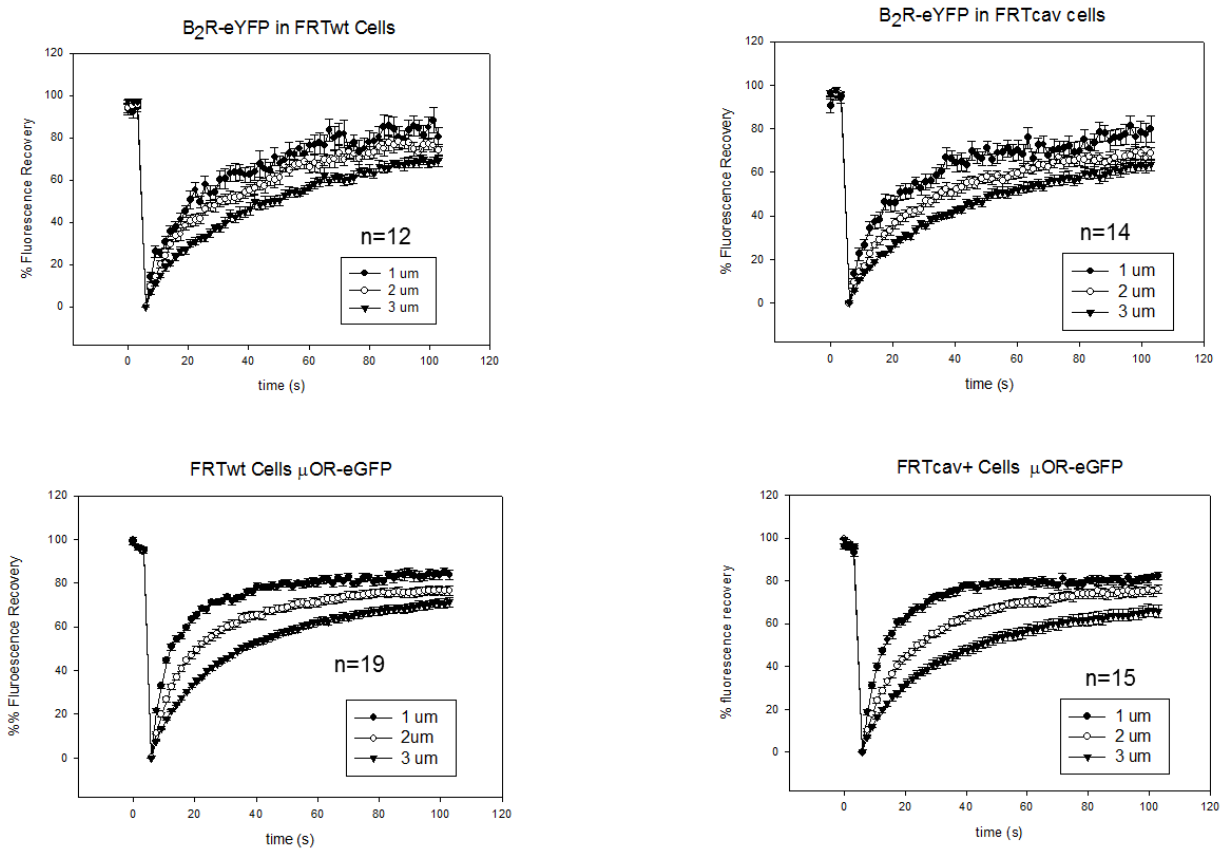

Figure III-4. FRAP measurements of B_2R and μOR in FRTwt and FRTcav+ cells taken at different bleach sizes. Recovery curves of **A** B_2R-GFP and **B** μOR-GFP diffusing in the bottom membrane of FRTwt and FRTcav+ cells where the size of the bleach spot was varied. While the calculated mobile fractions decreased ~3 fold with bleach size, no significant differences between diffusion coefficients for either receptor in FRTwt and FRTcav+ were found.

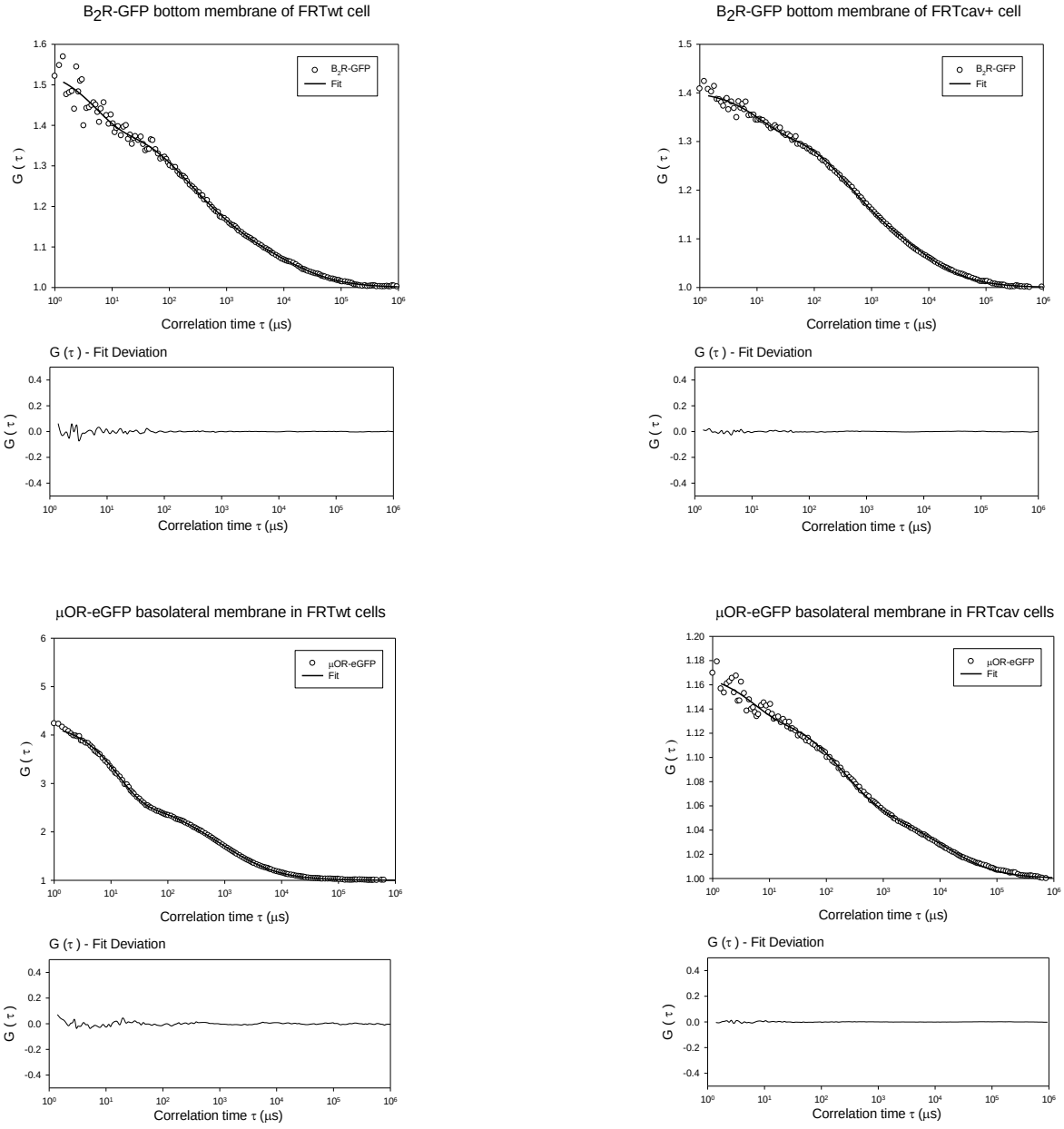

Figure III-5. Representative FCS curves of GPCRs in the bottom membranes of FRTwt and FRTcav+ cells A. B_2R-GFP **B.** μOR-eGFP

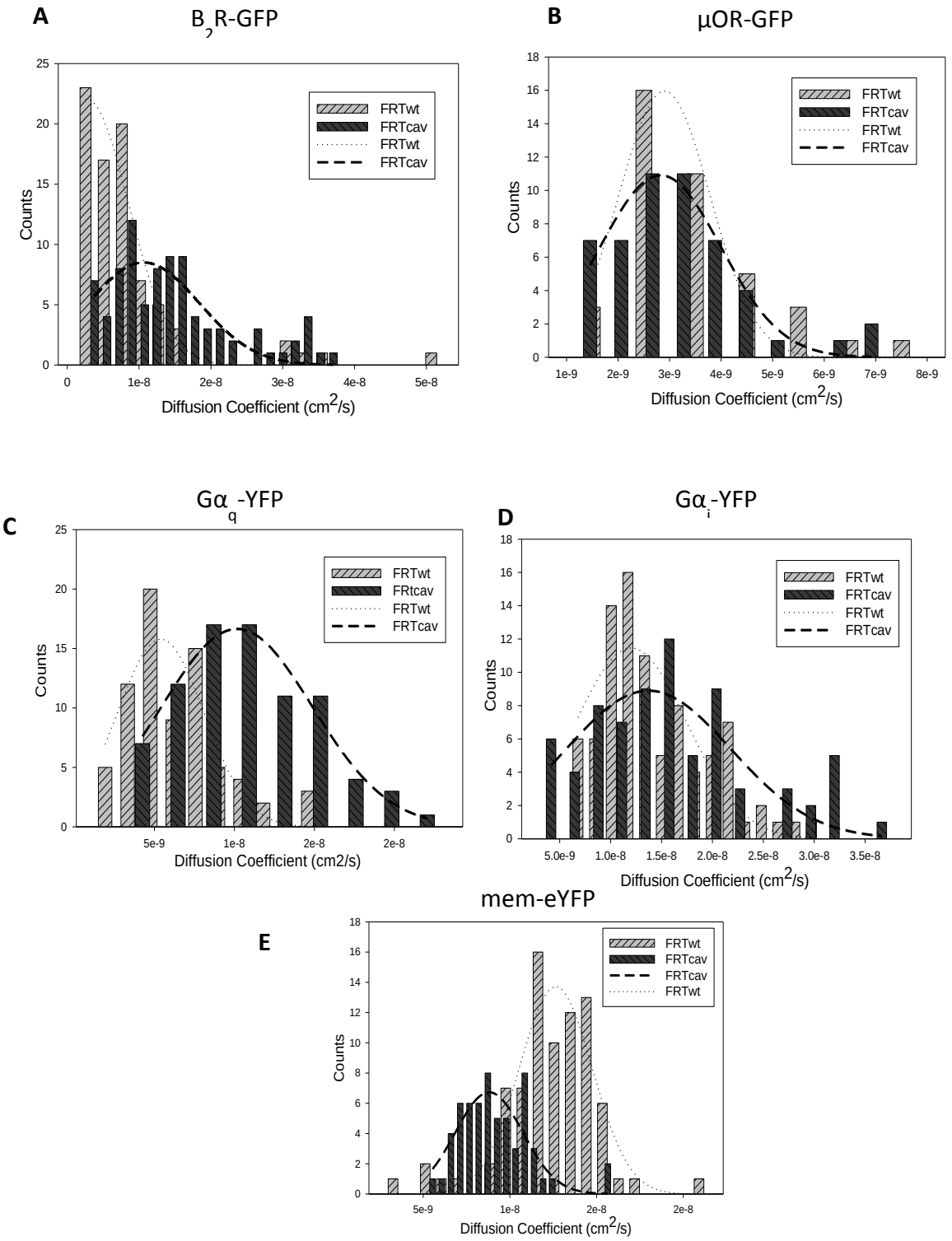

Figure III-6. Distribution of diffusion coefficients of membrane proteins in the bottom membrane of FRTwt and FRTcav+ extracted from FCS data Distribution of diffusion coefficients extracted from FCS data showing the broadening towards slower coefficients for membrane marker **(E)**, similar coefficients for μOR **(B)** and $G\alpha_i$ **(D)** and faster values for B_2R-GFP **(A)** and $G\alpha_q$ **(C)** in the presence of caveolae. Although the curves are fit to gaussian distributions, no model is intended.

B_2R diffusion coefficients differ in the two cell types (Figure III-6); a narrow distribution was seen for FRTwt cells as compared to a broader distribution in FRTcav+ cells. Similarly, a shift towards faster apparent diffusion coefficients in the presence of caveolae was seen for $G\alpha_q$–eGFP which has been shown to interact with caveolae ($6.2\pm0.3 \times 10^{-9}$ cm^2/s (n=75) for FRTwt and $11.0 \pm 0.1 \times 10^{-8}$ cm^2/s (n=74) for FRTcav. As a control, we monitored the diffusion of another G protein that does not interact with caveolae, $G\alpha_i$-eGFP (Oh and Schnitzer 2001) and found that caveolae does not affect its apparent diffusion coefficients ($1.4\pm0.1 \times 10^{-8}$ cm^2/s (n=88) for FRTwt, and $1.6\pm0.1 \times 10^{-8}$ cm^2/s (n=74) for FRTcav+ cells. The unexpected observation that B_2R and $G\alpha_q$ appear to diffuse more rapidly on the bottom membrane of FRTcav+ cells, whereas μOR and $G\alpha_i$ do not, indicates that caveolae are perturbing the movement and/or organization of these proteins (*see Discussion*).

Number and Brightness (N&B) studies.

It is possible that B_2R exists as an aggregate which can be disrupted by caveolae resulting in an increase in mobility. To determine whether this is the case, we monitored changes in the aggregation state of B_2R by N&B analysis (Dalal, Digman et al. 2008). N&B analysis reports on the molecular brightness and oligomerization of a fluorescent-tagged protein resulting in higher values of molecular brightness values compared to the brightness of a monomeric control. In these studies, brightness was measured by following changes in fluorescence intensity on a confocal microscope pixel by pixel over a time series of repetitive scans as previously described (Golebiewska, Johnston et al. 2011). However, we could not detect significant differences in the brightness of the bottom membrane populations of μOR in FRTwt or in FRTcav+ cells (29,904±166 versus 29,026±207 counts/s/molecule) or B_2R in FRTwt or in FRTcav+ cells (24,386±418 versus 24,014±704

counts/s/molecule). These results suggest that caveolae is not affecting the homo-oligomerization of these receptors.

DISCUSSION

Several methods have suggested that B_2R and $G\alpha_q$ localize to caveolae domains (de Weerd and Leeb-Lundberg 1997, Murthy and Makhlouf 2000, Oh and Schnitzer 2001, Lamb, Zhang et al. 2002, Sengupta, Philip et al. 2008, Calizo and Scarlata 2012). We have recently presented functional and FRET data supporting the idea that a subpopulation of B_2R localizes in caveolae domains (Calizo and Scarlata 2012). In this study, we have used diffusion measurements to test this idea. However, rather than support a caveolae localization of B_2R, we find a much more complicated picture. FRAP measurements showed that the presence of caveolae did not affect the diffusion coefficients of the membrane marker, the surface-associated protein $G\alpha_q$, or the two receptors. The inability of caveolae to affect diffusion of these proteins may be due to the large membrane area sampled in FRAP measurements that may include regions containing little caveolae. Additionally, the ability of a caveolin molecule in a caveola that contains over 100 caveolins as well as other proteins to fully compete with receptors for $G\alpha_q$, and the ability of $G\alpha_q$ to compete with other caveolin proteins in the domain, would most likely not result in a significant drop in $G\alpha_q$ mobility.

Since Cav1 is essentially immobile, then caveolae should increase the immobile population of the proteins. Although an ~10% increase in immobile population of B_2R was observed, a similar increase was seen for μOR receptors which do not appear to localize to caveolae domains based on functional and FRET studies (Calizo and Scarlata 2012). Thus, the mechanism underlying the

increase in immobile fraction with caveolae might be due to a general diffusion barrier of these domains that non-specifically impacts larger transmembrane proteins.

While FRAP studies could not detect differences between μOR and B_2R, FCS measurements which are more sensitive to local diffusion, show that caveolae domains give an apparent increase in the mobility of B_2R but not μOR. The faster mobility of B_2R in the presence of caveolae is unexpected since interaction with caveolae would be expected to impede diffusion. However, since caveolae is affecting the rate of B_2R diffusion and since Cav1 is close enough to participate in FRET with the receptor, we suggest that a novel model for B_2R–caveolae localization that may explain these seemingly contrary results. We propose that the faster apparent diffusion of B_2R in the presence of caveolae results from confined diffusion around the neck region of the domains rather than partitioning of the receptor into the domains. This peripheral association would result in a quasi-one dimensional circular diffusion on the caveolae exterior. How would this affect the observed diffusion? In FCS measurements, a membrane area of ~250 nm is illuminated and there is the possibility of viewing many caveolae of the bottom membrane since their diameters range from 50-100 nm and their density is high on the bottom membrane (see Figure III-1). If the domains are totally contained within the FCS illumination volume, their diffusion cannot be detected by FCS since FCS is only sensitive to movement of fluorophores in and out of the confocal volume. Alternately, if the domains are partially contained in the illuminated area, then the quasi-one dimensional diffusion of receptors along the caveolae periphery would give rise to a faster effective diffusion in the observation area since its diffusion is confined in the domain periphery. The variation in the number of caveolae, the amount of their circumference illuminated, as well as the amount of receptors associated to the periphery would give rise to a broadened distribution of observed diffusion coefficients towards faster values which is consistent with Figure III-6. A

peripheral localization would fit well with the functional, FRET and sedimentation studies previously described (de Weerd and Leeb-Lundberg 1997, Calizo and Scarlata 2012). This model is depicted in Figure III-7. While other interpretations are possible, a quasi-one-dimensional diffusion of receptor along the caveolae neck is the simplest. B_2R has been reported to internalize through a caveolae pathway (de Weerd and Leeb-Lundberg 1997), and if this were the case, one would expect a reduction of mobility with stimulation as the receptor incorporates into caveolae vesicles. The similar value of B_2R diffusion properties in the absence and presence of caveolae with bradykinin stimulation (Figure III-8) additionally support a peripheral localization.

In summary, this study highlights the dependence of diffusion measurements on the geometry of proteins diffusing in membranes and other confined systems. Care must be taken in both the analysis and interpretation.

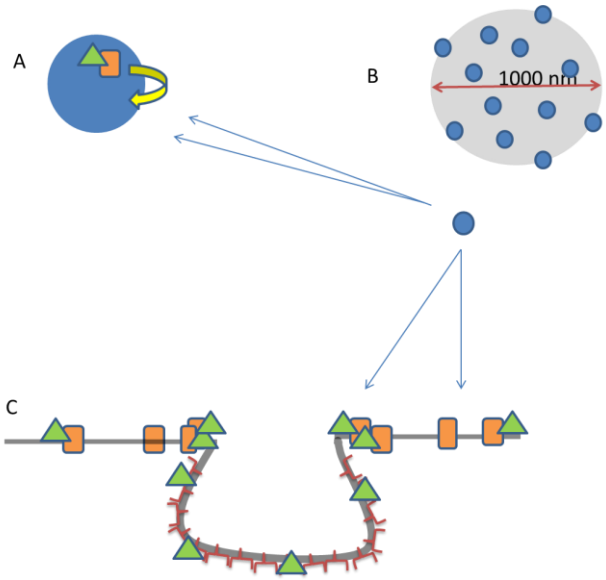

Figure III-7. Cartoon describing our proposed model of B_2R diffusion in the presence of caveolae. **A** B_2R, with its attached $G\alpha_q$ (orange rectangle) is transiently confined to diffuse on the periphery of caveolae (blue dots) due to strong interactions between $G\alpha_q$. **B** Cartoon depicts the illumination diameter in an FCS measurement focused on a plasma membrane region rich in caveolae (blue dots). **C** Side view of a caveolae domain in which B_2R remains in the neck region of the domain.

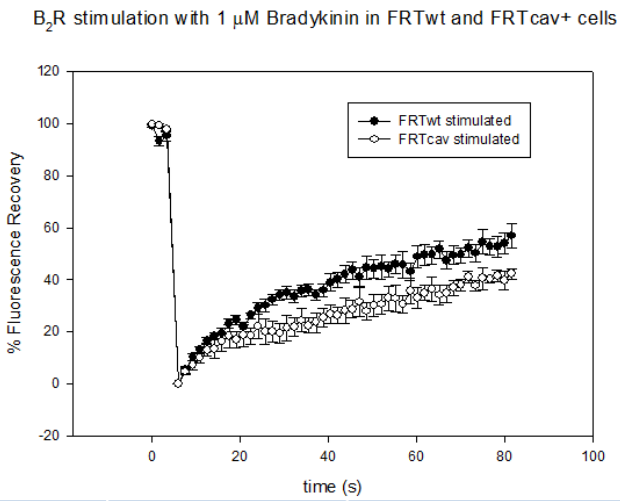

	Cell Type	Mobile Fraction	Diffusion Coefficient	N (cells)
Basal	FRTwt	0.63 ± 0.03	6.8 ± 0.7 x 10^{-11} cm^2/s	13
Basal	FRTcav	0.51 ± 0.03	6.0 ± 0.8 x 10^{-11} cm^2/s	12
Stimulated	FRTwt	0.55 ± 0.03	5.8 ± 0.6 x 10^{-11} cm^2/s	7
Stimulated	FRTcav	0.44 ± 0.04	4.5 ± 0.6 x 10^{-11} cm^2/s	6

Figure III-8. Diffusion of B_2R upon stimulation with bradykinin. Cells were stimulated at t=0 and immediately bleached. Intensities were collected at short times before receptor aggregation and internalization are seen, and less than ~20% of detachment of G proteins (see Philip et al., 2007J.Biol.Chem. 282, 19203). The similarities between the receptor response in FRTwt and FRTcav cells, along with the lack of a large and significant increase in B_2R mobility in FRTcav cells, is consistent with receptor localization

ACKNOWLEGEMENTS

The authors are grateful to Dr. Deborah Brown (Stony Brook University) for providing the FRT cells, to Dr. Lakshmi Devi (Mt. Sinai School of Medicine) for providing the DNA for the receptors and to Dr. Urszula Golebiewska (Queensborough Community College) for her advice. This work was supported by NIH053132.

CHAPTER IV– CONTROL OF THE RECEPTOR GRADIENT ON THE PLASMA MEMBRANE BY CELL SHAPE

ABSTRACT

Micropattern studies have suggested that signaling proteins and microdomains can be controlled by the cell shape and size, but little is known about whether the distribution of membrane bound receptors is influenced by cell shape. We hypothesize that plasma membrane curvature can modulate plasma membrane signal transduction processes. In this study, we use analytical approaches and experimental validation by fluorescence correlation spectroscopy (FCS) and quantitative immunofluorescence to determine the effect of cell shape on growth factor and G-protein coupled receptor (GPCR) signaling. Numerical simulations show the formation of transient microdomains of activated receptors in the cell body versus the cell tip. The formation of microdomains may be due to the balance of reaction-diffusion processes of soluble ligand and membrane-bound receptors along the plane of the membrane. FCS and quantitative imaging of epidermal growth factor receptor (EGFR) and bradykinin 2 receptor (B_2R) show varying diffusion coefficients and receptor concentration in different areas of the cell in elongated cell shapes which is not present in circular cells or a membrane protein that does not interact with an extracellular ligand, supporting the theory that cell shape may induce the transient accumulation of activated receptors in certain regions of the plasma membrane. This membrane heterogeneity may be carried over downstream the signal transduction process.

---

* Parts of the results section were taken from Cell. Rangamani, P et al., (in press) Decoding Information in cell shape.

INTRODUCTION

Maintenance of the cell shape is a complex phenomenon dictated by the interplay of numerous factors including the control of the cytoskeleton (Sheetz 2001, Hall 2012), membrane dynamics (endocytosis and exocytosis) and membrane tension (Diz-Muñoz, Fletcher et al. 2013) and most importantly, the extracellular matrix (ECM) (Geiger, Bershadsky et al. 2001). The cell is highly sensitive to the physical and mechanical cues that it senses from its microenvironment provided by the ECM. One way to mimic and reconstitute the properties of the ECM is by cell micropatterning. Micropatterning is a method wherein a defined cell adhesion pattern is fabricated on a culture substrate (for review see (Théry 2010)). Using this technique, numerous studies have demonstrated that the shape and size of the cellular microenvironment can dictate cell fate. Control of the cellular microenvironment, in particular alignment and constriction, can induce myogene differentiation of bone-marrow derived human mesenchymal stem cells (Yu, Chua et al. 2013). Cell shape and confinement can also influence the development of three-dimensional epithelial polarity by modulating the initial steps in the formation of the central lumen into the apical membrane (Rodríguez-Fraticelli, Auzan et al. 2012, Rodriguez-Fraticelli and Martin-Belmonte 2013) as well as microtubule nucleation and organization (Ghosh, Hentrich et al. 2013). A study on cell locomotion describes the relationship between the divergence angle of the micropattern and the migration speed as well as the relationship between the migration speed and the widths of the micropattern (Yoon, Kim et al. 2012). In turn, cell shape can contain information about signal transduction processes occurring within the cell. For this reason, pathology uses cell morphology as a diagnostic tool to study the disease states of tissues. Cells transformed with oncogenic Ras exhibit fusiform and elongated shape with compact nuclei and a

disrupted cytoskeleton (Kim, Burns et al. 1999), and is tightly coupled to DNA synthesis and growth in non-transformed cells (Folkman and Moscona 1978).

Several studies suggest that signaling proteins and microdomains can be controlled by the cell shape and size (Craske, Fivaz et al. 2005, Schneider, Parrish et al. 2005, Meyers, Craig et al. 2006). Glutamate and electrical stimulation results in the enrichment of PKCγ in synaptic spines and dendritic branches, which have a higher surface to volume ratio, compared to cell soma or thicker branches (Craske, Fivaz et al. 2005). Using a simple mathematical model of the antagonistic reactions of a plasma membrane activator such as a guanine exchange factor and a cytoplasmic deactivator such as a phosphatase, Meyers et al. (Meyers, Craig et al. 2006) demonstrated that as a model cell grows, the cytosolic substrate such as Cdc42 becomes progressively dephosphorylated as a result of decreased proximity to the activator. Conversely, as the cell flattens such as in the case of filopodia and lamellipodia, the substrate is highly phosphorylated. Constraining NIH3T3 fibroblasts on micropattern substrates induces an increase of a retrograde flux of actin cytoskeleton which may translate to downstream processes such as tyrosine phosphorylation (Guo and Wang 2007). For the β-adrenergic/cAMP/PKA/B-Raf/MAPK1,2 signaling cascade, microdomain characteristics are controlled by the cell shape as well as the presence of regulatory circuits and reaction rates (Neves, Tsokas et al. 2008). Using both simulation and experimental approaches, global activation of the β-adrenergic/cAMP/PKA/B-Raf/MAPK1,2 pathway resulted in the accumulation of cAMP microdomains in distal dendrites but little or no increase in cAMP in the cell body. Although the studies above demonstrate the significant role of cell shape on signaling proteins found in the cytosol, the effect of cell shape on cell surface proteins has not been fully explored.

In this dissertation chapter, we ask the question whether cell shape can affect the cell surface distribution of epidermal growth factor receptor (EGFR) and Bradykinin 2 Receptor (B_2R) in the basal and stimulated states. A combination of numerical simulation approach based on reaction-diffusion formulations of activated signaling components (for details, please see (Rangamani, Lipshtat et al. in press)) and experimental validation using fluorescence correlation spectroscopy and quantitative immunofluorescence were used to study the effect of cell shape on the cell surface distribution of EGFR and B_2R. From the numerical simulations, it is hypothesized that the curvature of the plasma membrane results in spatial gradients of signaling components on the plasma membrane. We validate the hypothesis by quantifying the distribution of cell surface receptors and components in different cell shapes in the basal and stimulated states by using fluorescence correlation spectroscopy (FCS) and quantitative immunofluorescence. We look at the Epidermal Growth Factor Receptor (EGFR), Bradykinin-2 Receptor (B_2R) to model the EGFR/Ras/MAPK cascade and GPCR pathways respectively. We use the ellipsoid cell shape which approaches the fusiform shape characteristic of neoplastic transformed cells, while we use the circular shape to model a normal spheroidal cell.

MATERIALS AND METHODS

Materials.

Micropatterned wells were a kind gift of Dr. Ravi Iyengar (Mt. Sinai Medical Center). The micropatterned wells had circular and elliptical wells and were microfabricated with standard photolithography techniques (Qin, Xia et al. 2010).

Cell culture.

COS-7 cells were a kind gift of Dr. Susana Neves (Mt. Sinai Medical Center). A10 cell line (rat aortic smooth muscle cells) from ATCC and COS-7 cell line were maintained at 37 °C in 5 % CO_2 supplemented with 10% FBS (Gemini) and 1 % pennicillin-streptomycin (Gibco). EGFR-eGFP is a kind gift from Dr. Linda Pike (Washington University School of Medicine, MO).

To seed cells on the micropattern, the micropattern coverslips were pre-treated with 500 μg/mL gentamicin (Sigma) and 0.5% pluronic F-127 (Sigma) for 1 hour, and washed with distilled water three times. Cells were reverse transfected with Fugene HD using manufacturer's instructions (Roche Diagnostics, IN). Briefly, EGFR-eGFP and Fugene HD were complexed in a 1:3 μg DNA:μL Fugene ratio and incubated with ~70,000 COS-7 cells in suspension. 36 hours post-transfection, cells were incubated in serum-starving media (DMEM, 0.1% FBS) for 12 hours. At least one hour before stimulation, cells were treated with 10 mM NaN_3, 2 mM NaF and 5 mM 2-deoxy-D-glucose to prevent the ATP-dependent internalization of EGFR (Liu, Sudhaharan et al. 2007).

Diffusion Measurements of EGFR-eGFP in COS-7 cells.

Fluorescence correlation spectroscopy (FCS) measurements were performed on cells expressing EGFR-eGFP using a Zeiss LSM 510 Confocor-2 system equipped with 40x (N.A. 1.2) water immersion objective. eGFP was excited using 488 nm Argon ion laser line and the fluorescence emission was recorded using an avalanche photodiode through a long pass emission

filter. The beam waist, ω_0 amd focal volume were determined using 10 nM rhodamine 6G solution (D = 2.8 x 10^{-6} cm^2/s). The power of the excitation laser was adjusted such that there is sufficient signal to noise ratio and minimal photobleaching. This was achieved using 55% output of a 500 mW maximum output 488 nm argon ion laser and 1% transmittivity. The focal volume was focused on either the cell body, which was aligned with the nucleus, or on the cell tip, designated as within 5 μm from the apex of the cell shape. A Z-axis scan of the cells showed 2 peaks corresponding to the basolateral and apical membrane populations of EGFR-eGFP. The apical peak was chosen for FCS measurements. Each FCS trace was measured for 20s. EGFR was stimulated using 100 ng/ml of EGF. Measurements were started immediately after EGF addition and were completed within 8 minutes. Time traces that showed a decrease or increase of intensity were not used for analysis. Autocorrelation functions were analyzed using a two component, pseudo-two dimensional diffusion model by modifying the three-dimensional fitting routine provided by the Confocor2 software, and setting the structural parameter to quasi-infinite:

$$G(\tau) = {N_{eff}}^{-1}\left(1 + \frac{\tau}{\tau_D}\right)^{-1}\left(1 + \frac{\tau}{S^2\tau_D}\right)^{-1/2}$$

where τ is the correlation time, τ_D the average time a particle spends in the confocal volume, N, the average number of molecules in the confocal volume and S, the structural parameter, where S is set to 100 (quasi-infinite) for 2-D diffusion. Diffusion Coefficient, *D*, is calculated from the τ_D of a molecule using Einstein relation for diffusion: $r^2 = 4D \times \tau_D$ where *r* is the radius of the observation volume.

To quantify the number of EGFR-eGFP on the membrane, N was obtained from the fit, which is the average number of molecules in the confocal volume. To determine the concentration of receptors per unit area, N was divided by the area of the beam waist obtained

through the calibration of the confocal volume with Rhodamine 6G (Elson and Webb 1975, Kim, Heinze et al. 2007).

Quantitative Imaging of Bradykinin-2 Receptor and membrane-marker.

A10 cells which endogenously express Bradykinin 2 Receptor were seeded on the micropattern coverslips which had been pre-treated with 0.5% pluronic F-127 (Sigma), at a density of 70,000 cells/35-mm dish. Before fixing, cells were serum-starved for 12 hours in serum-starving media (DMEM, 0.1 % FBS). Bradykinin-2 Receptor was stimulated with 0.1 µM Bradykinin for 1 min. Cells were fixed for 20 minutes with 3 % paraformaldehyde, 0.1% glutaraldehyde in phosphate buffered saline (PBS). Cells were then permeabilized with 0.2% Triton X-100 for 5 minutes and blocked with 3 % bovine serum albumin. Cells were incubated with polycolonal anti-B_2R (Santa Cruz Biotech, sc-15050) at a concentration of 20 µg/mL for 48 hours at 4 °C, followed by incubation with polyclonal Alexa 647 secondary antibody (Invitrogen) for 30 minutes. After washing, coverslips were mounted using Vectashield mounting media (Vector Laboratories).

To determine the distribution of a membrane marker, A10 cells were transfected with pEYFP-Mem (Clontech), which is a doubly palmitoylated fusion protein consisting of the N-terminal 20 amino acids of GAP43. Cells were transfected with Lipofectamine 2000 using manufacturer's instructions. Briefly, 70,000 cells were incubated with the lipofectamine-DNA complex at a ratio of 0.5 µg pEYFP : 1.5 µL Lipofectamine 2000 for 5 hours and then incubated in complete antibiotic free media (DMEM with 10% FBS). Transfected cells were detached and seeded on the micropattern coverslips after 24 hours and were allowed to attach to the

micropattern for at least 18 hours. Cells were then fixed for 20 minutes with 3% paraformaldehyde, 0.1 % glutaraldehyde in PBS.

Imaging was performed using Zeiss Confocal Laser Scanning Microscope equipped with a 40x (N.A. 1.2) objective and 643 nm HeNe laser. Z-stack were taken using a slice thickness of 0.5 μm.

Images were analyzed using ImageJ (NIH). Briefly, small regions of interest (ROIs) of the same size (0.7 μm circles) were selected on either the tip of the cell (within 5 μm from the cell tip) or the body of the cell (middle of the cell). This was done for over 10 ROIs and the intensities averaged, and then normalized by dividing the average intensities of the region by the average intensity of the entire cell. Comparison of the normalized intensities was performed using rank-sum test using SigmaPlot (Jandel Scientific, Inc.).

Numerical Simulation.

Partial differential equations based on the reaction diffusion system were solved using the Virtual Cell suite (Loew and Schaff 2001). The number of receptors along the curvature of the membrane is modeled as a reaction-diffusion system as Mathieu functions in elliptical coordinates for elongated or ellipsoid cells, and Bessel functions in polar coordinates for circular cell (Rangamani, Lipshtat et al. in press).

RESULTS

Numerical simulations predict a transient accumulation of activated cell surface receptors with an extracellular ligand in the cell body for an elongated cell shape.

In this study, we determine whether cell shape has an effect on the cell surface distribution of receptors in the activated, stimulated state. Numerical simulations were performed by Rangamani et al. (Rangamani, Lipshtat et al. in press) based on reaction-diffusion formulations of a soluble ligand binding to a receptor that diffuses on the plane of the membrane. The plasma membrane distribution of the receptor depends on the diffusion coefficient of the receptor and the k_{on} of the receptor-ligand complex. Based on this mathematical model, numerical simulations were performed on two cell shapes with different eccentricities, ε: a spheroidal cell shape, with ε=0 and an ellipsoid cell shape with ε=0.999. The spheroidal geometry models a normal cell whereas an ellipsoid models the fusiform morphology of a neoplastic transformed cell (Menezes, Miron-Mendoza et al. 2008). The results of the numerical simulation upon receptor activation are shown in Figure IV-1. Figure IV-1A shows the schematic of the theoretical model of an extracellular ligand, A, binding to the cell surface and forming an activated receptor-ligand complex, B, which diffuses on the plane of the membrane. The results of the numerical simulation performed by Virtual Cell, shows the cell surface distribution of receptors in 3D (Figure IV-1B) and 2D (Figure IV-1C) geometries. Results of the simplified 2-D simulations allow us to study the effect of curvature variation along a single axis (Figure IV-1B). The initial distribution of the cell surface receptor was assumed to be uniform on the plane of the plasma membrane, which reflects the basal, unstimulated state. In both 3D and 2D geometries, a

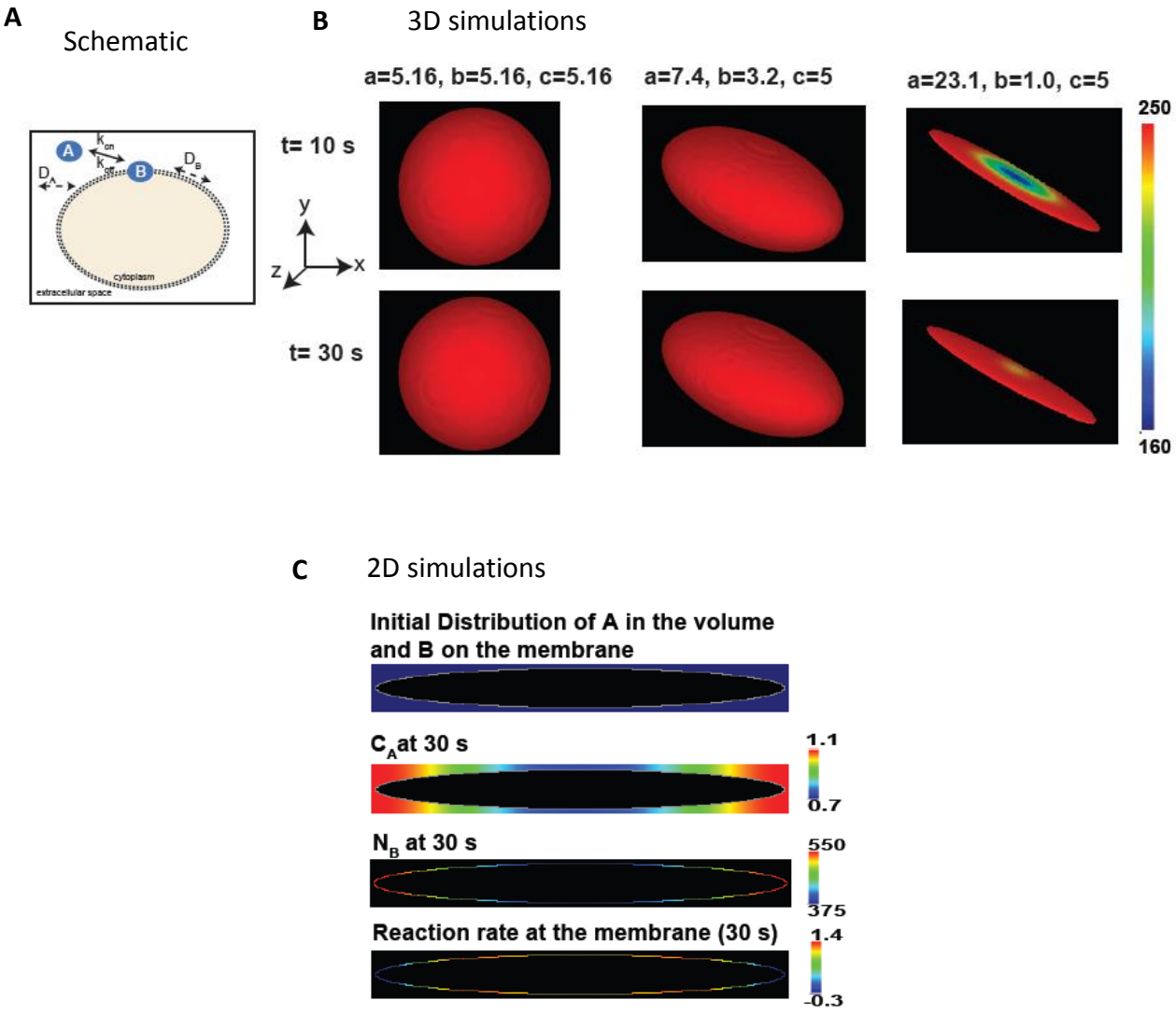

Figure IV-1. A. Numerical simulation of the effect of cell shape on the plasma membrane distribution of cell surface receptors with an extracellular, soluble ligand and a homogenous initial distribution. **A.** The reaction schematic shows the extracellular component A binding to the plasma membrane to form the plasma membrane bound receptor-ligand complex **B.** Cell surface distribution of B in 3D at 10 and 30 s in spherical and ellipsoidal cell shapes. A transient spatial heterogeneity is predicted for the elongated cell shape but not for the spherical cell shape. **C.** Distribution of the extracellular ligand, A and membrane bound receptor-ligand complex, B, in 2D geometry.

transient accumulation of activated receptor in the plasma membrane is predicted in the cell body for ellipsoid geometries, but no transient accumulation of receptors is predicted for a spheroidal cell shape.

Diffusion and concentration of EGFR on different regions of the cell.

We then verified the model experimentally by quantifying the number and concentration of EGFR in both the basal and stimulated states in circular and elliptical cellular geometries. We performed this by growing COS-7 cells transfected with eGFP tagged EGFR in circular and elliptical geometries. We verified that both circular and ellipsoid shapes have the same area (2000 μm^2) in the basal membrane, and the same height (Figure IV-2A). Because of the similarities in heights and areas, a two-dimensional model of the cell can be assumed, as performed in the simulations. We performed fluorescence correlation spectroscopy (FCS) on the tip (defined as within 5 μm from the apex of the cell) and the body of the transfected cell and extracted the diffusion coefficient and number of receptors in the confocal volume from the autocorrelation function. Results are shown in Figure IV-2. An increased diffusion coefficient was observed in the cell tip compared to the cell body in the ellipsoid cells after stimulation, but there was no difference between the diffusion coefficients of the cell tip and cell body in the basal, unstimulated state. We extracted the effective number of EGFR-eGFP (N_{eff}) from the autocorrelation function and estimated the concentration of receptors on the area of the plasma membrane (number of receptors/confocal area) in terms of N_{eff} per confocal volume by assuming a two-dimensional area on the plane of the membrane. For elongated cells, there was a decrease in concentration of EGFR in the stimulated cell tip compared to the unstimulated cell tip, suggesting the presence of a concentration gradient of EGFR-eGFP. For circular cells, no

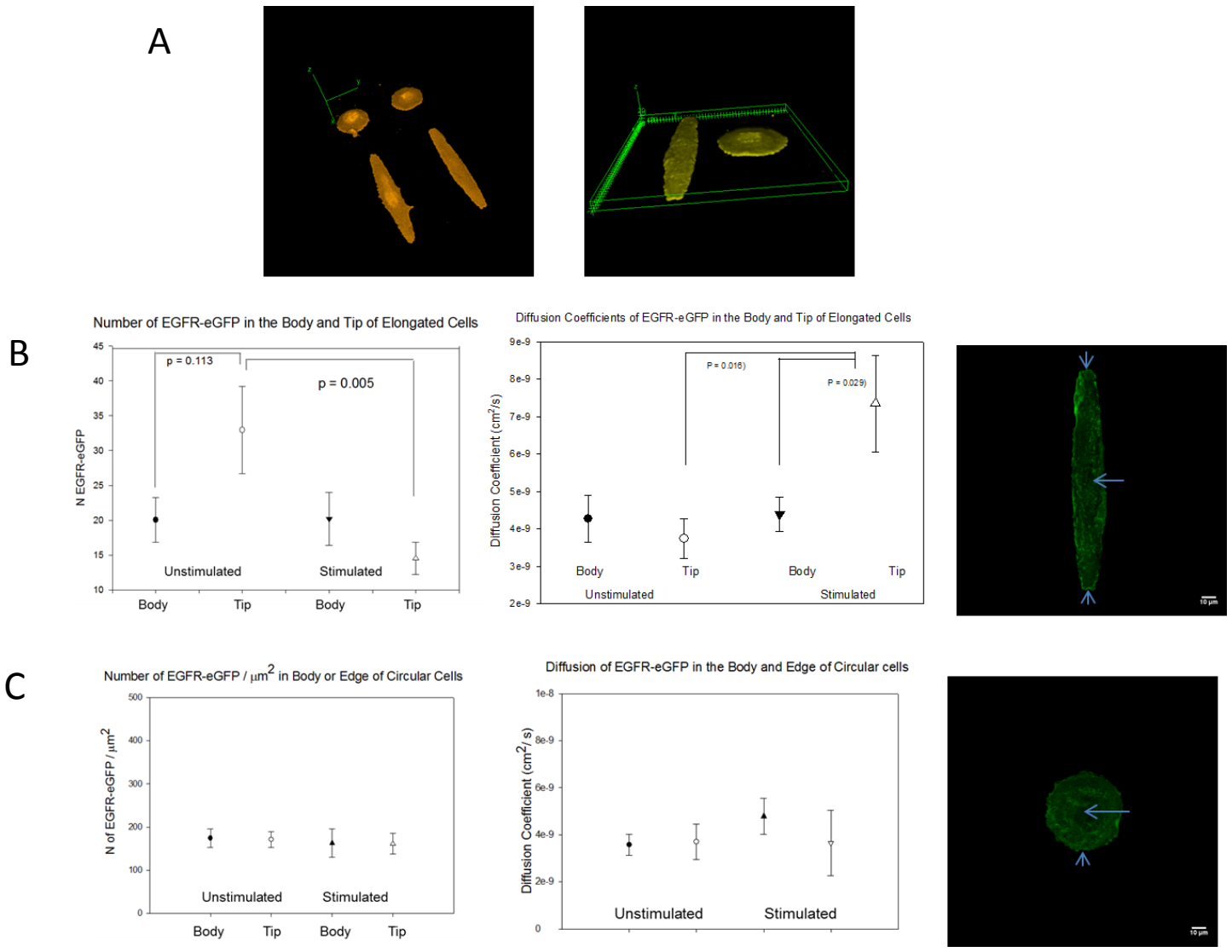

Figure IV-2. A. Volume projection of ellipsoid and circular cell shapes expressing EGFR-eGFP showing similar heights. Number and Diffusion Coefficients extracted from the autocorrelation functions of elliptical (**B**) and spherical cells (**C**). Representative cells showing the sites where the excitation laser was parked for FCS measurement are shown. For elliptical cells, FCS measurements were performed on the cell tip and the cell body, while for circular cells, the measurements were performed on the cell periphery and the cell body.

difference in both diffusion coefficients and number of receptors is observed between the periphery and cell body suggesting that a concentration gradient is absent.

Distribution of B_2R in A10 cells.

The numerical simulations predict that other cell surface receptors which bind to a soluble, extracellular ligand will also have a similar gradient distribution upon stimulation. To determine if this is true in other cell surface proteins, quantitative immunofluorescence was performed on an endogenously expressed G-protein coupled receptor. The probability of artifacts because of protein overexpression is also prevented by looking at endogenous proteins instead of transient overexpression. We chose A10 cells which is a vascular smooth muscle cell line that expresses bradykinin 2-receptor, (B_2R) (Calizo and Scarlata 2012). The amount of B_2R was quantified using immunofluorescence and confocal imaging. We find that at the basal, unstimulated state, there is increased B_2R intensity at the tip of the cell than at the body in ellipsoid cells. The behavior reverses upon stimulation, with the cell body exhibiting increased intensity compared to the cell tip (Figure IV-6). No such difference in distribution was observed in circular cells, when we compared the north-south axis to the east-west axis of the cell in both the stimulated and unstimulated states. This observation is similar with EGFR and agrees with the theoretical model wherein a concentration gradient is observed in greater degree for ellipsoid cell shapes compared to circular cell shapes, even for endogenous G-protein coupled receptors.

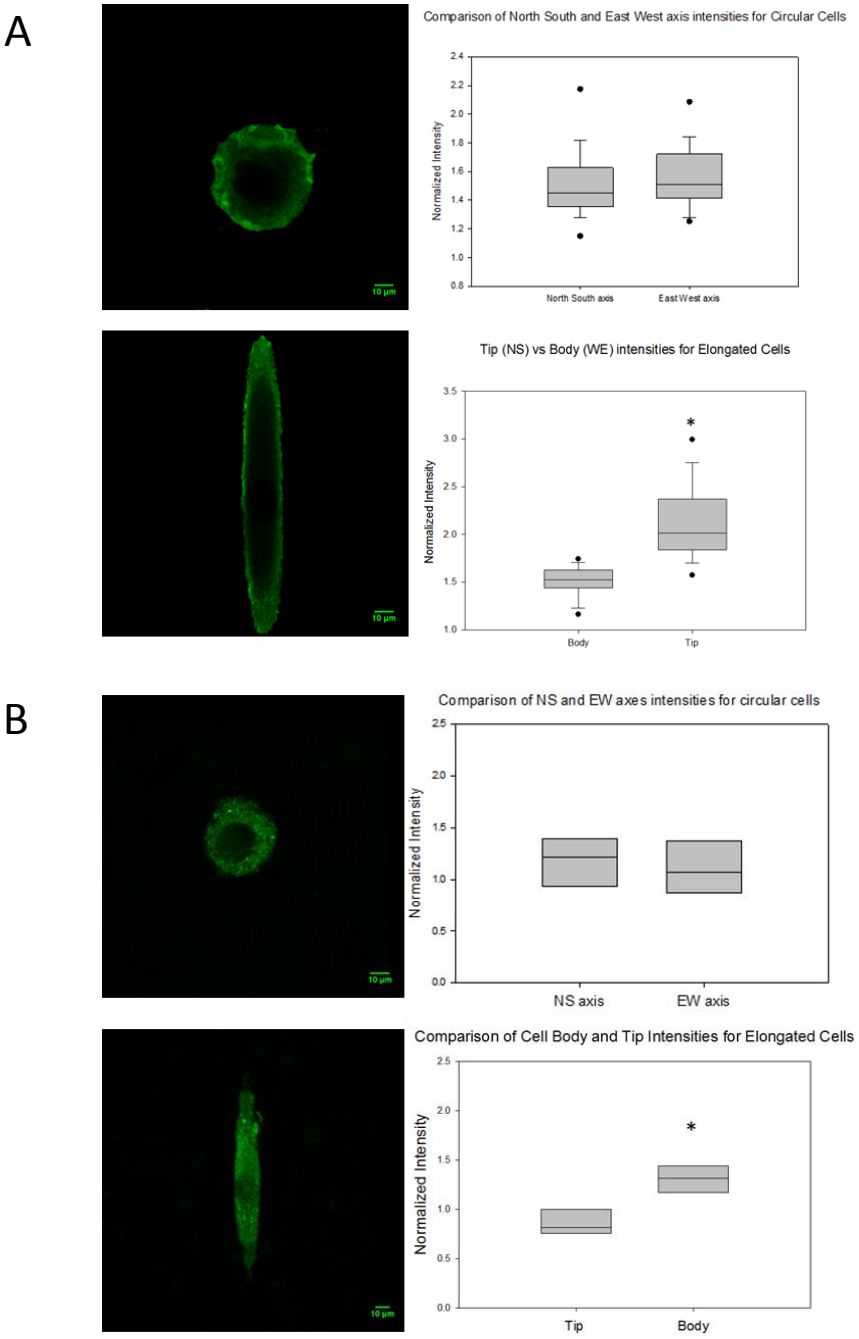

Figure IV-3. A. Comparison of B_2R immunofluorescence intensities in circular and elongated cells in the basal, unstimulated state. Data are shown as box plots of the intensities in the cell body and cell tip of elongated and circular cells, where N = 5 for elongated cells and N = 4 for circular cells. **B.** Same as Figure **3A.** but after stimulation of B_2R with 100 nM of bradykinin. N = 8 for elongated cells and N = 5 for circular cells. Asterisk indicates a statistically significant difference between the cell body and cell tip intensities by Mann-Whitney rank sum test ($p \leq 0.005$).

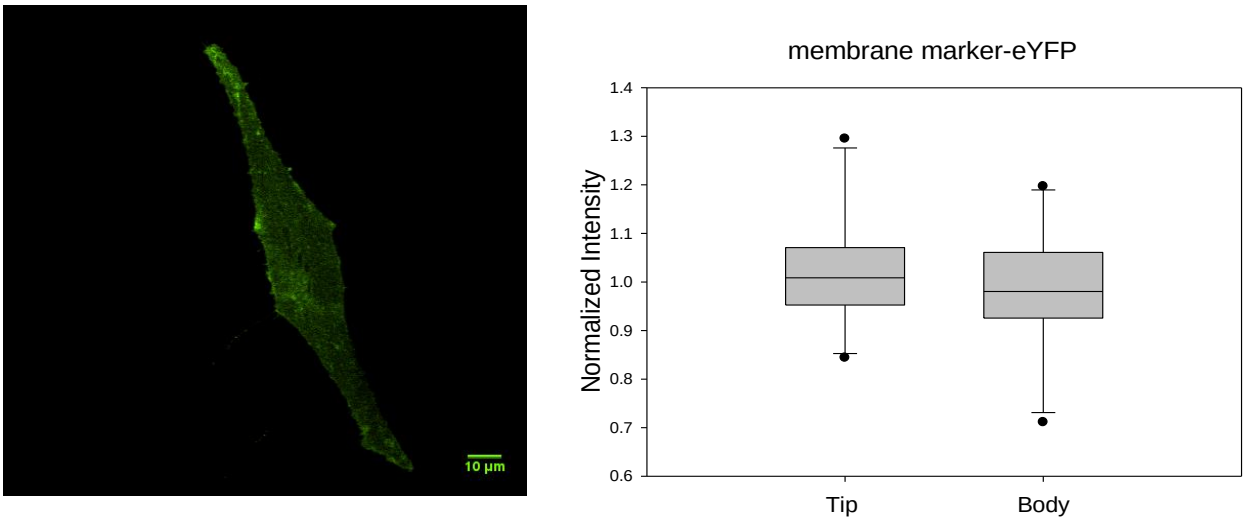

Figure IV-4. Comparison of membrane marker intensities in the body and tip of elongated cells showing no difference in intensities between the body and the tip of elongated cells. Data is shown as a box plot showing the distribution of intensities where N = 10 cells

Mobility and distribution of fluorescently labeled membrane marker in different cell shapes.

We further tested the hypothesis from the numerical simulations in other membrane proteins that are not cell surface receptors. Because of the absence of the soluble extracellular ligands, the model predicts that there will be no concentration gradient on the cell surface. Furthermore, we wanted to verify whether the concentration gradient apparent in our measurements is not an artifact of the cellular geometry. We repeated diffusion and intensity measurements on cells transiently expressing pEYFP-mem, which is a doubly palmitoylated marker with the first 20 amino acids of GAP43 tagged with eYFP. No difference was observed between the diffusion coefficients of pEYFP-mem on the body and tip of elongated cells. Furthermore, no difference was observed between the intensities of pEYFP-mem in the tip and the body in elongated cells. These results suggest that the observed concentration gradient is not due to an artifact of the cellular geometry, and also confirms that cell surface proteins that do not

interact with a soluble, extracellular ligand, do not display the concentration gradient observed in cell surface receptors.

Distribution of Cav1 in A10 cells.

Caveolae have been proposed to be a signaling platform which sequesters a multitude of signaling proteins including G-protein coupled receptors and their downstream signaling components (Anderson 1993, Lisanti, Scherer et al. 1994, Insel, Head et al. 2005). Recently, caveolae's role as a sensor of membrane tension has been suggested in experiments where Cav1 positive structures disassembles under high membrane tension such as hypo-osmolarity (Hill, Bastiani et al. 2008, Liu and Pilch 2008). Cell shape can also cause high membrane tension as the cell conforms to an eccentric shape in the micropattern wells. We determined the effect of cell shape eccentricity on the distribution of Cav1. We quantified the amount of Cav1 at the bottom membrane by converting the images to a binary distribution and quantifying the Cav1 positive spots. We found the typically punctate distribution of Cav1 and were enriched at the cell cortex. A decreased number of Cav1 positive spots were observed in elongated cells compared to circular cells. This data is in accord with the observation that high membrane tension, as can be caused by increased cell eccentricity, can disrupt caveolae domains. Cav1 did not exhibit a concentration gradient of cell surface receptors as with EGFR and B_2R.

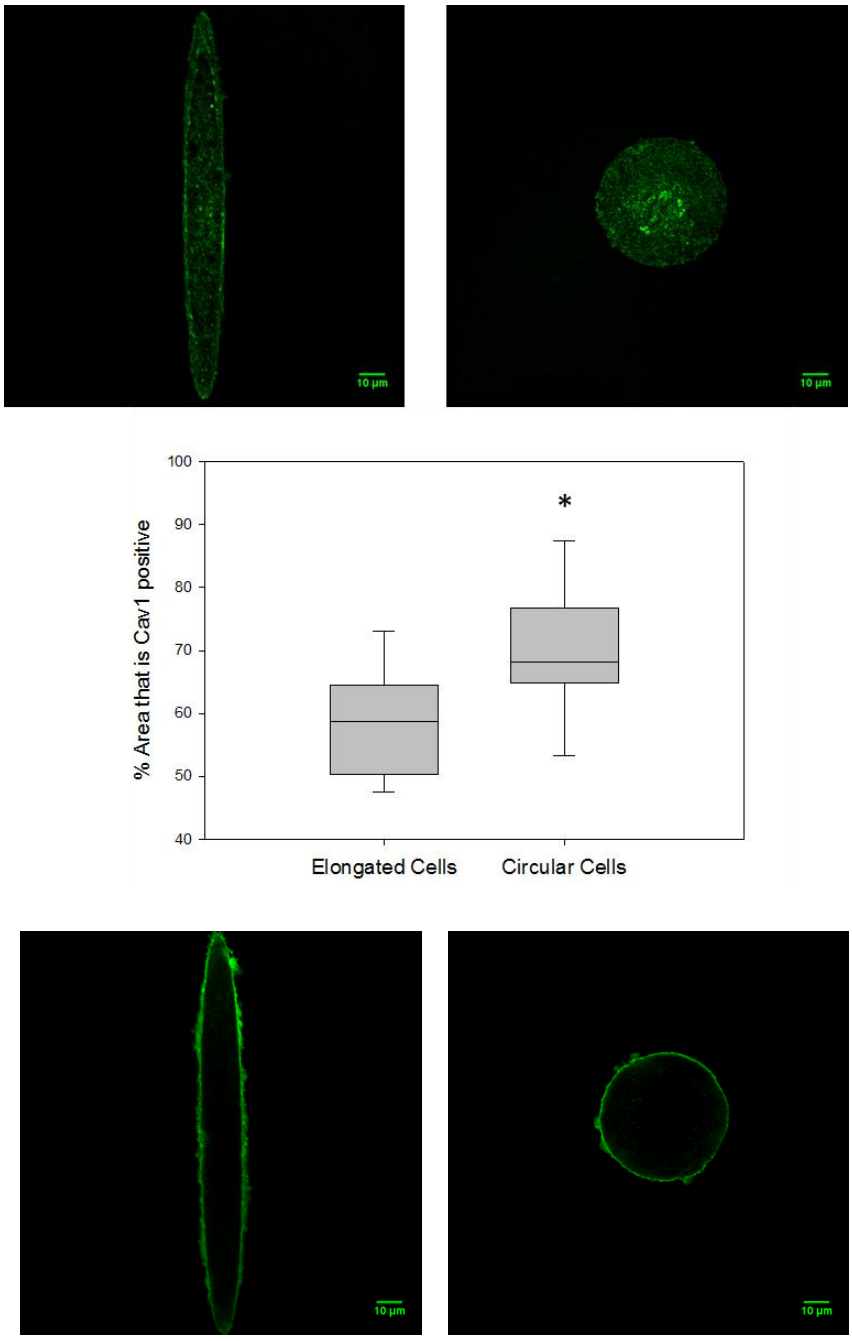

Figure IV-5. A. Comparison of Cav1 marker intensities in elongated and circular cells. Data is shown as a box plot showing the distribution of intensities where N = 16 for elongated cells and N=12 for circular cells. Asterisk indicates a statistically significant difference between the cell body and cell tip intensities by t-test ($p \leq 0.005$). **B.** Actin staining of elongated and circular cells showing that actin is on the cell cortex but is not preferentially distributed on any site on the plasma membrane.

Distribution of actin on different cell shapes.

We wanted to verify whether the distribution of the receptors at the cell tip or the cell body resulted from cytoskeletal rearrangement. To this end, we stained for actin in different cell shapes (Figure IV-5B). We found that actin was enriched on the cell cortex and very little was found on the cell body. However, actin was not sequestered to any particular site in the cell shape. This result suggests that the concentration gradient observed on membrane receptors may not be due to actin rearrangement.

DISCUSSION

In this dissertation chapter, the effect of cell shape on the distribution of cell surface receptors was studied and verified through simulation and micropattern cell culture methods. Numerical simulations and theory support the idea that a concentration gradient of membrane receptor exists on the plasma membrane which increases with the eccentricity of the cell shape. The theoretical basis of this concentration gradient may be the local competition between reaction and diffusion. The balance between the two processes can be described by the Thiele modulus, ϕ_{local}, which is a term used in chemical engineering to characterize processes that involve reaction-diffusion on immobilized surfaces.

$$\Phi_{\text{local}} = R_c \sqrt{\frac{k_{on}}{D_B}}$$

where k_{on} and D_B are the reaction rates and diffusion constants, respectively. The Thiele modulus is a periodic function which depends on, R_c which is defined as the distance from the center of the ellipse to the membrane. For ellipsoid cells, ϕ_{local} fluctuates along the length of the cell shape as R_c changes while for circular cells, R_c is constant and ϕ_{local} does not change along the membrane. As the eccentricity of the ellipsoid increases, the range in the R_c also increases, hence the gradient gets steeper for ellipsoids compared to circular shapes.

The direct relationship of the steepness of the Thiele modulus gradient with eccentricity of the cell shape may explain the transient heterogeneity of activated cell surface receptors in an elongated cell shape, which does not appear to be present in a spherical cell shape.

We tested this for the EGFR/Ras/MAPK1,2 pathway. By fluorescence correlation spectroscopy, we find that an EGFR gradient exists on the plasma membrane in ellipsoidal cells but none exists on the circular cells. MAPK1,2 activity in the nucleus are increased in elliptical cells compared to circular cells, consistent with the model that the plasma membrane gradient will be transmitted in the downstream signaling components (Rangamani, Lipshtat et al. in press). We tested experimentally whether the model holds true for other cell surface proteins that reacts with a soluble, extracellular ligand such as the G-protein coupled receptor B_2R. Using quantitative immunofluorescence, we find that a receptor gradient exists also exists in ellipsoid cells, similar to the EGFR distribution, but none or very little in circular cells and agrees with the results of the simulation. We find that this is not true for membrane marker and Caveolin-1 and this gradient does not seem to arise because of a cytoskeletal rearrangement.

This study provides evidence that cell shape can play a role in signal transduction due to the balance of reaction-diffusion processes on the plane of the membrane. This may provide

another level of regulation of cell surface protein heterogeneity aside from the presence of lipid rafts, cytoskeleton and protein domains such as caveolae. It would be interesting to determine how the combination of the factors mentioned above would modify the gradient dynamics of cell surface proteins. Studies are underway to determine how caveolae domains would influence the G-protein coupled receptor pathway along with cell shape.

ACKNOWLEDGMENTS

This study was performed in collaboration with the laboratory of Dr. Ravi Iyengar (Mt. Sinai Medical Hospital). We would like to thank Dr. Padmini Rangamani for performing all the numerical and theoretical simulations, Dr. Susana Neves and Dr. Evren Azeloglu for the micropattern slides and insightful discussion and suggestions.

CHAPTER V – CONCLUSION,

GENERAL DISCUSSION AND FUTURE DIRECTIONS

The heterogeneity of the plasma membrane can explain many aspects of signal transduction. It can explain the efficiency, divergence, convergence and cross-talk of several signaling pathways. Compartmentalization of signaling components could facilitate the efficiency and direct signal transduction by bringing related signaling molecules in close proximity to each other. Evidence of how membrane heterogeneity influences signaling pathways through lipid domains, PIP_2 microdomains, cytoskeleton corrals and caveolae are just being unveiled in recent years because of the development of techniques that have sufficient spatio-temporal resolution leading to a more detailed understanding of the plasma membrane. In this thesis, we made efforts to elucidate the influence of membrane heterogeneity on $G\alpha_q$ and $G\alpha_i$ signaling pathways by using a variety of fluorescent and imaging experiments that have sufficient temporal resolution (FCS) and nanometer sensitivity (FRET microscopy). We also included the epidermal growth factor signaling pathway. We were able to demonstrate that the nanoscale heterogeneity of the plasma membrane (i.e. caveolae domains) was able to influence the G-protein signaling pathway. We also find that the cell microenvironment and shape also exerts control on the distribution of plasma membrane proteins. The effects of these membrane heterogeneities can propagate downstream the signaling cascade and may ultimately dictate cell fate.

Our initial aim was to determine whether all or some G-protein coupled receptors localize to caveolae domains. Furthermore, we wanted to determine whether caveolae domains would

affect the secondary messenger signaling downstream of the GPCR pathway. These aims are described and discussed in the second chapter of this thesis. We looked at two representative GPCR pathways: the B_2R / $G\alpha_q$ / PLCβ and the μOR / $G\alpha_i$ / AC pathways. We find that GPCRs have different tendencies to localize to caveolae domains: a significant population (~20%) of B_2R is sequestered in caveolae domains, while none or very little μOR is close to caveolae domains. $G\alpha_q$ has two-fold higher FRET efficiency suggesting that it interacts more with Cav1 than the receptor to which it is coupled to, B_2R. We hypothesized that $G\alpha_q$ may act as a scaffold between B_2R and Cav1 and tested this by disrupting the interaction of $G\alpha_q$ and Cav1, and measuring the FRET between Cav1 and B_2R. Disruption of the interaction between $G\alpha_q$ and Cav1 was achieved either by microinjection of a peptide that competes with the binding between $G\alpha_q$ and Cav1, or through siRNA mediated downregulation of $G\alpha_q$. The decrease in FRET between B_2R and Cav1 upon disruption of $G\alpha_q$–Cav1 interaction supports the hypothesis that $G\alpha_q$ may scaffold B_2R to caveolae domains. The interaction of B_2R or $G\alpha_q$ with Cav1 impacts the function of this pathway as evidenced by an increased magnitude and duration of Ca^{2+} response in the presence of Cav1. The same behavior is seen in other $G\alpha_q$ pathways such as the muscarinic and histamine receptor pathways, where the Ca^{2+} response was enhanced by the presence of caveolae. The study makes the prediction that $G\alpha_q$ coupled GPCRs are more likely to localize in caveolae domains and functionally be affected by the presence of caveolae domains. It would be interesting to see if other $G\alpha_q$ and $G\alpha_i$ coupled receptors that were not tested in this study would exhibit the same increase in intracellular Ca^{2+} release in the presence of caveolae and the same degree of proximity to caveolae domains.

Many GPCRs have been reported to localize to caveolae domains (Chini and Parenti 2004) but the mechanism of their localization is not well understood. The initial hypothesis was

that receptors may direct themselves to caveolae domains, bringing with them their intracellular binding partners. From our observations, we found that the reverse is true wherein G proteins can direct the receptors to membrane domains.

What is the basis of sequestration of signaling proteins in caveolae domains? The presence of a caveolin binding motif (CBM) in the signaling protein may sequester it to caveolae via the caveolin scaffolding domain (CSD) (Couet, Li et al. 1997). B_2R, μOR, $G\alpha_q$, and $G\alpha_i$ all have a caveolin binding motifs. Both B_2R and μOR have the caveolin binding motif on their C-termini which may interact with Cav1 molecules on the inner leaflet of the plasma membrane. For $G\alpha_i$ the caveolin-scaffolding domain is located in one of the β-strands in the Ras-like domain, while for $G\alpha_q$ the region is in a linker region between two alpha helices in the Ras-like domain towards the C-terminus. This region is exposed even when it is bound to PLCβ and may be accessible for Cav1 binding.

For future studies, the Cav1 interacting region of $G\alpha_q$ may be swapped with the corresponding C-terminal region of $G\alpha_i$ and see if this chimera would still exhibit FRET with Cav1. We can also determine whether the presence of this chimera would remove the population of B_2R associated with caveolae.

Another possible mechanism of sequestration may be though lipid modification of the proteins. Many signaling proteins are lipid modified to facilitate membrane anchorage and to bring them closer to their membrane bound substrates. As most Class A GPCRs, both B_2R and μOR contain the CAAX box palmitoylation sites on their C-terminal domain. Although this site has not been shown to be palmitoylated in the case of μOR, this sequence has been shown to be palmitoylated in the case of B_2R by mass spectrometry.

The activity and localization of G-proteins are highly dependent on lipid modification. $G\alpha_i$ is a substrate for N-myristolyation through N-myristoyl transferase, but $G\alpha_s$, $G\alpha_q$, $G\alpha_{12}$ are not. $G\alpha_i$ may also be palmitoylated on its N-terminus but this process is dependent on its myristoylation state. While myristoylation increases the hydrophobicity of $G\alpha_i$, it has been shown to be insufficient for membrane attachment (Peitzsch and McLaughlin 1993), and may require palmitoylation or interaction with geranylgeranylated $G\beta\gamma$. In the case of $G\alpha_i$, palmitoylation and interaction with $G\beta\gamma$ are two redundant mechanisms to target $G\alpha_i$ to the membrane.

For $G\alpha_q$ and $G\alpha_s$, palmitoylation is the sole fatty acid modification. As opposed to myristoylation, palmitoylation is reversible and is not required for membrane anchorage of both $G\alpha_q$ and $G\alpha_s$. Palmitoylation is necessary for the function of G-proteins. Non-palmitoylated mutants of $G\alpha_q$ have a reduced ability to activate PLCβ in vitro. It is possible that palmitoylation may serve two different functions for the $G\alpha_q$ and $G\alpha_i$; for $G\alpha_i$ palmitoylation occurs for membrane anchorage, a function which is redundant to that of $G\beta\gamma$, while for $G\alpha_q$ and $G\alpha_s$, palmitoylation modifies their function or association with other plasma membrane proteins. $G\alpha_q$ is doubly palmitoylated at cysteines 9 and 10 (Wedegaertner, Chu et al. 1993). Dual palmitoylation has been shown to play a role in the partitioning of proteins into cholesterol rich domains such as caveolae. Therefore, the double palmitoylation of $G\alpha_q$ may play a role in its own partitioning, as well as its upstream receptor, to caveolae domains. Since $G\alpha_s$ is also dually palmitoylated (Kleuss and Krause 2003) and several $G\alpha_s$ receptors also localize to caveolae domains, it would also be interesting to test whether $G\alpha_s$ coupled receptors localize to caveolae domains through their $G\alpha_s$ binding partners.

How is intracellular calcium release potentiated by the presence of caveolae domains? The second chapter of this dissertation, along with previous studies (Sengupta, Philip et al. 2008, Guo, Golebiewska et al. 2011) suggest that Cav1 may stabilize the activated state of $G\alpha_q$ and prolong the recombination time of the heterotrimer. These results are consistent with the increased magnitude and duration of calcium release in the presence of Cav1. While this explanation may be consistent with the results, other possible explanations may exist. Several downstream effectors may be concentrated in caveolae domains leading to their increased activity. While PLCβ does not appear to be sequestered in caveolae domains, PIP_2 substrates have been found to localize in caveolae domains (Pike and Casey 1996, Fujita, Cheng et al. 2009). PIP_2 has been shown to localize in the neck region of caveolae domains (Fujita, Cheng et al. 2009) suggesting that the neck region may be a specialized subdomain. Furthermore, several calcium signaling proteins have been found to localize in caveolae domains such as ion channels and STIM (Isshiki and Anderson 1999, Daniel, El-Yazbi et al. 2006, Pani and Singh 2009). The activation of G-proteins may stimulate certain ion channels and increase calcium flux. All of these observations reinforce the idea that caveolae are important sites of calcium signaling as proposed by other groups.

In this study, we have used FRET microscopy techniques to study nanometer-sized domains. Although FRET is sensitive to proximity related changes in the order of 5-10 nm, one concern with FRET microscopy is that caveolae domains are diffraction limited, such that one pixel observed in this particular FRET microscopy method might correspond to an area of the membrane that is much bigger than the caveolae themselves resulting in a broadening of the FRET values. The pixel size of our FRET microscope is in the order of 167 nm, which is twice as big as caveolae domains. One way to overcome this limitation is through the use of super-

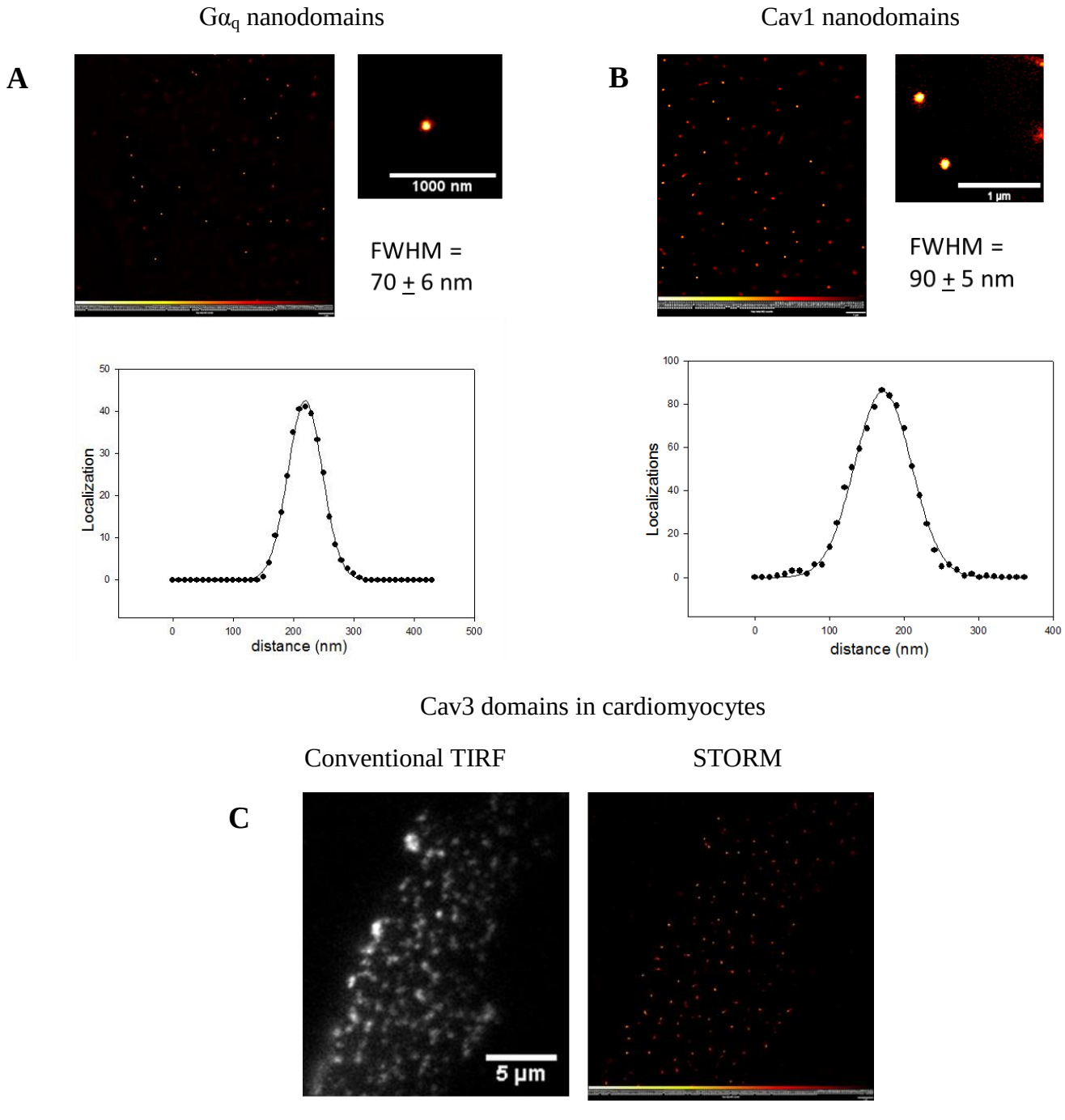

Figure V-1. Caveolin-1 and $G\alpha_q$ form similarly sized domains on the membrane surface of A10 muscle cell line as seen in super-resolution imaging. STORM imaging of **A** $G\alpha_q$ and **B** Cav1 showing ~90 nm and ~70 nm nanodomains respectively. **C** Comparison of TIRF and STORM images of Cav3 on cardiomyocytes.

resolution imaging which improves the resolution of fluorescence microscopy techniques to 20-30 nm which is ideal for the size of caveolae domains. We have attempted to perform super-resolution microscopy by using stochastic optical reconstruction microscopy (STORM) (Rust, Bates et al. 2006, Huang, Bates et al. 2009). In this method, organic fluorophores such as oxazine and rhodamine dyes are induced to stochastically blink, resulting in a sparse population of fluorophores that are on at a given acquisition frame. The exact location of each spot is obtained by assuming a Gaussian distribution of the light emitted by the single molecule fluorophore. The process is iterated until a dataset consisting of thousands of frames each containing a sparse number of molecules is acquired and each spot localized, and gives a super-resolution image. We performed preliminary STORM studies looking at Cav1 and $G\alpha_q$. With Cav1, we were able to reconstruct images that showed 70 nm sized clusters which is approximately the size of caveolae domains (Figure V-1). We compared this with $G\alpha_q$ and obtained similarly sized clusters (~80 nm). The similarly sized clusters suggest that both proteins form microdomains. Whether they are in the same clusters or not may be answered by performing super-resolution colocalization with two color dyes. Another complication of the STORM technique is that the cup-shaped geometry of caveolae domains may give rise to out of focus light that may not be resolved using the STORM technique. For future directions, it would interesting to determine whether the two-proteins indeed colocalize by performing 2-color STORM in 3D.

In the third chapter, we determined the influence of caveolae domains on the mobilities of G-protein coupled receptors. The diffusion properties of the B_2R / $G\alpha_q$ and μOR / $G\alpha_i$ were compared in the presence and absence of caveolae domains. We have used two diffusion methods that were expected to give complementary results: FRAP, which requires the photobleaching of fluorescently tagged proteins and measurement of the rate of recovery of the

unbleached population into the bleached spot, and FCS, which measures the diffusion coefficient of a fluorophore as it moves in and out of a small excitation volume. A small (~10%) decrease in the mobile fraction extracted from FRAP measurements was observed in FRTcav+ cells compared to FRTwt cells for both B_2R and μOR receptors, but no difference in mobile fractions was observed between FRTwt and FRTcav+ for mm-eYFP and $G\alpha_q$. We attribute this decrease in mobile fractions of B_2R and μOR in the presence of caveolae, as caveolae acting as diffusion barriers for transmembrane proteins but not for peripheral membrane proteins. However, in FCS measurements, B_2R and $G\alpha_q$ exhibited faster diffusion coefficients in the presence of caveolae while the distribution of mobilities of μOR and $G\alpha_i$ were not changed in the presence of caveolae. Instead of exhibiting a reduced diffusion coefficient because of interaction with Cav1 domains as discussed in the first chapters, membrane proteins such as B_2R and $G\alpha_q$ that interact with Cav1 exhibited higher mobilities in FCS. Caveolae slowed down the doubly palmitoylated membrane marker, pEYFP-Mem. Interestingly, this membrane marker has the first 20 amino acids of GAP-43 which localize to lipid rafts by virtue of its double palmitoylation motif. Therefore, the behavior of pEYFP-Mem is not surprising since Cav1 may also stabilize both planar and nonplanar lipid rafts. We propose that the geometry of caveolae gives rise to a confined diffusion of its attached membrane proteins resulting in an apparent increase in mobility.

From the conclusions drawn from chapter 2 and 3, we propose a model of how caveolae may sequester GPCR and intracellular binding partners (Figure V-2): Some GPCRs, such as the $G\alpha_i$ coupled μOR, does not have any affinity for caveolae domains, by virtue of their Gα subunits which do not have preferential interactions with Cav1 and are not sequestered to caveolae domains. $G\alpha_q$, through its specific molecular interaction with Cav1, can scaffold

receptors to caveolae domains. The lower FRET values between B_2R and Cav1 compared to $G\alpha_q$ and Cav1 suggests that the receptors are located farther away from Cav1 molecules than $G\alpha_q$. We propose that the receptors are concentrated in the neck region / periphery of caveolae domains while $G\alpha_q$, can easily access the caveolae bulb. The population of receptors that interact with Cav1 domains may be confined in the periphery of caveolae domains and exhibit an anomalous diffusion resulting in an increased apparent diffusion coefficient, despite its interaction or sequestration by caveolae. Furthermore, $G\alpha_q$, a peripheral membrane protein, does not exhibit entrapment in caveolae domains and can detach and attach to the caveolae surface with no significant change in mobile fraction as seen in the FRAP results. Although other models are plausible, we believe that this model can explain the results that we have seen in Chapter 2 and 3.

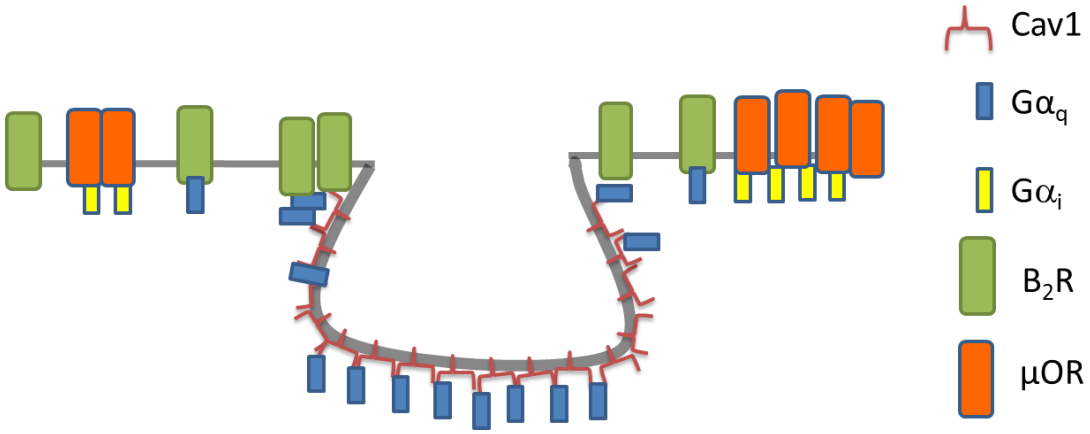

Figure V-2. Proposed model of caveolae sequestration of GPCRs and intracellular binding partners: G proteins mediate receptor association with caveolae domains. GPCRs coupled to $G\alpha_q$ might interact more extensively with cav1 than receptors coupled to $G\alpha_i$. The localizing effect of these proteins by caveolae increases their signaling potential.

The current model for the function of caveolae domains is a membrane mechanosensor that could disassemble during states of high membrane tension. If membrane tension can disassemble caveolae domains, it can also perturb the interactions between Cav1 and protein complexes that are attached to Cav1 domains, such as $G\alpha_q$ and its corresponding receptors. The B_2R / $G\alpha_q$ pathway is involved in mechanosensing in endothelial and vascular smooth muscle cells which exhibits elevated IP_3, cGMP, PGI_2 and NO (Gudi, Clark et al. 1996). It can therefore be hypothesized that membrane tension may alter the number of caveolae domains which in turn can alter the B_2R / $G\alpha_q$ signaling pathway. Furthermore, an agonist-independent activation of $G\alpha_q$ due to membrane stretch may occur and the presence of caveolae domains may alter their signaling properties. It would be interesting to find out how caveolae can modify the membrane tension sensed by the cell through $G\alpha_q$ pathways.

On the fourth chapter, the role of cell shape on membrane heterogeneity is explored. Using quantitative fluorescence, we were able to show that membrane receptors (EGFR and B_2R) are not uniformly distributed along the plane of the membrane, but may accumulate transiently at certain regions of the cell, such as the cell body. Experimentally, different cell shapes were achieved by using micropattern technology and performing quantitative fluorescence studies on the cells that have conformed to a particular cell shape. The theoretical basis of this concentration gradient is the balance of reaction-diffusion processes. The concentration gradient of signaling proteins on the plasma membrane may be carried over to the downstream signaling cascade resulting in the formation of signaling microdomains in the cytosol. Furthermore, we found that increasing the membrane tension such as increasing the eccentricity of cell shape affects the number of caveolae. If caveolae are sites which concentrate

signaling proteins, the effect of cell shape could impact the number of signalosomes on the membrane and affect the downstream signaling pathways.

The control of cell shape on the signal transduction of G-protein coupled receptors adds another layer of regulation and complexity in the control of membrane domains, aside from well-established factors such as lipids, proteins and the cytoskeleton.

For future studies it would be interesting to find out the effect of plasma membrane components in combination with the effects of cell shape. We would like to determine the role of membrane heterogeneities in either increasing or decreasing the effects of cell shape on membrane signal transduction. The effects of the cytoskeletal proteins such as actin on the formation of plasma membrane microdomains may be studied as well. It would also be interesting to determine the effect of cell shape on the downstream signaling components of B_2R / $G\alpha_q$ / PLCβ pathway. In particular, what is the effect of cell shape on the secondary messengers calcium and IP_3? We can hypothesize that an elongated cell shape, or a shape with a higher surface to volume ratio will cause the formation of calcium microdomains, which may be visualized using live cell imaging. Since we do not yet know the duration of these microdomains inside the cell, and may exist only for a few seconds, these experiments would benefit from techniques that have high temporal resolution.

LITERATURE CITED

Alberts, B., D. Bray, J. Lewis, M. Raff, K. Roberts and J. Watson (1994). Molecular Biology of the Cell. New York, Garland.

Alexrod, D., D. Koppel, J. Schlessinger, E. Elson and W. Webb (1976). "Mobility measurements by analysis of fluorescence photobleaching recovery kinetics." Biophys.J. **16**: 1055-1069.

Anderson, R. G. (1993). "Caveolae: where incoming and outgoing messengers meet." Proceedings of the National Academy of Sciences **90**(23): 10909-10913.

Anderson, R. G. (1998). "The caveolae membrane system." Annu.Rev.Biochem. **67**: 199-225.

Anderson, R. G. (1998). The caveolae membrane system. Annual review of biochemistry. **67:** 199-225.

Bachvarov, D. R., S. Houle, M. Bachvarova, J. Bouthillier, A. Adam and F. Marceau (2001). "Bradykinin B(2) receptor endocytosis, recycling, and down-regulation assessed using green fluorescent protein conjugates." J Pharmacol Exp Ther **297**(1): 19-26.

Bastiani, M., L. Liu, M. M. Hill, M. P. Jedrychowski, S. J. Nixon, H. P. Lo, D. Abankwa, R. Luetterforst, M. Fernandez-Rojo, M. R. Breen, S. P. Gygi, J. Vinten, P. J. Walser, K. N. North, J. F. Hancock, P. F. Pilch and R. G. Parton (2009). "MURC/Cavin-4 and cavin family members form tissue-specific caveolar complexes." The Journal of Cell Biology **185**(7): 1259-1273.

Bastiani, M. and R. G. Parton (2010). "Caveolae at a glance." Journal of Cell Science **123**(22): 3831-3836.

Berg, K. A., G. Zardeneta, K. M. Hargreaves, W. P. Clarke and S. B. Milam (2007). "Integrins regulate opioid receptor signaling in trigeminal ganglion neurons." Neuroscience **144**(3): 889-897.

Boucrot, E., M. T. Howes, T. Kirchhausen and R. G. Parton (2011). "Redistribution of caveolae during mitosis." Journal of Cell Science **124**(12): 1965-1972.

Breen, M. R., M. Camps, F. Carvalho-Simoes, A. Zorzano and P. F. Pilch (2012). "Cholesterol Depletion in Adipocytes Causes Caveolae Collapse Concomitant with Proteosomal Degradation of Cavin-2 in a Switch-Like Fashion." PLoS ONE **7**(4): e34516.

Brock, R., M. A. Hink and T. M. Jovin (1998). "Fluorescence Correlation Microscopy of Cells in the Presence of Autofluorescence." Biophysical journal **75**(5): 2547-2557.

Brown, D. A. (2006). "Lipid Rafts, Detergent-Resistant Membranes, and Raft Targeting Signals." Physiology **21**(6): 430-439.

Brown, D. A. and E. London (1998). "FUNCTIONS OF LIPID RAFTS IN BIOLOGICAL MEMBRANES." Annual Review of Cell and Developmental Biology **14**(1): 111-136.

Burch, R. M. and J. Axelrod (1987). "Dissociation of bradykinin-induced prostaglandin formation from phosphatidylinositol turnover in Swiss 3T3 fibroblasts: evidence for G protein regulation of phospholipase A2." Proceedings of the National Academy of Sciences **84**(18): 6374-6378.

Cabrera-Vera, T. M., J. Vanhauwe, T. O. Thomas, M. Medkova, A. Preininger, M. R. Mazzoni and H. E. Hamm (2003). "Insights into G Protein Structure, Function, and Regulation." Endocrine Reviews **24**(6): 765-781.

Calizo, R. C. and S. Scarlata (2012). "A Role for G-Proteins in Directing G-Protein-Coupled Receptor–Caveolae Localization." Biochemistry **51**(47): 9513-9523.

Cézanne, L., S. Lecat, B. Lagane, C. Millot, J.-Y. Vollmer, H. Matthes, J.-L. Galzi and A. Lopez (2004). "Dynamic Confinement of NK2 Receptors in the Plasma Membrane: IMPROVED FRAP ANALYSIS AND BIOLOGICAL RELEVANCE." Journal of Biological Chemistry **279**(43): 45057-45067.

Chang, W. J., Y. S. Ying, K. G. Rothberg, N. M. Hooper, A. J. Turner, H. A. Gambliel, J. De Gunzburg, S. M. Mumby, A. G. Gilman and R. G. Anderson (1994). "Purification and characterization of smooth muscle cell caveolae." The Journal of Cell Biology **126**(1): 127-138.

Chen, C. A. and D. R. Manning (2001). "Regulation of G proteins by covalent modification." Oncogene **20**(No. 13): 1643-1652.

Chen, Y., M. Elangovan and A. Periasamy (2005). FRET Data Analysis: The Algorithm. Molecular Imaging: FRET Microscopy and Spectroscopy. P. a. Day. New YorkOxford University Press**:** Chap. 7.

Chini, B. and M. Parenti (2004). "G-protein coupled receptors in lipid rafts and caveolae: how, when and why do they go there?" J Mol Endocrinol **32**(2): 325-338.

Chun, M., U. K. Liyanage, M. P. Lisanti and H. F. Lodish (1994). "Signal transduction of a G protein-coupled receptor in caveolae: colocalization of endothelin and its receptor with caveolin." Proceedings of the National Academy of Sciences **91**(24): 11728-11732.

Couet, J., S. Li, T. Okamoto, T. Ikezu and M. Lisanti (1997). "Identification of peptide and protein ligands for the caveolin-scaffolding domain. Implications for the interaction of caveolin with caveolae-associated proteins." J Biol Chem **272**: 6525 - 6533.

Craske, M. L., M. Fivaz, N. N. Batada and T. Meyer (2005). "Spines and neurite branches function as geometric attractors that enhance protein kinase C action." The Journal of Cell Biology **170**(7): 1147-1158.

Dalal, R. B., M. A. Digman, A. F. Horwitz, V. Vetri and E. Gratton (2008). "Determination of Particle Number and Brightness Using a Laser Scanning Confocal Microscope Operating in the Analog Mode." Microscopy Research and Technique **81**: 69-81.

Daniel, E. E., A. El-Yazbi and W. J. Cho (2006). "Caveolae and calcium handling, a review and a hypothesis." Journal of Cellular and Molecular Medicine **10**(2): 529-544.

de Weerd, W. and L. Leeb-Lundberg (1997). "Bradykinin sequesters B2 bradykinin receptors and the receptor coupled G alpha sunuits G alpha(q) and G alpha (i) in caveolae in DDT1 MF-2 smooth muscle cells." Journal of Biological Chemistry **272**: 17858-17866.

de Weerd, W. F. C. and L. M. F. Leeb-Lundberg (1997). "Bradykinin Sequesters B2 Bradykinin Receptors and the Receptor-coupled Gα Subunits Gαq and Gαiin Caveolae in DDT1 MF-2 Smooth Muscle Cells." Journal of Biological Chemistry **272**(28): 17858-17866.

Defer, N., M. Best-Belpomme and J. Hanoune (2000). "Tissue specificity and physiological relevance of various isoforms of adenylyl cyclase." American Journal of Physiology - Renal Physiology **279**(3): F400-F416.

Dessy, C., R. A. Kelly, J.-L. Balligand and O. Feron (2000). "Dynamin mediates caveolar sequestration of muscarinic cholinergic receptors and alteration in NO signaling." EMBO J **19**(16): 4272-4280.

Dietzen, D., W. Hastings and D. Lublin (1995). "Caveolin is palmitoylated on multiple cysteine residues: palmitoylation is not necessary for localization of caveolin to caveolae." J Biol Chem **270**: 6838 - 6842.

Digman, M. A., P. W. Wiseman, C. Choi, A. R. Horwitz and E. Gratton (2009). "Stoichiometry of molecular complexes at adhesions in living cells." PNAS **106**: 1-6.

Diz-Muñoz, A., D. A. Fletcher and O. D. Weiner (2013). "Use the force: membrane tension as an organizer of cell shape and motility." Trends in Cell Biology **23**(2): 47-53.

Dowal, L., P. Provitera and S. Scarlata (2006). "Stable association between G alpha(q) and phospholipase C beta 1 in living cells." J Biol Chem **281**(33): 23999-24014.

Downes, G. B. and N. Gautam (1999). "The G Protein Subunit Gene Families." Genomics **62**(3): 544-552.

Drab, M., P. Verkade, M. Elger, M. Kasper, M. Lohn, B. Lauterbach, J. Menne, C. Lindschau, F. Mende, F. C. Luft, A. Schedl, H. Haller and T. V. Kurzchalia (2001). "Loss of Caveolae,

Vascular Dysfunction, and Pulmonary Defects in Caveolin-1 Gene-Disrupted Mice." Science **293**(5539): 2449-2452.

Dreja, K., M. Voldstedlund, J. Vinten, J. Tranum-Jensen, P. Hellstrand and K. Sward (2002). "Cholesterol Depletion Disrupts Caveolae and Differentially Impairs Agonist-Induced Arterial Contraction." Arterioscler Thromb Vasc Biol **22**(8): 1267-1272.

Drmota, T., J. Novotny, G. W. Gould, P. Svoboda and G. Milligan (1999). "Visualization of distinct patterns of subcellular redistribution of the thyrotropin-releasing hormone receptor-1 and gqalpha /G11alpha induced by agonist stimulation." Biochem. J. **340**(2): 529-538.

Elson, E. L. and W. W. Webb (1975). "Concentration Correlation Spectroscopy: A New Biophysical Probe Based on Occupation Number Fluctuations." Annual Review of Biophysics and Bioengineering **4**(1): 311-334.

Engelman, J. A., C. C. Wykoff, S. Yasuhara, K. S. Song, T. Okamoto and M. P. Lisanti (1997). "Recombinant Expression of Caveolin-1 in Oncogenically Transformed Cells Abrogates Anchorage-independent Growth." Journal of Biological Chemistry **272**(26): 16374-16381.

Faussner, A., J. M. Bathon and D. Proud (1999). "Comparison of the responses of B1 and B2 kinin receptors to agonist stimulation." Immunopharmacology **45**(1-3): 13-20.

Feron, O., T. W. Smith, T. Michel and R. A. Kelly (1997). "Dynamic Targeting of the Agonist-stimulated m2 Muscarinic Acetylcholine Receptor to Caveolae in Cardiac Myocytes." Journal of Biological Chemistry **272**(28): 17744-17748.

Folkman, J. and A. Moscona (1978). "Role of cell shape in growth control." Nature **273**(5661): 345-349.

Fotiadis, D., B. Jastrzebska, A. Philippsen, D. J. Müller, K. Palczewski and A. Engel (2006). "Structure of the rhodopsin dimer: a working model for G-protein-coupled receptors." Current Opinion in Structural Biology **16**(2): 252-259.

Fotiadis, D., Y. Liang, S. Filipek, D. A. Saperstein, A. Engel and K. Palczewski (2003). "Atomic-force microscopy: Rhodopsin dimers in native disc membranes." Nature **421**(6919): 127-128.

Fra, A. M., E. Williamson, K. Simons and R. G. Parton (1995). "De novo formation of caveolae in lymphocytes by expression of VIP21-caveolin." Proceedings of the National Academy of Sciences **92**(19): 8655-8659.

Fujita, A., J. Cheng, K. Tauchi-Sato, T. Takenawa and T. Fujimoto (2009). "A distinct pool of phosphatidylinositol 4,5-bisphosphate in caveolae revealed by a nanoscale labeling technique." Proceedings of the National Academy of Sciences **106**(23): 9256-9261.

Galbiati, F., J. A. Engelman, D. Volonte, X. L. Zhang, C. Minetti, M. Li, H. Hou, B. Kneitz, W. Edelmann and M. P. Lisanti (2001). "Caveolin-3 Null Mice Show a Loss of Caveolae, Changes in the Microdomain Distribution of the Dystrophin-Glycoprotein Complex, and T-tubule Abnormalities." Journal of Biological Chemistry **276**(24): 21425-21433.

Gaudreault, S. B., J.-F. Blain, J.-P. Gratton and J. Poirier (2005). "A role for caveolin-1 in post-injury reactive neuronal plasticity." Journal of Neurochemistry **92**(4): 831-839.

Geiger, B., A. Bershadsky, R. Pankov and K. M. Yamada (2001). "Transmembrane crosstalk between the extracellular matrix and the cytoskeleton." Nat Rev Mol Cell Biol **2**(11): 793-805.

Gervásio, O. L., W. D. Phillips, L. Cole and D. G. Allen (2011). "Caveolae respond to cell stretch and contribute to stretch-induced signaling." Journal of Cell Science **124**(21): 3581-3590.

Ghosh, S., C. Hentrich and T. Surrey (2013). "Micropattern-Controlled Local Microtubule Nucleation, Transport, and Mesoscale Organization." ACS Chemical Biology **8**(4): 673-678.

Glenney, J. and D. Soppet (1992). "Sequence and expression of caveolin, a protein component of caveolae plasma membrane domains phosphorylated on tyrosine in Rous sarcoma virus-transformed fibroblasts." Proc Natl Acad Sci USA **89**: 10517 - 10521.

Glenney, J. R. and L. Zokas (1989). "Novel tyrosine kinase substrates from Rous sarcoma virus-transformed cells are present in the membrane skeleton." The Journal of Cell Biology **108**(6): 2401-2408.

Golebiewska, U., J. M. Johnston, L. Devi, M. Filizola and S. Scarlata (2011). "Differential Response to Morphine of the Oligomeric State of μ-Opioid in the Presence of δ-Opioid Receptors." Biochemistry **50**(14): 2829-2837.

Gosens, R., G. L. Stelmack, G. Dueck, M. M. Mutawe, M. Hinton, K. D. McNeill, A. Paulson, S. Dakshinamurti, W. T. Gerthoffer, J. A. Thliveris, H. Unruh, J. Zaagsma and A. J. Halayko (2007). "Caveolae facilitate muscarinic receptor-mediated intracellular Ca2+ mobilization

and contraction in airway smooth muscle." American Journal of Physiology - Lung Cellular and Molecular Physiology **293**(6): L1406-L1418.

Grynkiewicz, G., M. Poenie and R. Y. Tsien (1985). "A new generation of Ca2+ indicators with greatly improved fluorescence properties." Journal of Biological Chemistry **260**(6): 3440-3450.

Gudi, S. R. P., C. B. Clark and J. A. Frangos (1996). "Fluid Flow Rapidly Activates G Proteins in Human Endothelial Cells: Involvement of G Proteins in Mechanochemical Signal Transduction." Circulation Research **79**(4): 834-839.

Guo, W.-h. and Y.-l. Wang (2007). "Retrograde Fluxes of Focal Adhesion Proteins in Response to Cell Migration and Mechanical Signals." Molecular Biology of the Cell **18**(11): 4519-4527.

Guo, Y., U. Golebiewska and S. Scarlata (2011). "Modulation of Ca2+ Activity in Cardiomyocytes through Caveolae-G[alpha]q Interactions." Biophysical Journal **100**(7): 1599-1607.

Guo, Y., U. Golebiewska and S. Scarlata (2011). "Modulation of Ca2+ Activity in Cardiomyocytes through Caveolae-Gαq Interactions." Biophysical Journal **100**(7): 1599-1607.

Haasemann, M., J. Cartaud, W. Muller-Esterl and I. Dunia (1998). "Agonist-induced redistribution of bradykinin B2 receptor in caveolae." Journal of Cell Science **111**(7): 917-928.

Haasemann, M., J. Cartaud, W. Muller-Esterl and I. Dunia (1998). "Agonist-induced redistribution of bradykinin B2 receptor in caveolae." J Cell Sci **111 (Pt 7)**: 917-928.

Haasemann, M., J. Cartaud, W. Muller-Esterl and I. Dunia (1998). "Agonist-induced redistribution of bradykinin B2 receptor in caveolae." J Cell Sci **111**(7): 917-928.

Hagiwara, Y., T. Sasaoka, K. Araishi, M. Imamura, H. Yorifuji, I. Nonaka, E. Ozawa and T. Kikuchi (2000). "Caveolin-3 deficiency causes muscle degeneration in mice." Human Molecular Genetics **9**(20): 3047-3054.

Hailstones, D., L. S. Sleer, R. G. Parton and K. K. Stanley (1998). "Regulation of caveolin and caveolae by cholesterol in MDCK cells." Journal of Lipid Research **39**(2): 369-379.

Hall, A. (2012). "Rho family GTPases." Biochem. Soc. Trans. **40**(No. 6): 1378-1382.

Hansen, C. G. and B. J. Nichols (2010). "Exploring the caves: cavins, caveolins and caveolae." Trends in Cell Biology **20**(4): 177-186.

Hayer, A., M. Stoeber, C. Bissig and A. Helenius (2010). "Biogenesis of Caveolae: Stepwise Assembly of Large Caveolin and Cavin Complexes." Traffic **11**(3): 361-382.

Head, B. P., H. H. Patel, D. M. Roth, N. C. Lai, I. R. Niesman, M. G. Farquhar and P. A. Insel (2005). "G-protein-coupled Receptor Signaling Components Localize in Both Sarcolemmal and Intracellular Caveolin-3-associated Microdomains in Adult Cardiac Myocytes." Journal of Biological Chemistry **280**(35): 31036-31044.

Hill, M. M., M. Bastiani, R. Luetterforst, M. Kirkham, A. Kirkham, S. J. Nixon, P. Walser, D. Abankwa, V. M. J. Oorschot, S. Martin, J. F. Hancock and R. G. Parton (2008). "PTRF-

Cavin, a Conserved Cytoplasmic Protein Required for Caveola Formation and Function." Cell **132**(1): 113-124.

Holmes, W. R. and L. Edelstein-Keshet (2012). "A Comparison of Computational Models for Eukaryotic Cell Shape and Motility." PLoS Comput Biol **8**(12): e1002793.

Huang, B., M. Bates and X. Zhuang (2009). "Super-Resolution Fluorescence Microscopy." Annual Review of Biochemistry **78**(1): 993-1016.

Igarashi, J. and T. Michel (2000). "Agonist-modulated Targeting of the EDG-1 Receptor to Plasmalemmal Caveolae." Journal of Biological Chemistry **275**(41): 32363-32370.

Insel, P. A., B. P. Head, R. S. Ostrom, H. H. Patel, J. S. Swaney, C.-M. Tang and D. M. Roth (2005). "Caveolae and Lipid Rafts: G Protein-Coupled Receptor Signaling Microdomains in Cardiac Myocytes." Annals of the New York Academy of Sciences **1047**(1): 166-172.

Insel, P. A., B. P. Head, H. H. Patel, D. M. Roth, R. A. Bundey and J. S. Swaney (2005). "Compartmentation of G-protein-coupled receptors and their signalling components in lipid rafts and caveolae." Biochem. Soc. Trans. **33**(Pt 5): 1131-1134.

Isshiki, M. and R. G. W. Anderson (1999). "Calcium signal transduction from caveolae." Cell Calcium **26**(5): 201-208.

Isshiki, M., J. Ando, R. Korenaga, H. Kogo, T. Fujimoto, T. Fujita and A. Kamiya (1998). "Endothelial Ca2+ waves preferentially originate at specific loci in caveolin-rich cell edges." Proceedings of the National Academy of Sciences **95**(9): 5009-5014.

Isshiki, M., J. Ando, K. Yamamoto, T. Fujita, Y. Ying and R. G. W. Anderson (2002). "Sites of Ca2+ wave initiation move with caveolae to the trailing edge of migrating cells." Journal of Cell Science **115**(3): 475-484.

Jaqaman, K. and S. Grinstein (2012). "Regulation from within: the cytoskeleton in transmembrane signaling." Trends in Cell Biology **22**(10): 515-526.

Ju, H., V. J. Venema, H. Liang, M. B. Harris, R. Zou and R. C. Venema (2000). "Bradykinin activates the Janus-activated kinase/signal transducers and activators of transcription (JAK/STAT) pathway in vascular endothelial cells: localization of JAK/STAT signalling proteins in plasmalemmal caveolae." Biochem. J. **351**(1): 257-264.

Kabayama, K., T. Sato, K. Saito, N. Loberto, A. Prinetti, S. Sonnino, M. Kinjo, Y. Igarashi and J.-i. Inokuchi (2007). "Dissociation of the insulin receptor and caveolin-1 complex by ganglioside GM3 in the state of insulin resistance." Proceedings of the National Academy of Sciences **104**(34): 13678-13683.

Kang, M. J., Y. H. Chung, C. Hwang, M. Murata, T. Fujimoto, I. H. Mook-Jung, C. I. Cha and W.-Y. Park (2006). "Caveolin-1 upregulation in senescent neurons alters amyloid precursor protein processing " Experimental and Molecular Medicine **38**: 126-133.

Kim, S. A., K. G. Heinze and P. Schwille (2007). "Fluorescence correlation spectroscopy in living cells." Nat Meth **4**(11): 963-973.

Kim, Y., A. Burns, P. Goldsmith, C. Heppner, S. Park, S. Chandrasekharappa, F. Collins, A. Spiegel and S. Marx (1999). "Stable overexpression of MEN1 supresses tumorigenicity of RAS." Oncogene **18**: 5936-5942.

Kirkham, M., S. J. Nixon, M. T. Howes, L. Abi-Rached, D. E. Wakeham, M. Hanzal-Bayer, C. Ferguson, M. M. Hill, M. Fernandez-Rojo, D. A. Brown, J. F. Hancock, F. M. Brodsky and R. G. Parton (2008). "Evolutionary analysis and molecular dissection of caveola biogenesis." Journal of Cell Science **121**(12): 2075-2086.

Kleuss, C. and E. Krause (2003). "G[alpha]s is palmitoylated at the N-terminal glycine." EMBO J **22**(4): 826-832.

Kogo, H. and T. Fujimoto (2000). "Caveolin-1 isoforms are encoded by distinct mRNAs: Identification of mouse caveolin-1 mRNA variants caused by alternative transcription initiation and splicing." FEBS Letters **465**(2–3): 119-123.

Koleske, A. J., D. Baltimore and M. P. Lisanti (1995). "Reduction of caveolin and caveolae in oncogenically transformed cells." Proceedings of the National Academy of Sciences **92**(5): 1381-1385.

Krisch, B., J. Feindt and R. Mentlein (1998). "Immunoelectronmicroscopic Analysis of the Ligand-induced Internalization of the Somatostatin Receptor Subtype 2 in Cultured Human Glioma Cells." Journal of Histochemistry & Cytochemistry **46**(11): 1233-1242.

Kurzchalia, T., P. Dupree, R. Parton, R. Kellner, H. Virta, M. Lehnert and K. Simons (1992). "VIP 21, A 21-kDa membrane protein is an integral component of trans-Golgi-network-derived transport vesicles." J Cell Biol **118**: 1003 - 1014.

Kusumi, A., C. Nakada, K. Ritchie, K. Murase, K. Suzuki, H. Murakoshi, R. S. Kasai, J. Kondo and T. Fujiwara (2005). "PARADIGM SHIFT OF THE PLASMA MEMBRANE CONCEPT FROM THE TWO-DIMENSIONAL CONTINUUM FLUID TO THE PARTITIONED

FLUID: High-Speed Single-Molecule Tracking of Membrane Molecules." Annual Review of Biophysics and Biomolecular Structure **34**(1): 351-378.

Lakowicz, J. (2006). Principles of Fluorescence Spectroscopy, Third Edition. New York, Springer Science

Lamb, M., C. Zhang, T. Shea, D. Kyle and L. M. F. Leeb-Lundberg (2002). "Human B1 and B2 bradykinin receptors and their agonists target caveolae-related lipid rafts to different degrees in HEK293 cells." Biochem. **41**: 14340-14347.

Lamb, M. E., C. Zhang, T. Shea, D. J. Kyle and L. M. F. Leeb-Lundberg (2002). "Human B1 and B2 Bradykinin Receptors and Their Agonists Target Caveolae-Related Lipid Rafts to Different Degrees in HEK293 Cells†." Biochemistry **41**(48): 14340-14347.

Langlois, S., K. N. Cowan, Q. Shao, B. J. Cowan and D. W. Laird (2008). "Caveolin-1 and -2 Interact with Connexin43 and Regulate Gap Junctional Intercellular Communication in Keratinocytes." Mol. Biol. Cell **19**(3): 912-928.

Langlois, S., K. N. Cowan, Q. Shao, B. J. Cowan and D. W. Laird (2008). "Caveolin-1 and -2 Interact with Connexin43 and Regulate Gap Junctional Intercellular Communication in Keratinocytes." Molecular Biology of the Cell **19**(3): 912-928.

Law, P.-Y., Y. H. Wong and H. H. Loh (2000). "Molecular Mechanisms and Regulation of Opioid Receptor Signaling." Annual Review of Pharmacology and Toxicology **40**(1): 389-430.

Leeb-Lundberg, L. M. F., F. Marceau, W. Müller-Esterl, D. J. Pettibone and B. L. Zuraw (2005). "International Union of Pharmacology. XLV. Classification of the Kinin Receptor Family: from Molecular Mechanisms to Pathophysiological Consequences." Pharmacological Reviews **57**(1): 27-77.

Levental, I., D. Lingwood, M. Grzybek, Ü. Coskun and K. Simons (2010). "Palmitoylation regulates raft affinity for the majority of integral raft proteins." Proceedings of the National Academy of Sciences.

Li, S., T. Okamoto, M. Chun, M. Sargiacomo, J. E. Casanova, S. H. Hansen, I. Nishimoto and M. P. Lisanti (1995). "Evidence for a Regulated Interaction between Heterotrimeric G Proteins and Caveolin." Journal of Biological Chemistry **270**(26): 15693-15701.

Lipardi, C., R. Mora, V. Colomer, S. Paladino, L. Nitsch, E. Rodriguez-Boulan and C. Zurzolo (1998). "Caveolin Transfection Results in Caveolae Formation but Not Apical Sorting of Glycosylphosphatidylinositol (GPI)-anchored Proteins in Epithelial Cells." The Journal of Cell Biology **140**(3): 617-626.

Lipardi, C., R. Mora, V. Colomer, S. Paladino, L. Nitsch, E. Rodriguez-Boulan and C. Zurzolo (1998). "Caveolin transfection results in caveolae formation but not apical sorting of glycosylphosphatidylinositol (GPI)-anchored proteins in epithelial cells." J.Cell Biol. **140**: 617-626.

Lisanti, M. P., P. E. Scherer, Z. Tang and M. Sargiacomo (1994). "Caveolae, caveolin and caveolin-rich membrane domains: a signalling hypothesis." Trends in Cell Biology **4**(7): 231-235.

Liu, L. and P. F. Pilch (2008). "A Critical Role of Cavin (Polymerase I and Transcript Release Factor) in Caveolae Formation and Organization." Journal of Biological Chemistry **283**(7): 4314-4322.

Liu, P., M. Rudick and R. Anderson (2002). "Multiple functions of caveolin-1." J Biol Chem **277**: 41295 - 41298.

Liu, P., T. Sudhaharan, R. M. L. Koh, L. C. Hwang, S. Ahmed, I. N. Maruyama and T. Wohland (2007). "Investigation of the Dimerization of Proteins from the Epidermal Growth Factor Receptor Family by Single Wavelength Fluorescence Cross-Correlation Spectroscopy." Biophysical Journal **93**(2): 684-698.

Loew, L. M. and J. C. Schaff (2001). "The Virtual Cell: a software environment for computational cell biology." Trends in biotechnology **19**(10): 401-406.

Makino, C. L., X.-H. Wen and J. Lem (2003). "Piecing together the timetable for visual transduction with transgenic animals." Current Opinion in Neurobiology **13**(4): 404-412.

Marceau, F. and D. Regoli (2004). "Bradykinin receptor ligands: therapeutic perspectives." Nat Rev Drug Discov **3**(10): 845-852.

McMahon, K.-A., H. Zajicek, W.-P. Li, M. J. Peyton, J. D. Minna, V. J. Hernandez, K. Luby-Phelps and R. G. W. Anderson (2009). "SRBC/cavin-3 is a caveolin adapter protein that regulates caveolae function." EMBO J **28**(8): 1001-1015.

Menezes, G. C., M. Miron-Mendoza, C.-H. Ho, H. Jiang and F. Grinnell (2008). "Oncogenic Ras-transformed human fibroblasts exhibit differential changes in contraction and migration in 3D collagen matrices." Experimental Cell Research **314**(16): 3081-3091.

Mentlein, R., J. Held-Feindt and B. Krisch (2001). "Topology of the signal transduction of the G protein-coupled somatostatin receptor sst₂ in human glioma cells." Cell and Tissue Research **303**(1): 27-34.

Meyers, J., J. Craig and David J. Odde (2006). "Potential for Control of Signaling Pathways via Cell Size and Shape." Current Biology **16**(17): 1685-1693.

Monier, S., D. J. Dietzen, W. R. Hastings, D. M. Lublin and T. V. Kurzchalia (1996). "Oligomerization of VIP21-caveolin in vitro is stabilized by long chain fatty acylation or cholesterol." FEBS Lett **388**: 143-149.

Monier, S., R. G. Parton, F. Vogel, J. Behlke, A. Henske and T. V. Kurzchalia (1995). "VIP21-caveolin, a membrane protein constituent of the caveolar coat, oligomerizes in vivo and in vitro." Molecular Biology of the Cell **6**(7): 911-927.

Mora, R., V. L. Bonilha, A. Marmorstein, P. E. Scherer, D. Brown, M. P. Lisanti and E. Rodriguez-Boulan (1999). "Caveolin-2 localizes to the golgi complex but redistributes to plasma membrane, caveolae, and rafts when co-expressed with caveolin-1." J Biol Chem **274**(36): 25708-25717.

Morris, J. B., H. Huynh, O. Vasilevski and E. A. Woodcock (2006). "α1-Adrenergic receptor signaling is localized to caveolae in neonatal rat cardiomyocytes." Journal of Molecular and Cellular Cardiology **41**(1): 17-25.

Murata, M., J. Peranen, R. Schreiner, F. Wieland, T. Kurzchalia and K. Simons (1995). "VIP21/caveolin is a cholesterol-binding protein." Proc Natl Acad Sci USA **92**: 10339 - 10343.

Murthy, K. S. and G. M. Makhlouf (2000). "Heterologous desensitization mediated by G protein-specific binding to caveolin." J.Biol.Chem. **275 (39)**: 30211-30219.

Navratil, A. M., S. P. Bliss, K. A. Berghorn, J. M. Haughian, T. A. Farmerie, J. K. Graham, C. M. Clay and M. S. Roberson (2003). "Constitutive Localization of the Gonadotropin-releasing Hormone (GnRH) Receptor to Low Density Membrane Microdomains Is Necessary for GnRH Signaling to ERK." Journal of Biological Chemistry **278**(34): 31593-31602.

Neves, S. R., P. Tsokas, A. Sarkar, E. A. Grace, P. Rangamani, S. M. Taubenfeld, C. M. Alberini, J. C. Schaff, R. D. Blitzer, I. I. Moraru and R. Iyengar (2008). "Cell Shape and Negative Links in Regulatory Motifs Together Control Spatial Information Flow in Signaling Networks." Cell **133**(4): 666-680.

Nomura, R., C. Inuo, Y. Takahashi, T. Asano and T. Fujimoto (1997). "Two-dimensional distribution of Gi2α in the plasma membrane: a critical evaluation by immunocytochemistry." FEBS Letters **415**(2): 139-144.

Oh, P. and J. E. Schnitzer (2001). "Segregation of heterotrimeric G proteins in cell surface microdomains. G(q) binds caveolin to concentrate in caveolae, whereas G(i) and G(s) target lipid rafts by default." Mol Biol Cell **12**(3): 685-698.

Oh, P. and J. E. Schnitzer (2001). "Segregation of Heterotrimeric G Proteins in Cell Surface Microdomains: Gq Binds Caveolin to Concentrate in Caveolae, whereas Gi and Gs Target Lipid Rafts by Default." Molecular Biology of the Cell **12**(3): 685-698.

Ostrom, R. S., S. R. Post and P. A. Insel (2000). "Stoichiometry and Compartmentation in G Protein-Coupled Receptor Signaling: Implications for Therapeutic Interventions Involving Gs." Journal of Pharmacology and Experimental Therapeutics **294**(2): 407-412.

Palmer, R. M. J., A. G. Ferrige and S. Moncada (1987). "Nitric oxide release accounts for the biological activity of endothelium-derived relaxing factor." Nature **327**(6122): 524-526.

Pani, B. and B. B. Singh (2009). "Lipid rafts/caveolae as microdomains of calcium signaling." Cell Calcium **45**(6): 625-633.

Park, D. S., S. E. Woodman, W. Schubert, A. W. Cohen, P. G. Frank, M. Chandra, J. Shirani, B. Razani, B. Tang, L. A. Jelicks, S. M. Factor, L. M. Weiss, H. B. Tanowitz and M. P. Lisanti (2002). "Caveolin-1/3 Double-Knockout Mice Are Viable, but Lack Both Muscle and Non-Muscle Caveolae, and Develop a Severe Cardiomyopathic Phenotype." The American Journal of Pathology **160**(6): 2207-2217.

Parton, R. G. (1994). "Ultrastructural localization of gangliosides; GM1 is concentrated in caveolae." Journal of Histochemistry & Cytochemistry **42**(2): 155-166.

Parton, R. G. and K. Simons (2007). "The multiple faces of caveolae." Nat. Rev. Mol. Cell Biol **8**: 185-194.

Parton, R. G. and K. Simons (2007). "The multiple faces of caveolae." Nat Rev Mol Cell Biol **8**(3): 185-194.

Patel, H. H., F. Murray and P. A. Insel (2008). G-Protein-Coupled Receptor-Signaling Components in Membrane Raft and Caveolae Microdomains. Protein-Protein Interactions as New Drug Targets. E. Klussmann and J. Scott, Springer Berlin Heidelberg. **186:** 167-184.

Pawson, A. J., S. R. Maudsley, J. Lopes, A. A. Katz, Y.-M. Sun, J. S. Davidson and R. P. Millar (2003). "Multiple Determinants for Rapid Agonist-Induced Internalization of a Nonmammalian Gonadotropin-Releasing Hormone Receptor: A Putative Palmitoylation Site and Threonine Doublet within the Carboxyl-Terminal Tail Are Critical." Endocrinology **144**(9): 3860-3871.

Peitzsch, R. M. and S. McLaughlin (1993). "Binding of acylated peptides and fatty acids to phospholipid vesicles: Pertinence to myristoylated proteins." Biochemistry **32**(39): 10436-10443.

Pelkmans, L., T. Bürli, M. Zerial and A. Helenius (2004). "Caveolin-Stabilized Membrane Domains as Multifunctional Transport and Sorting Devices in Endocytic Membrane Traffic." Cell **118**(6): 767-780.

Pelkmans, L. and M. Zerial (2005). "Kinase-regulated quantal assemblies and kiss-and-run recycling of caveolae." Nature **436**(7047): 128-133.

Philip, F., G. Kadamur, R. G. Silos, J. Woodson and E. M. Ross (2010). "Synergistic Activation of Phospholipase C-β3 by Gαq and Gβγ Describes a Simple Two-State Coincidence Detector." Current Biology **20**(15): 1327-1335.

Philip, F., P. Sengupta and S. Scarlata (2007). "Signaling through a G Protein Coupled Receptor and its corresponding G protein follows a stoichometrically limited model." J.Biol.Chem. **282**: 19203-19216.

Pike, L. J. and L. Casey (1996). "Localization and Turnover of Phosphatidylinositol 4,5-Bisphosphate in Caveolin-enriched Membrane Domains." Journal of Biological Chemistry **271**(43): 26453-26456.

Pin, J.-P., R. Neubig, M. Bouvier, L. Devi, M. Filizola, J. A. Javitch, M. J. Lohse, G. Milligan, K. Palczewski, M. Parmentier and M. Spedding (2007). "International Union of Basic and Clinical Pharmacology. LXVII. Recommendations for the Recognition and Nomenclature of G Protein-Coupled Receptor Heteromultimers." Pharmacological Reviews **59**(1): 5-13.

Popot, J. L. and D. M. Engelman (1990). "Membrane protein folding and oligomerization: the two-stage model." Biochemistry **29**(17): 4031-4037.

Prakash, Y. S., M. A. Thompson, B. Vaa, I. Matabdin, T. E. Peterson, T. He and C. M. Pabelick (2007). "Caveolins and intracellular calcium regulation in human airway smooth muscle." American Journal of Physiology - Lung Cellular and Molecular Physiology **293**(5): L1118-L1126.

Qin, D., Y. Xia and G. M. Whitesides (2010). "Soft lithography for micro- and nanoscale patterning." Nat. Protocols **5**(3): 491-502.

Rangamani, P., A. Lipshtat, E. Azeloglu, R. Calizo, M. Hu, S. Ghassemi, J. Hone, S. Scarlata, S. Neves and R. Iyengar (in press). "Decoding Information in Cell Shape. ." Cell.

Rasmussen, S. G. F., B. T. DeVree, Y. Zou, A. C. Kruse, K. Y. Chung, T. S. Kobilka, F. S. Thian, P. S. Chae, E. Pardon, D. Calinski, J. M. Mathiesen, S. T. A. Shah, J. A. Lyons, M. Caffrey, S. H. Gellman, J. Steyaert, G. Skiniotis, W. I. Weis, R. K. Sunahara and B. K. Kobilka (2011). "Crystal structure of the [bgr]2 adrenergic receptor-Gs protein complex." Nature **477**(7366): 549-555.

Razani, B., J. A. Engelman, X. B. Wang, W. Schubert, X. L. Zhang, C. B. Marks, F. Macaluso, R. G. Russell, M. Li, R. G. Pestell, D. Di Vizio, H. Hou, B. Kneitz, G. Lagaud, G. J. Christ, W. Edelmann and M. P. Lisanti (2001). "Caveolin-1 Null Mice Are Viable but Show Evidence of Hyperproliferative and Vascular Abnormalities." Journal of Biological Chemistry **276**(41): 38121-38138.

Reits, E. A. J. and J. J. Neefjes (2001). "From fixed to FRAP: measuring protein mobility and activity in living cells." Nat Cell Biol **3**(6): E145-E147.

Rhee, S. G. (2001). "REGULATION OF PHOSPHOINOSITIDE-SPECIFIC PHOSPHOLIPASE C*." Annual Review of Biochemistry **70**(1): 281-312.

Richter, T., M. Floetenmeyer, C. Ferguson, J. Galea, J. Goh, M. R. Lindsay, G. P. Morgan, B. J. Marsh and R. G. Parton (2008). "High-Resolution 3D Quantitative Analysis of Caveolar Ultrastructure and Caveola–Cytoskeleton Interactions." Traffic **9**(6): 893-909.

Rodriguez-Fraticelli, A. and F. Martin-Belmonte (2013). "Mechanical control of epithelial lumen formation." Small GTPases **4**(2).

Rodriguez-Fraticelli, A. E., M. Auzan, M. A. Alonso, M. Bornens and F. Martin-Belmonte (2012). "Cell confinement controls centrosome positioning and lumen initiation during epithelial morphogenesis." J Cell Biol **198**(6): 1011-1023.

Rodríguez-Fraticelli, A. E., M. Auzan, M. A. Alonso, M. Bornens and F. Martín-Belmonte (2012). "Cell confinement controls centrosome positioning and lumen initiation during epithelial morphogenesis." The Journal of Cell Biology **198**(6): 1011-1023.

Rothberg, K. G., J. E. Heuser, W. C. Donzell, Y.-S. Ying, J. R. Glenney and R. G. W. Anderson (1992). "Caveolin, a protein component of caveolae membrane coats." Cell **68**(4): 673-682.

Rothberg, K. G., J. E. Heuser, W. C. Donzell, Y. S. Ying, J. R. Glenney and R. G. W. Anderson (1992). "Caveolin, a protein component of caevolae membrane coats." Cell **68**: 673-682.

Rothberg, K. G., Y. S. Ying, B. A. Kamen and R. G. W. Anderson (1990). "Cholesterol controls the clustering of the glycophospholipid-anchored membrane receptor for 5-methyltetrahydrofolate." J.Cell Biol. **111**: 2931-2938.

Runnels, L. W. and S. F. Scarlata (1999). "Determination of the Affinities between Heterotrimeric G Protein Subunits and Their Phospholipase C-β Effectors†." Biochemistry **38**(5): 1488-1496.

Rust, M. J., M. Bates and X. Zhuang (2006). "Sub-diffraction-limit imaging by stochastic optical reconstruction microscopy (STORM)." Nat Meth **3**(10): 793-796.

Rybin, V. O., X. Xu, M. P. Lisanti and S. F. Steinberg (2000). "Differential targeting of beta -adrenergic receptor subtypes and adenylyl cyclase to cardiomyocyte caveolae. A mechanism to functionally regulate the cAMP signaling pathway." J Biol Chem **275**(52): 41447-41457.

Salanueva, I. J., A. Cerezo, M. C. Guadamillas and M. A. Del Pozo (2007). "Integrin regulation of caveolin function." Journal of Cellular and Molecular Medicine **11**(5): 969-980.

Sargiacomo, M., P. E. Scherer, Z. Tang, E. Kübler, K. S. Song, M. C. Sanders and M. P. Lisanti (1995). "Oligomeric structure of caveolin: implications for caveolae membrane organization." Proceedings of the National Academy of Sciences **92**(20): 9407-9411.

Sargiacomo, M., M. Sudol, Z. Tang and M. Lisanti (1993). "Signal transducing molecules and glycosyl-phosphatidylinositol-linked proteins form a caveolin-rich insoluble complex in MDCK cells." The Journal of Cell Biology **122**(4): 789-807.

Saulière-Nzeh, A. N., C. Millot, M. Corbani, S. Mazères, A. Lopez and L. Salomé (2010). "Agonist-selective Dynamic Compartmentalization of Human Mu Opioid Receptor as Revealed by Resolutive FRAP Analysis." Journal of Biological Chemistry **285**(19): 14514-14520.

Saulière, A., G. Gaibelet, C. Millot, S. Mazères, A. Lopez and L. Salomé (2006). "Diffusion of the mu opioid receptor at the surface of human neuroblastoma SH-SY5Y cells is restricted to permeable domains." FEBS letters **580**(22): 5227-5231.

Scherer, P., T. Okamoto, M. Chun, I. Nishimoto, H. Lodish and M. Lisanti (1996). "Identification, sequence and expression of caveolin-2 defines a caveolin gene family." Proc Natl Acad Sci USA **93**: 131 - 135.

Scherer, P. E., R. Y. Lewis, D. Volonté, J. A. Engelman, F. Galbiati, J. Couet, D. S. Kohtz, E. van Donselaar, P. Peters and M. P. Lisanti (1997). "Cell-type and Tissue-specific Expression of Caveolin-2: CAVEOLINS 1 AND 2 CO-LOCALIZE AND FORM A STABLE HETERO-OLIGOMERIC COMPLEX IN VIVO." Journal of Biological Chemistry **272**(46): 29337-29346.

Schlegel, A., D. Volonte, J. A. Engelman, F. Galbiata, P. Mehta, X.-L. Zhange, P. Scherer and M. P. Lisanti (1998). "Crowded little caves: structure and function of caveolae." Cell Signal. **10**: 457-463.

Schneider, I. C., E. M. Parrish and J. M. Haugh (2005). "Spatial Analysis of 3′ Phosphoinositide Signaling in Living Fibroblasts, III: Influence of Cell Morphology and Morphological Polarity." Biophysical Journal **89**(2): 1420-1430.

Schnitzer, J. E., P. Oh, B. S. Jacobson and A. M. Dvorak (1995). "Caveolae from luminal plasmalemma of rat lung endothelium: microdomains enriched in caveolin, Ca(2+)-ATPase, and inositol trisphosphate receptor." Proceedings of the National Academy of Sciences **92**(5): 1759-1763.

Schubert, A.-L., W. Schubert, D. C. Spray and M. P. Lisanti (2002). "Connexin Family Members Target to Lipid Raft Domains and Interact with Caveolin-1†." Biochemistry **41**(18): 5754-5764.

Schwille, P., U. Haupts, S. Maiti and W. W. Webb (1999). "Molecular dynamics in living cells observed by fluorescence correlation spectroscopy with one- and two-photon excitation." Biophys. J. **77**: 2251-2265.

Schwille, P., S. Kummer, A. A. Heikal, W. E. Moerner and W. W. Webb (2000). "Fluorescence correlation spectroscopy reveals fast optical excitation-driven intramolecular dynamics of yellow fluorescent proteins." Proceedings of the National Academy of Sciences **97**(1): 151-156.

Sengupta, P., F. Philip and S. Scarlata (2008). "Caveolin-1 alters Ca2+ signal duration through specific interaction with the G{alpha}q family of G proteins." J Cell Sci **121**(9): 1363-1372.

Sezgin, E. and P. Schwille (2011). "Fluorescence Techniques to Study Lipid Dynamics." Cold Spring Harbor Perspectives in Biology **3**(11).

Shaul, P. W., E. J. Smart, L. J. Robinson, Z. German, I. S. Yuhanna, Y. Ying, R. G. W. Anderson and T. Michel (1996). "Acylation Targets Endothelial Nitric-oxide Synthase to Plasmalemmal Caveolae." Journal of Biological Chemistry **271**(11): 6518-6522.

Sheetz, M. P. (2001). "Cell control by membrane–cytoskeleton adhesion." Nat Rev Mol Cell Biol **2**(5): 392-396.

Simons, K. and M. J. Gerl (2010). "Revitalizing membrane rafts: new tools and insights." Nat Rev Mol Cell Biol **11**(10): 688-699.

Singer, S. J. and G. L. Nicolson (1972). "The Fluid Mosaic Model of the Structure of Cell Membranes." Science **175**(4023): 720-731.

Sinha, B., D. Köster, R. Ruez, P. Gonnord, M. Bastiani, D. Abankwa, R. V. Stan, G. Butler-Browne, B. Vedie, L. Johannes, N. Morone, R. G. Parton, G. Raposo, P. Sens, C. Lamaze

and P. Nassoy (2011). "Cells Respond to Mechanical Stress by Rapid Disassembly of Caveolae." Cell **144**(3): 402-413.

Smotrys, J. E. and M. E. Linder (2004). "PALMITOYLATION OF INTRACELLULAR SIGNALING PROTEINS: Regulation and Function." Annual Review of Biochemistry **73**(1): 559-587.

Song, K., P. Scherer, Z. Tang, T. Okamoto, S. Li, M. Chafel, C. Chu, D. Kohtz and M. Lisanti (1996). "Expression of caveolin-3 in skeletal, cardiac, and smooth muscle cells. Caveolin-3 is a component of the sarcolemma and co-fractionates with dystrophin and dystrophin-associated glycoproteins." J Biol Chem **271**: 15160 - 15165.

Song, K. S., S. Li, T. Okamoto, L. A. Quilliam, M. Sargiacomo and M. P. Lisanti (1996). "Co-purification and Direct Interaction of Ras with Caveolin, an Integral Membrane Protein of Caveolae Microdomains: DETERGENT-FREE PURIFICATION OF CAVEOLAE MEMBRANES." Journal of Biological Chemistry **271**(16): 9690-9697.

Soskic, V., E. Nyakatura, M. Roos, W. Müller-Esterl and J. Godovac-Zimmermann (1999). "Correlations in Palmitoylation and Multiple Phosphorylation of Rat Bradykinin B2 Receptor in Chinese Hamster Ovary Cells." Journal of Biological Chemistry **274**(13): 8539-8545.

Sotgia, F., J. K. Lee, K. Das, M. Bedford, T. C. Petrucci, P. Macioce, M. Sargiacomo, F. D. Bricarelli, C. Minetti, M. Sudol and M. P. Lisanti (2000). "Caveolin-3 Directly Interacts with the C-terminal Tail of β-Dystroglycan: IDENTIFICATION OF A CENTRAL WW-LIKE DOMAIN WITHIN CAVEOLIN FAMILY MEMBERS." Journal of Biological Chemistry **275**(48): 38048-38058.

Sprang, S. R., Z. Chen and X. Du (2007). Structural Basis of Effector Regulation and Signal Termination in Heterotrimeric Gα Proteins. Advances in Protein Chemistry. R. S. Stephen, Academic Press. **Volume 74:** 1-65.

Stan, R.-V. (2002). "Structure and function of endothelial caveolae." Microscopy Research and Technique **57**(5): 350-364.

Stan, R. V. (2005). "Structure of caveolae." Biochimica et Biophysica Acta (BBA) - Molecular Cell Research **1746**(3): 334-348.

Stan, R. V., E. Tkachenko and I. R. Niesman (2004). "PV1 Is a Key Structural Component for the Formation of the Stomatal and Fenestral Diaphragms." Molecular Biology of the Cell **15**(8): 3615-3630.

Sun, Y., H. Wallrabe, S.-A. Seo and A. Periasamy (2011). "FRET Microscopy in 2010: The Legacy of Theodor Förster on the 100th Anniversary of his Birth." ChemPhysChem **12**(3): 462-474.

Suzuki, K., K. Ritchie, E. Kajikawa, T. Fujiwara and A. Kusumi (2005). "Rapid Hop Diffusion of a G-Protein-Coupled Receptor in the Plasma Membrane as Revealed by Single-Molecule Techniques." Biophysical Journal **88**(5): 3659-3680.

Tagawa, A., A. Mezzacasa, A. Hayer, A. Longatti, L. Pelkmans and A. Helenius (2005). "Assembly and trafficking of caveolar domains in the cell: caveolae as stable, cargo-triggered, vesicular transporters." The Journal of Cell Biology **170**(5): 769-779.

Tang, Z., P. Scherer, T. Okamoto, K. Song, C. Chu, D. Kohtz, I. Nishimoto, H. Lodish and M. Lisanti (1996). "Molecular cloning of caveolin-3, a novel member of the caveolin gene family expressed predominantly in muscle." J Biol Chem **271**: 2255 - 2261.

Tang, Z., P. E. Scherer, T. Okamoto, K. Song, C. Chu, D. S. Kohtz, I. Nishimoto, H. F. Lodish and M. P. Lisanti (1996). "Molecular Cloning of Caveolin-3, a Novel Member of the Caveolin Gene Family Expressed Predominantly in Muscle." Journal of Biological Chemistry **271**(4): 2255-2261.

Teixeira, A., N. Chaverot, C. Schröder, A. D. Strosberg, P.-O. Couraud and S. Cazaubon (1999). "Requirement of Caveolae Microdomains in Extracellular Signal-Regulated Kinase and Focal Adhesion Kinase Activation Induced by Endothelin-1 in Primary Astrocytes." Journal of Neurochemistry **72**(1): 120-128.

Théry, M. (2010). "Micropatterning as a tool to decipher cell morphogenesis and functions." Journal of Cell Science **123**(24): 4201-4213.

Thomsen, P., K. Roepstorff, M. Stahlhut and B. van Deurs (2002). "Caveolae Are Highly Immobile Plasma Membrane Microdomains, Which Are not Involved in Constitutive Endocytic Trafficking." Molecular Biology of the Cell **13**(1): 238-250.

Venkatakrishnan, A. J., X. Deupi, G. Lebon, C. G. Tate, G. F. Schertler and M. M. Babu (2013). "Molecular signatures of G-protein-coupled receptors." Nature **494**(7436): 185-194.

Volontè, D., F. Galbiati and M. P. Lisanti (1999). "Visualization of caveolin-1, a caveolar marker protein, in living cells using green fluorescent protein (GFP) chimeras: The

subcellular distribution of caveolin-1 is modulated by cell-cell contact." FEBS letters **445**(2): 431-439.

Waldhoer, M., S. E. Bartlett and J. L. Whistler (2004). "OPIOID RECEPTORS." Annual Review of Biochemistry **73**(1): 953-990.

Wedegaertner, P. B., D. H. Chu, P. T. Wilson, M. J. Levis and H. R. Bourne (1993). "Palmitoylation is required for signaling functions and membrane attachment of Gq alpha and Gs alpha." Journal of Biological Chemistry **268**(33): 25001-25008.

Weidemann, T. and P. Schwille (2009). Fluorescence Correlation Spectroscopy in Living Cells. Handbook of Single-Molecule Biophysics. P. Hinterdorfer and A. van Oijen. New York, Springer Science

Williams, T. and M. Lisanti (2004). "The caveolin proteins." Genome Biology **5**(3): 214.

Woodman, S. E., D. S. Park, A. W. Cohen, M. W.-C. Cheung, M. Chandra, J. Shirani, B. Tang, L. A. Jelicks, R. N. Kitsis, G. J. Christ, S. M. Factor, H. B. Tanowitz and M. P. Lisanti (2002). "Caveolin-3 Knock-out Mice Develop a Progressive Cardiomyopathy and Show Hyperactivation of the p42/44 MAPK Cascade." Journal of Biological Chemistry **277**(41): 38988-38997.

Yamada, E. (1955). "THE FINE STRUCTURE OF THE RENAL GLOMERULUS OF THE MOUSE." The Journal of Biophysical and Biochemical Cytology **1**(6): 551-566.

Yamaguchi, T., Y. Murata, Y. Fujiyoshi and T. Doi (2003). "Regulated interaction of endothelin B receptor with caveolin-1." European Journal of Biochemistry **270**(8): 1816-1827.

Yoon, S.-H., Y. K. Kim, E. D. Han, Y.-H. Seo, B. H. Kim and M. R. K. Mofrad (2012). "Passive control of cell locomotion using micropatterns: the effect of micropattern geometry on the migratory behavior of adherent cells." Lab on a Chip **12**(13): 2391-2402.

Yu, C., S. Rouen and R. T. Dobrowsky (2008). "Hyperglycemia and downregulation of caveolin-1 enhance neuregulin-induced demyelination." Glia **56**(8): 877-887.

Yu, T., C. K. Chua, C. Y. Tay, F. Wen, H. Yu, J. K. Y. Chan, M. S. K. Chong, D. T. Leong and L. P. Tan (2013). "A Generic Micropatterning Platform to Direct Human Mesenchymal Stem Cells from Different Origins Towards Myogenic Differentiation." Macromolecular Bioscience: n/a-n/a.

Zajchowski, L. D. and S. M. Robbins (2002). "Lipid rafts and little caves. Compartmentalized signalling in membrane microdomains." Eur J Biochem **269**: 737-752.

Zhang, F. L. and P. J. Casey (1996). "Protein Prenylation: Molecular Mechanisms and Functional Consequences." Annual Review of Biochemistry **65**(1): 241-269.

Zhao, H., H. H. Loh and P. Y. Law (2006). "Adenylyl Cyclase Superactivation Induced by Long-Term Treatment with Opioid Agonist Is Dependent on Receptor Localized within Lipid Rafts and Is Independent of Receptor Internalization." Molecular Pharmacology **69**(4): 1421-1432.

Zheng, H., J. Chu, Y. Qiu, H. H. Loh and P.-Y. Law (2008). "Agonist-selective signaling is determined by the receptor location within the membrane domains." Proceedings of the National Academy of Sciences.